# Nanosized systems for efficient delivery of antitumoral and anti-inflammatory drugs

Università degli Studi di Cagliari
PhD Program in Scienze e Tecnologie Farmaceutiche
SSD Chim/09
A.A.: 2013-2014 ciclo XXVII

PhD Candidate: Rosa Pireddu
PhD Program Coordinator: Prof. Elias Maccioni
Supervisor: Dr. Francesco Lai


REGIONE AUTONOMA DELLA SARDEGNA

Rosa Pireddu gratefully acknowledges Sardinia Regional Government for the financial support of her PhD scholarship (P.O.R. Sardegna F.S.E. Operational Programme of the Autonomous Region of Sardinia, European Social Fund 2007-2013 - Axis IV Human Resources, Objective 1.3, Line of Activity 1.3.1.)

## Contents

# I. Liposomes

# 1.Liposomes for triiodothyronine delivery to hepatoma cells: development, characterization and *in vitro* studies



## 1. Introduction

Hepatocellular carcinoma (HCC) is one of the most common malignant tumors which can result from several liver diseases such as hepatitis B and C infections, metabolic liver diseases and non-alcoholic fatty liver diseases [1]. Malignant transformations of hepatocytes induced by viral factors and several mediators in the chronically inflamed area lead to hepatocarcinogenesis. HCC is the sixth most common cancer (in male) and the third leading cause of cancer associated deaths in the world [2,3].

### 1.1. Triiodothyronine (T3) and Thyroid hormone receptors (TRs)

3,5,3'-triiodo-L-thyronine (T3) (Figure 1), a thyroid hormone (TH) normally synthesized and secreted by the thyroid gland, influences a variety of physiological processes, including cell growth and metabolism in mammals, metamorphosis in amphibians, and development of the vertebrate nervous system [4]. Most of the effects of T3 are mediated by thyroid hormone nuclear receptors, the TRs, which act as transcription factors [5,6]. TRs are members of the steroid/thyroid receptor superfamily of nuclear hormone receptors, which includes the two retinoid acid receptors (RAR and RXR), the vitamin D receptor (VDR), the peroxisome proliferators-activated receptor (PPAR), the constitutive androstane receptor (CAR), and some orphan receptors [7]. Two different TR subtypes, TRα and TRβ, have been identified which are the products of distinct genes [8]. The TRα1 and the TRβ1 isoforms bind thyroid hormone with near-equal affinity, and are ubiquitously expressed, although TRα1 predominates in the heart (50—70% of TRs) while TRβ1 predominates in the liver (80% of TRs) [7]. Data collected from various TR knockout mice suggest that TRα1 mediates the effects of thyroid hormones of heart rate, whereas TRβ1 is important in mediating the cholesterol-lowering and TSH suppressant effects of T3 [8]. Paradoxically, al-

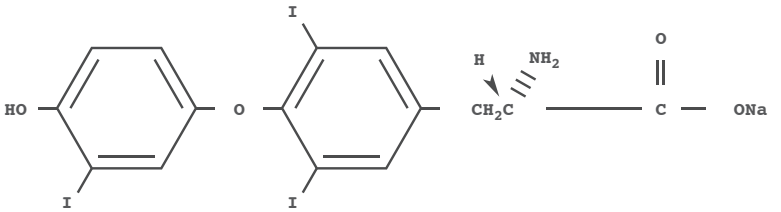


**Figure 1** 3,5,3'-triiodo-L-thyronine (T3) structure



though the thyroid hormones stimulate liver proliferation and enhance liver regeneration, they also induce a rapid regression of carcinogen-induced hepatic nodules, and reduce the incidence of hepatocarcinoma and lung metastasis [9,10]. TRβ-specific agonist GC-1 also reduces the number of preneoplastic foci generated in experimental models of liver carcinogenesis in rodents but T3 exhibits a stronger effect than GC-1, suggesting that TRα could also contribute to the antineoplastic effects of the hormone [11]. The biochemical phenotype of the preneoplastic hepatocytes closely resembles that of immature hepatocytes since they lack hepatocyte differentiation markers while expressing genes normally present during the fetal or neonatal period. Treatment with T3 or GC-1 causes the loss of several markers associated with preneoplasia showing that TRs ligands promote remodeling of the preneoplastic lesions. Therefore, it has been postulated that the mitogenic activity mediated by activated TRs is associated with or followed by a process of differentiation [11]. In contrast to the mitogenic effect of THs in the liver, in hepatocarcinoma cells transfected with TR, T3 down-regulates expression of pituitary tumor-transforming 1 (PTTG1), a critical mitotic checkpoint protein [12]. Furthermore, expression of TRβ1 in hepatocarcinoma cells retards tumor growth, causes partial mesenchymal to epithelial cell transition and has a strong inhibitory effect on invasion, extravasation and metastasis formation in nude mice [13,14]. In cultured hepatocarcinoma cells, and also in breast cancer cells, TRβ1 abolishes anchorage-independent growth and migration, disrupts the mitogenic action of growth factors suppressing activation of signaling pathways that are crucial for cell proliferation and invasiveness, and represses expression of genes that are relevant for metastatic progression [14]. Notably, the antitumoral property of T3 appears to be

specific and not shared by other liver mitogens, such as ciprofibrate, a member of the class of peroxisome proliferators [10]. All these findings suggest that thyroid hormone receptors constitute a novel therapeutic target in cancer. However, T3 administration is associated with serious side effects, particularly cardiac dysfunction, i.e. tachycardia, arrhythmias, and precipitation of ischemic episodes or heart failure [15].

### 1.2. Nanosized vehicles for drug delivery in cancer

The ideal nanoscale drug delivery system should ensure that the conjugated or bound drug–carrier complex arrives and acts preferentially at the selected target. Targeting of the drug–nanocarrier complex can be active, whereby the complex incorporates a ligand specific for the receptor or epitope of the target tissue. In passive targeting, complexes diffuse and accumulate at sites with excessively leaky microvasculature, such as tumours and inflamed tissues, with normal endothelium being much less permeable. Subsequent extravasation of complexes takes place either via transcytosis, whereby macromolecules are internalized from the blood at points of invagination of the cell membrane, or paracellularly, via diffusion through the tight junctions of endothelial cells. Particularly in cancers, an imbalance in factors that regulate angiogenesis, such as overexpression of vascular endothelial growth factor (VEGF), results in both increased vascular permeability and chaotic tumour-vessel architecture. In combination, these effects cause enhanced permeation and retention (EPR) [16], resulting in high local drug concentrations (Figure 2). Key properties of any nanomaterial used in drug delivery are its biocompatibility and biodegradability, so that the unloaded carrier is degraded or metabolized into non-toxic components and cleared through the circulation. Materials are cleared according to their size. Small particles (0–30 nm) are rap-



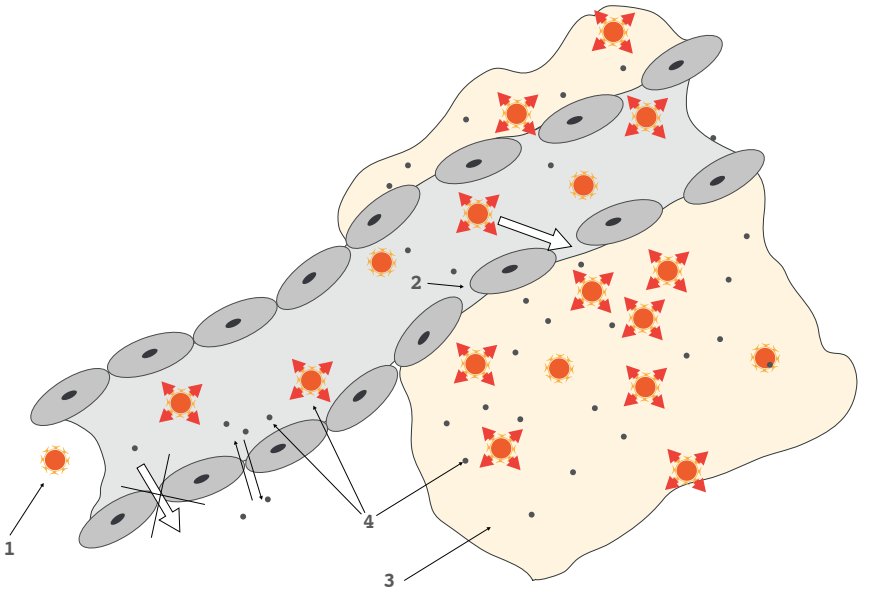


**Figure 2** Schematics of the Enhanced Permeability and Retention (EPR) effect or "passive" targeting. Passive tissue targeting is achieved by extravasation of nanoparticles through increased permeability of the tumor vasculature and ineffective lymphatic drainage (EPR effect). (1) Drug-loaded nanocarrier; it cannot extravasate through normal endothelium and only small molecules of free drug (4) can traverse normal endothelium to a certain extent in both directions; (2) gaps between endothelial cells appear in pathological areas (3) (such as tumors, infarcts, and inflammations), through which nanoparticles can extravasate and accumulate in such areas creating high local drug concentrations. Adapted from Ref. [23]

idly cleared by renal excretion. Nanocarriers >30 nm are cleared by the mononuclear phagocytic system (MPS), consisting of macrophages located in the liver (Kupffer cells) and the spleen [17], which act as phagocytotic scavengers. Clearance is also dependent on endothelial fenestral size [17]. Fenestrae are highly variable, so it is difficult to determine the efficacy and toxicity of nanomedicines in different individuals because age, sex and genetics influence their rate of clearance [18]. Whether nanocarriers are taken up by macrophages depends on opsonization by the innate immune system [19]. Opsonins, molecules that bind to foreign materials and enhance phagocytosis, include IgG and IgA antibodies, the complement cascade system and mannose-binding lectin [20]. Therefore, the surface properties of nanocarriers can significantly affect the rate of clearance by the MPS. A useful method for evading opsonization of large narrow carriers was developed in Rutgers University in the 1960s [21]: in a process called PEGylation, a polymer, poly(ethylene glycol) (PEG; [CH2CH2O]n), is conjugated to the drug carrier.
Overall, use of ligand—drug—nanocarrier complexes improves the drug therapeutic index. The high selectivity and specificity of the complex, increases the amount of drug delivered to the target tissue and decreases the amount at unwanted sites. Therefore, less systemic drug needs to be administered to ensure a sufficient concentration at the site of action and the minimum efficacious dose is also lower. In addition, because less drug is present at unwanted sites, the maximum non-toxic is higher. The overall effect is a drastic decrease in toxicity and adverse side effects [22].

### 1.2.1. Liposomes

Liposomes are closed spherical vesicles consisting of one or more lipid bilayers that encapsulate an aqueous phase in which hydrophilic drugs can be stored while hydrophobic molecules can be



dissolved into lipid bilayer. The size of liposome depends on their composition and preparation method and can vary from approximately 50 nm to greater than 1 $\mu$m in diameter. The lipid bilayer can be composed of either synthetic or natural phospholipids. The predominant physical and chemical properties of liposomes are based on the net properties of the constituent phospholipids [24], including permeability, charge density and steric hindrance. The lipid bilayer closes in on itself due to interactions between water molecules and the hydrophobic phosphate groups of the phospholipids. This process of liposome formation is spontaneous because the amphiphilic phospholipids self-associate into bilayers. Drug loading into liposomes can be achieved through (i) liposome formation in an aqueous solution saturated with soluble drug; (ii) the use of organic solvents and solvent exchange mechanisms; (iii) the use of lipophilic drugs; and (iv) pH gradient methods [25] (Figure 3). Liposomes generally reach their site of action by extravasation into the interstitial space from the bloodstream. Liposomes can target specific tissues through both active and passive targeting strategies (Figure 4). This is because they can easily be manipulated by linking additional molecules to the outer surface of the lipid bilayer. Liposomes are rapidly cleared by the MPS due to their size. Reducing opsonization of liposomes by PEGylation therefore reduces clearance by the MPS, increasing the circulation half-life. Opsonization presents such a problem to the development of therapeutically useful liposomes that nearly all research reported in the literature involves PEG-coated or PEGylated liposomes. Liposomal formulations of anticancer drugs have already been approved for human use. Doxil® is a liposomal formulation of the anthracycline drug doxorubicin used to treat cancer in AIDS-related Kaposi sarcoma and multiple myeloma [26]. Its advantages over free dox-

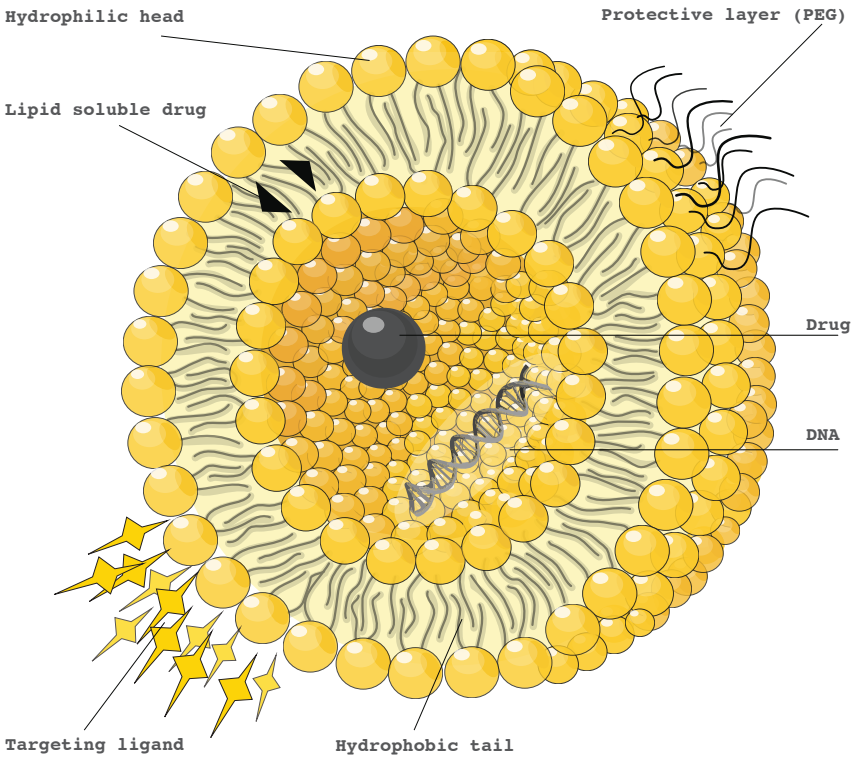


**Figure 3** Diagram of a bilaminar liposome. The hydrophobic region traps drugs in the central core when the liposomes are prepared. The outer surface can be functionalized with ligands for active targeting or PEGylated. Liposomes can vary in the number of lipid bilayers they possess and can be classified into three categories: (i) multilamellar vesicles, (ii) large unilamellar vesicles and (iii) small unilamellar vesicles. Adapted from Ref. [29]



orubicin are greater efficacy and lower cardiotoxicity. These advantages are attributed to passive targeting of tumours, due to leaky tumour vasculature [27] and the EPR effect, and to lower concentrations of free doxorubicin at healthy tissue sites. There is evidence that liposomal Doxil® is metabolized by leukaemia cells via a different mechanism than that for free doxorubicin, which might explain the improved efficacy and lower toxicity. Furthermore, Doxil® is under clinical trial for the treatment of breast cancer.
One of the most interesting developments in this field is the potential of liposomes to overcome the increasing problem of multidrug resistance (MDR) acquired by cancers, which drastically reduces chemotherapeutic efficacy. Ogawara et al. recently investigated the effect of PEG liposomal doxorubicin (Doxil®) in a male mouse tumour model inoculated with either colon cancer (C26) cells or their doxorubicin-resistant (MDR) subclone, which overexpresses P-gp efflux pumps [28]. The results showed that PEG liposomal doxorubicin had anti-tumour effects on both doxorubicin-resistant and non-doxorubicin-resistant C26 cells. With increasing incidence of resistance to chemotherapy, the use of liposomes offers effective treatment without the need for the costly discovery of new chemotherapeutic drugs because current drugs can be reformulated. Liposomes are firmly established with the success of Doxil®, and new liposomal formulations of other anticancer drugs are now being intensively explored to improve chemotherapy outcomes and reduce toxicity.

### 1.3. Liver targeting

The liver is well known for its high drug uptake because of its first pass-effect and its prominent role in the metabolism and excretion of many compounds including therapeutic drugs. It receives blood (oxygenated and deoxygenated) from the gut and heart via the portal vein and hepatic artery, respectively. Blood

circulates through a permeable discontinuous capillary network term as the sinusoids to reach the central and hepatic veins (Figure 4). The sinusoids are small blood vessels (5 to 10μm wide) between the radiating rows of hepatocytes having fenestrations of size 100–150 nm (depending on the type of animal species). They allow almost unrestricted passage of plasma components to the perisinusoidal space, where the cords of parenchymal cells called as hepatocytes are situated. Inside the sinusoid capillaries, the Kupffer cells are responsible for phagocytic activity of the liver [30].

One of the most prominent cell types in the liver are obviously the hepatocytes. The strategic localization of hepatocytes combined with a high expression of many transporters and endocytotic receptors is often a driving force for the accumulation of xenobiotics in this cell type. Consequently, many drugs are taken up and cleared from the circulation by this cell type without any targeting system. However, although hepatocytes represent more than 80% of the total number of resident hepatic cells, uptake in other cell-types like Kupffer cells may occur as well, and high uptake of viruses, antibodies or other biological compounds into these cells often leads to complete degradation of such compounds [31,32], which in some cases destroys their therapeutic activity. It seems clear that although drugs do accumulate rapidly in liver they simply do not accumulate in the proper intrahepatic cell-type [33], thus for specific cell, there should be specific delivery system and ligand for targeting. There may be five different cells types present in liver for active targeting of drug, namely, (i) hepatocytes, (ii) Kupffer and sinusoidal endothelial cells, (iii) hepatic stellate cells (HSC), (iv) bile duct epithelial cells, and, in the presence of a neoplasia (v) hepatocellular carcinoma cells (Figure 5). In particular, strategies for hepatocytes-and hepatocellular carcinoma cells-selective drug targeting will be detailed in the following sections.



**1.3.1. Delivery systems to hepatocytes**

In several pathological conditions, such as viral hepatitis (Hepatitis A, B or C), alcohol-induced steatohepatitis (ASH), non-alcohol-induced steatohepatitis (NASH), some genetic diseases like Wilson's disease, hemochromatosis, α1antitrypsin deficiency, and several other metabolic disorders, hepatocytes represent the most relevant target cells. In all these conditions, hepatocytes are infected or damaged and they are directly involved in the pathogenesis of these diseases. Drug uptake by this particular cell-type is in general not a major issue due to the first pass effect and the presence of many transporters and endocytotic receptors that take up drugs. In the past decades, many methods for hepatocyte-selective drug targeting have been explored in order to enhance the therapeutic effects of several antitumoral, antiviral and gene-based therapies or to reduce side-effects of antiviral or anticancer drugs [33]. In most cases, the asialoglycoprotein receptor (ASGP-R) has been used as the target receptor for drug delivery to the hepatocytes. Galactose residues [35,36] or lactose moieties [37] have been coupled to proteins, polymers or incorporated into the outer layer of liposomes [38]. The asialoglycoprotein receptor is specifically and abundantly present on hepatocytes [35–37,39] and this receptor has been used to deliver all kinds of therapeutic compounds ranging from therapeutic proteins, antiviral agents [40] to anticancer drugs into hepatocytes [41–43]. In particular, ASGP-R-targeted liposomes have been widely used for the delivery of drugs, genes and oligonucleotides to this cell type. Indeed, delivery of liposomes and proteins to the hepatocytes using this ASGP-R as a target receptor was one of the first options for the cell-specific delivery to liver cells, and

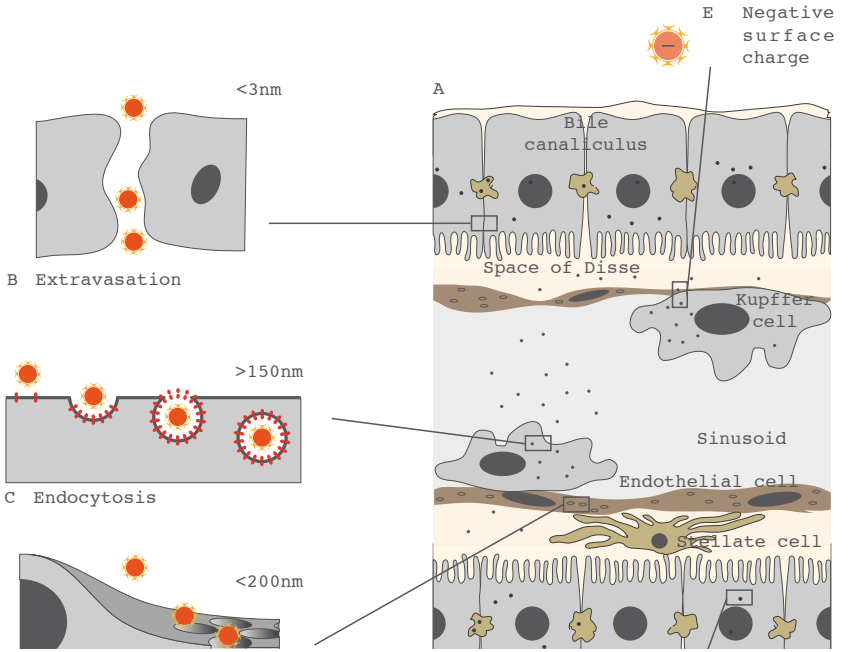


**Figure 4** Mechanisms of nanoparticles passively targeting the liver. (A) Microscopic structure of liver sinusoid in hepatic lobules. (B) Nanoparticles smaller than 3 nm in diameter could extravasate different tissues nonspecifically. (C) Nanoparticles with large negative surface charge or larger than 150 nm in diameter could be captured by Kupffer cells. (D) Nanoparticles less than 200 nm in diameter could pass through sinusoidal fenestrations after intravenous administration. (E) Nanoparticles with negative surface charge tend to be taken up by Kupffer cells and endothelial cells. (F) Nanoparticles with positive surface charge tend to be taken up by hepatocytes. Adapted from Ref. [34]



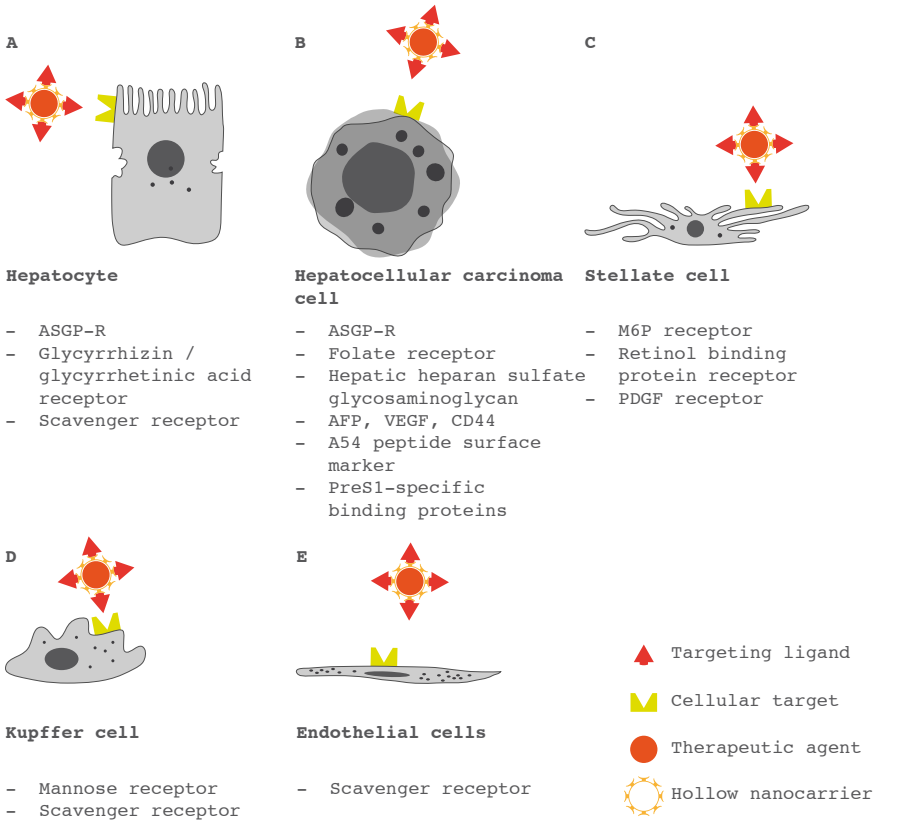


**Figure 5** Receptors or cellular targets on liver cells for nanoparticles actively targeting the liver. After intravenous administration, nanoparticles modified with specific surface ligands could be recognized by their receptors or cellular targets on a specific type of liver cells ((A) hepatocyte. (B) Hepatocellular carcinoma cell. (C) Hepatic stellate cells (HSC). (D) Kupffer cell. (E) Endothelial cells), and then the drug/gene was released. Adapted from Ref. [34]

even to date, much research in the liposomal drug delivery area is still dedicated to targeting to this ASGP-R on hepatocytes [39,44], although this has not led to any clinical application yet. ASGP-receptor ligands have also been applied for the delivery of siRNA to hepatocytes [45,46].

### 1.3.2. Delivery systems to hepatocellular carcinoma cells

In well-differentiated HCC cells, asialoglycoprotein (ASPG) receptor is highly expressed [47]. Several drug delivery systems have already been developed to deliver drugs to this receptor using lactosaminated or galactosamine substituted drug carriers. In particular, polymers have been applied for the purpose of drug delivery to HCC [42,48,49] but modified albumins have also been explored [50,51]. The ASGP-receptor has also been employed as a target receptor for the delivery of genes with antineoplastic effects to the hepatocytes by making complexes of plasmids and polymers coupled to ASGP-receptor binding ligands [52,53]. Moreover, other drug delivery systems such as cationic liposomes, virosomes, and adenoviral vectors have been exploited for the delivery of anticancer drugs and genes in HCC. Cheng et al. [54] synthesized GC/5-FU nanoparticles by combining galactosylated chitosan (GC) material with 5-FU, and tested its effect on liver cancer cells *in vitro* and *in vivo.* They concluded that sustained releases of GC/5-FU nanoparticles are more effective in targeting hepatic cancer cells than 5-FU monotherapy, as shown in mouse orthotropic liver cancer model. In the same year, Li et al. [55] stated that the encapsulation of tetrandrine (Tet) and paclitaxel (Ptx) into nanoparticles retain the synergistic anticancer efficiency of Tet and Ptx against mice hepatoma H22 cells. Other researchers, Zhou et al. [56], synthesized N-lactosyl-ioleoylphosphatidylethanolamine (Lac-DOPE) and evaluated it as a liver-specific targeting ligand via ASGP-R



receptors for liposomal delivery of doxorubicin. It reported that lactosylated liposomes are promising drug delivery vehicles for hepatocellular carcinoma. Recently, Zhang et al. [57] reported that mixed copolymer nanoparticles (NPs), self-assembled from β-cyclodextrin-grafted hyperbranched polyglycerol (HPG-g-CD) and lactobionic acid (LA)-grafted hyperbranched polyglycerol (HPG-g-LA), were utilized as carriers for paclitaxel, resulting in enhanced hepatocellular-carcinoma uptake of these nanoparticles. Therefore, it was concluded that mixed copolymer NPs are efficient nanocarriers for hepatoma-targeted delivery of potent antitumor drugs.

To enhance the specificity for HCC, other targeting strategies using monoclonal antibodies (mAb), and growth factor-recognizing oligopeptides have been utilized. The HCC-specific monoclonal antibody AF-20, directed against a 180 kDa-cell-surface glycoprotein which is highly expressed on HCC [58] has been explored, but recently research focused on the use of antibodies against growth factor receptors that are expressed on HCC. Similar to other tumors, HCC tissues express epidermal growth factor (EGF) receptors and a chimeric (mouse/human) antibody against this EGF-receptor (Cetuximab) has been examined in clinical trials [59,60]. Several studies show that this antibody is beneficial in patients with HCC and may be used in combination with other drugs. However, antibodies have not been applied as drug carrier to HCC. For that purpose oligopeptides recognizing the EGF receptor have been used. Liu et al. and Lee et al. both applied an EGFR-binding peptide for gene delivery to HCC [61,62]. Liu et al. demonstrated that delivery of human cyclin-dependent kinase inhibitor gene p21WAF-1 and murine cytokine gene GM-CSF using EGF receptor oligopeptides produced potent antitumor effects in hepatoma-bearing mice [61], and beneficial effects were also obtained us-

ing EFG itself as homing ligand [63]. Although many of HCC targeted cell-selective therapies applied an intra- or peri-tumor inoculation of the compounds [62], Liu et al. demonstrated beneficial effects after systemic administration of the EGF-R targeted genes [64]. The use of the EGF ligand itself to direct compounds to the EGF-receptor was applied by Wolschek et al. They used these compounds to deliver the reporter gene beta-galactosidase into HCC after systemic administration into mice [63].
Significant tumor accumulation of drugs can already be obtained in patients with HCC based on the enhanced permeability and retention (EPR) effect [65] if a drug delivery tool with the proper molecular size is used. Combined with a HCC-selective molecule, additional cell-selectivity and thus therapeutic effectiveness may be obtained. In the area of drug targeting to HCC, significant advancement has been made in recent years, leading to an improved management of HCC in patients.

### 1.3.3. Lactoferrin as ligand for liver targeting

In order to enhance the targeting efficiency of drug delivery systems to receptors in hepatocytes, several novel materials have been employed and, among them, we have selected Lactoferrin (Lf). It is a mammalian cationic iron binding glycoprotein belonging to the transferrin (Tf) family [66]. Recently this glycoprotein is becoming increasingly attractive because of its multifunctional and mediating biological activities with Lf receptors (Lf-R) [67,68]. Formerly Lf-R was successfully utilized as a targeting ligand for brain delivery due to the presence of Lf receptor on blood brain barrier (BBB) [69–71]. Likewise, many recent studies revealed that lactoferrin could bind to multiple receptors on hepatocytes prior to internalization, including low-density lipoprotein receptor-related protein receptors (LRP-R) [72,73] and the asialoglycoprotein receptors (ASGP-R) [74,75], which also belong to LfR [67,76,77]. It has been demonstrated that Lf binds ASGP-R with high affinity (Kd approx. 80 nM) in a galactose-independent manner [78], implying Lf is a good ligand to ASGP-R binding. For instance, Wei et al. reported Lf-PEGylated liposomes (PLS) as a promising drug delivery system for hepatocellular carcinoma therapy with lower toxicity and enhanced efficacy [79]. It has been validated that Lf-R binds to ASGP-R with high affinity, implying that Lf-R is a good ligand to ASGPR binding. Due to its specific binding, Lf-R has been applied to gene delivery successfully, for the transfer of genetic material to the hepatocytes [80]. These exciting evidences suggested that Lf-R might be a promising candidate for hepatocellular carcinoma targeting due to its high affinity for ASGP-R, and that is highly possible to develop a hepatic carcinoma targeting drug delivery system employing the ASGP-R targeting ability of Lf-R.



## 2. The aim of the work

Given the T3 anticancer potential in the treatment of hepatocellular carcinoma, the aim of this work was to develop an effective hepatocellular carcinoma targeting drug delivery system to improve the T3 delivery to hepatic cancer cells and, at the same time, to reduce toxic side effects. Three different liposome systems, such as, conventional, Stealth (PEGylated) and Lf-modified-Stealth liposomes were developed and characterized. Liposomes cell interactions and cellular uptake were evaluated in FaO, HepG2 and SKHep cells by confocal microscopy using liposomes labeled with the lipophilic marker 1,2-dioleolylsn-glycero-3-phosphoethanolamine-N-(lissamine rhodamine B sulfonyl) (Rho-PE) and loaded with the hydrophilic probe 5(6)-carboxyfluorescein (CF). Finally, in vitro cytotoxicity studies were carried out by using MTT assay to evaluate the toxicity of the liposome delivery system and to test the effect of T3 when in-

corporated into liposomes.

## 3. Materials and methods

### 3.1 Materials

1-Palmitoyl-2-oleylphosphatydilcholine (POPC), dimethyldioctadecylammonium (DDAB), DSPE-PEG-maleimide and 1,2-dioleolylsn-glycero-3-phosphoethanolamine-N-(lissamine rhodamine B sulfonyl) (Rho-PE) were purchased from Avanti Polar Lipids (Alabaster, USA). 1,2-distearoyl-sn-glycero-3-phosphoethanolamine-N-[methoxy (polyethylene glycol)-2000]-(DSPE-PEG2000) was purchased from Lipoid GmbH (Ludwigshafen, Germany). Phosphate buffer solution (PBS, pH 7) was purchased from Carlo Erba Reagents (Rodano, Italy). 3,3',5-Triiodo-L-thyronine sodium salt (T3), 2-iminothiolane (Traut's reagent), Lactoferrin, from bovine colostrum (Lf), Sepharose CL-4B, 5(6)-carboxyfluorescein (CF) and all the other products were purchased from Sigma–Aldrich (Milan, Italy). Centriprep-30 (molecular weight cut-off: 30,000) concentrators were from Amicon (Billerica, Massachusetts).

### 3.2. Liposomes preparation

All liposome formulations were prepared according to the film hydration method. Conventional liposomes (Conv-LIPO) were obtained by dissolving in a chloroform/methanol (1/1, v/v) mixture POPC (78.94 μmol) (1-Palmitoyl-2-oleylphosphatydilcholine), DDAB (0.63μmol) (Dimethyldioctadecylammonium) and T3 (10 μmol) (as methanol solution). By adding to this mixture DSPE-PEG2000 (2.4 μmol)(1,2-distearoyl-sn-glycero-3-phosphoethanolamine-N-[methoxy (polyethylene glycol)-2000] and the linker lipid DSPE-PEG-maleimide (0.72 μmol) Stealth liposomes (Stealth-LIPO) and targeted liposomes (Lf-Stealth-LIPO) were respectively produced. The lipid mixtures were deposited as a thin film in a roundbottom flask by rotoevaporating (Rotavapor Büchi R110, Flawil, Switzerland) the chloroform/methanol under vacuum. The thin lipid films were hydrated at 65°C with 1 mL of PBS solution (pH 7) by mechanical shaking for 2 h. The resulting liposome dispersions were sonicated with a Soniprep 150 ultrasonic disintegrator (MSE Crowley, London, United Kingdom) until a clear opalescent dispersion was obtained (5 seconds on and 2 seconds off, 60 cycles). The liposomes were then purified on a Sepharose CL-4B gel filtration column using phosphate buffer as eluent.

### 3.3. Lactoferrin conjugation

To prepare targeted liposomes (Lf-Stealth-LIPO), Lactoferrin was conjugated to the liposome by means of thioether-bonds between the protein and the linker lipids of the liposomes. Here, the Lf molecules are thiolated using 2-iminothiolane (Traut's reagent) and react with the maleimide groups on the PEG terminus. Then, 3.38 mg/ml (42,3 nmol) Lf was added to 2 ml borate–EDTA buffer (0.15 M Na borate, 0.1 mM EDTA, pH 8.5) containing 1692 nmol of fresh Traut's reagent. This mixture was incubated for 60 min on a rotational shaker (at 110 rpm) at room temperature. Thiolated Lf solutions were concentrated and the buffer exchanged with phosphate buffer solution using a Centriprep-30 concentrator (molecular weight cut-off: 30,000, Amicon). The concentrated lactoferrin was immediately added to the maleimide grafted liposomes and left to react overnight at room temperature. Lastly, the lactoferrin-conjugated liposomes were separated from T3 and free Lf by Sepharose CL-4B gel filtration as described above [81].

### 3.4. Liposomes characterization

#### 3.4.1. Particle size and zeta potential

Size distribution (average diameter and polydispersity index (PI)) of the samples was determined by photon correlation spectroscopy using a Zetasizer nano (Malvern Instrument, Worcestershire, United Kingdom). Before counting, the samples were diluted with PBS. Samples were backscattered by helium–neon laser (633 nm) at an angle of 173° and at con-

stant temperature of 25°C. Zeta potential was estimated using the Zetasizer nano by means of the M3-PALS (phase analysis light scattering) technique, which measures the particle electrophoretic mobility in a thermostated cell. A long-term stability study of formulations stored at 4 ± 1°C was performed by monitoring the vesicle average size, polydispersity index and surface charge over 90 days.

**3.4.2. Encapsulation efficiency**

Encapsulation efficiency (E%), expressed as the percentage of the encapsulated drug respect to the amount of T3 initially used in liposomal preparation, was determined by gel filtration chromatography. Briefly, 800 $\mu$l of the samples were loaded on a Sepharose CL-4B column which was pre-equilibrated with PBS buffer and then eluted with the buffer. T3 loaded liposomes were collected and diluted with methanol. T3 content was quantified by HPLC method.

**3.4.3. Transmission Electron Microscope (TEM)**

The morphological characteristics of the liposomes were examined using a Transmission Electron Microscope (TEM). Liposomes were deposited for 2 minutes on carbon coated 200 mesh copper grids and negatively stained with 2.5% uranyl acetate for 2 minutes, washed with water, drained and observed at 80 kV with a Tecnai 12 (Fei) TEM.

**3.4.4. HPLC analysis for T3**

T3 content was quantified at 226 nm using a chromatograph Alliance 2690 (Waters, Milan, Italy), equipped with a photodiode array detector and a computer integrating apparatus (Empower 3). The column was a SunFire C18 (3.5 $\mu$m, 4.6 mm × 100 mm, Waters), and the mobile phase was a mixture of water, methanol, acetonitrile and acetic acid (41.92:40:18:0.08, v/v), delivered at a flow rate of 0.7 ml/min.

A standard calibration curve was built up by using working, standard solutions. Calibration graphs were plotted according to the linear regression analysis, which gave a correlation coefficient value (R2) of 0.999.



**3.5. Cell experiments**

**3.5.1. Cell line culture**

FaO, rat hepatoma cell line and human hepatocarcinoma cell line, HepG2, were supplied by Interlab Cell Line Collection (Servizio Biotecnologie, IST, Genova, Italy) and maintained in Dulbecco's medium (DMEM plus Glutamax I) (Invitrogen). The liver human cells SKHep were a gentle gift from Prof. Silvia Giordano (Istituto Oncologico Candiolo, Torino, Italy) and were maintained in Minimun Essential Medium (Invitrogen). Both culture medium, DMEM and MEM, were supplemented with penicillin, streptomycin and 10% heat-inactivated fetal calf-serum (FCS) (Invitrogen) and the cells maintained in a humidified atmosphere of 5% CO2/95% air, at 37°C. After 19 hours of incubation, the medium was replaced with fresh medium without serum and the cells were treated with different concentration of empty and drug loaded formulations as indicated in the figures.

**3.5.2. Western Blot Analysis**

After treatment, total protein extracts were obtained using M-PER Mammalian Protein Extraction Reagent (Thermos Scientific, Rockford, IL, USA) plus Halt Protease Inhibitor Cocktail (Thermo Scientific) and according to manufacturer's instruction. Protein concentration of the total extracts was determined according to the method of Bradford [82] using BSA as standard (DC Protein Assay, Bio Rad Laboratories, Hercules, CA). For immunoblotting analysis, equal amounts of proteins were electrophoresed on SDS 10% polyacrilamyde gels. After gel electrotransfer onto nitrocellulose membranes, to ensure equivalent protein loading and transfer in all lanes, the membranes were stained with 0.5% (w/v) Ponceau S red (ICN Biomedicals) in 1% acetic acid for 5 minutes. After blocking in TBS containing 0.5% Tween 20 (Sigma) (TBS-T) and 5% non-fat dry milk for 1 hour at

room temperature or overnight at 4° C, membranes were washed in TBS-T and incubated with the appropriate primary antibodies diluted in blocking buffer. Whenever possible, the same membrane was used to detect the expression of different proteins. Depending on the origin of primary antibody, filters were incubated with anti-mouse, anti-goat or anti-rabbit horseradish peroxidase-conjugated IgG (Santa Cruz Biotechnology, Santa Cruz, CA). Immunoreactive bands were identified by chemiluminescence detection system, as described by the manufacturer (Supersignal Substrate, Pierce, Rockford, IL). For immunoblotting experiments mouse monoclonal anti-actin (clone AC-40, Sigma) and Thyroid Hormone Receptor beta-1 (J52, Thermo Scientific) antibodies were used.

**3.5.3. Cellular uptake of fluorescent liposomes**

Cell interactions and cellular uptake were investigated by confocal microscopy using liposomes labeled with a lipophilic fluorescent marker 1,2-dioleolyl-sn-glycero-3-phosphoethanolamine-N-(lissamine rhodamine B sulfonyl) (0.035 mg/ml; RhoPE) and loaded with a hydrophilic fluorescent marker 5(6)-carboxyfluorescein (0.025 mg/ml; CF). Liposomes were purified from the non-entrapped markers by gel filtration as described above. Cells (3 x 105/3ml medium) were grown in collagen coated slides seated in 6 wells plate, and the experiments were performed to the achievement of subconfluence. FaO, HepG2 and SKHep cells were incubated at 37°C with the different formulation and a solution of CF for 1 and 3 hours at the highest concentration used for the cytotoxicity study (1:100). At the end of the experiment, the cells were washed twice with PBS (EuroClone, Italy) and fixed with a solution of 4% buffered formaldeyde (pH 7.4) (Sigma, Milan, Italy) and treated with triton X-100 (0.1%, Sigma, Milan, Italy) to increase the permeability of the cells. The fixed cells were washed with PBS and then stained with Hoechts 33258 blue (Life Technologies, Invitrogen, Milan, Italy) to display the nucleus. After staining, the cells were again washed with PBS and were mounted with Mounting Medium (BioSystem, Italia).

The fluorescence images were analyzed with the laser scanning confocal microscope (FluoView, FV10i, Olympus). CF, RhoPE and Hoechst 33258 fluorescence was observed with 470 ± 20/535 ± 40, 546 ± 6/620 ± 60 and 360 ± 20/460 ± 25 excitation/emission filters respectively.

**3.5.4. Cell viability studies**

The toxic effect of liposomes was determined by the cell viability MTT (tetrazolium salt, 3-(4,5-dimethylthiazol-2yl)-2,5-diphenyltetrazolium bromide) assay. 200 mL of 1:10 diluted MTT stock (5 mg/mL of MTT in Hanks' balanced salt solution) was added to each culture. The formed crystals were solubilized in a solution of isopropanol-10% NP40-0.4N HCl, and absorbance values were measured at the wavelength of 570 nm with the background subtraction at 690 nm in a Packard Spectra Count microplate reader (Packard Instrument Co, Downers Grove, IL). Cells (2 x 104 cells/well) were seeded in 96 well plates with 200 $\mu$l of culture medium. Nineteen hours after seeding the medium was replaced with fresh medium without FCS, and cells were treated with both empty and drug loaded formulations at different dilutions (1:100, 1:200, 1:400, 1:800, 1:1600 for empty formulations and 1:100, 1:200, 1:1000 for T3 loaded formulations). In parallel, hepatoma cells were treated with T3 solutions at different dilutions (1:100, 1:200, 1:1000). T3 was dissolved in 1N NaOH and neutralized with cultured medium. Each sample was tested in triplicate for at least three times. The untreated cells were used as negative control.

**3.6. Statistical analysis of data**

Instat software (GraphPad Prism4, San Diego, CA) was used to analyze the data.

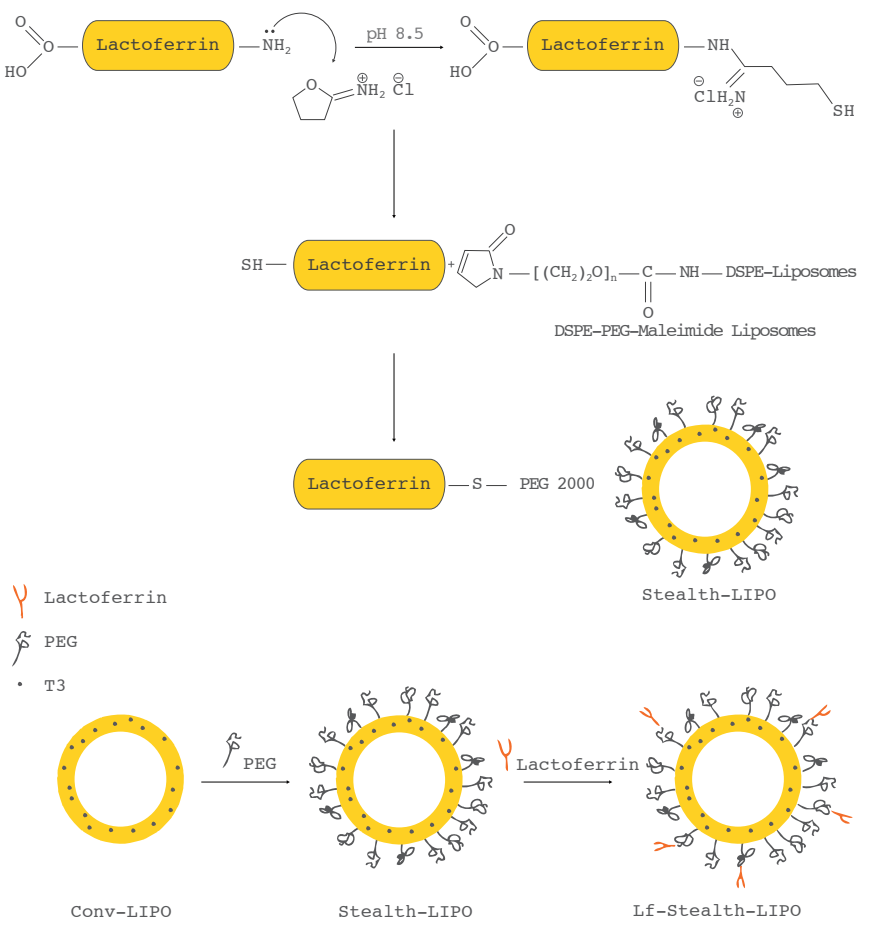


**Figure 6** Schematic representation of conventional liposomes (Conv-LIPO), stealth liposomes (Stealth-LIPO) and liposomes conjugated to lactoferrin (Lf-Stealth-LIPO) and schematic preparation and covalent attachment of Lf to stealth liposome surface.



One-way analysis of variance (ANOVA) with post hoc analysis using Tukey's multiple comparison test was used for parametric data. The results of multiple observations were presented as the means ± S.D of at least 3 separate experiments. A p value of $<0.05$ was considered statistically significant.

## 4. Results and discussion

### 4.1. Preparation and characterization of empty and drug-loaded liposomes

Liposomes (see Figure 6 for schematic representation) were successfully prepared using the film hydration method. As shown in Table 1, six different formulations were prepared. Empty and drug loading conventional liposomes (Conv-LIPO) were prepared using only POPC and DDAB. Then, the outer surface of liposomes was modified by adding a pegylated lipid (DSPE-PEG) to the composition of conventional formulation (Stealth-LIPO). Finally, for the preparation of targeted liposomes (Lf-Stealth-LIPO) the lipid linker DSPE-PEG-maleimide was incorporated in the lipid mixture. Lf was covalently conjugated to the distal end of DSPE-PEG- maleimide lipid by thioether bond and loaded onto Stealth liposomes surface as targeting moiety. To bind the linker with a thioether bond Lf was thiolated using 1:40 Lf/iminothiolane molar ratio [81]. Liposomes TEM visualization (Figure 7) shows multi-lamellar vesicles, small in size and with spherical shape. The physical properties of liposomes are shown in Table 2. PCS measurements showed a mean diameter of empty and T3 loaded-formulations ranging between 86 and 126 nm, which are preferable for tumor accumulation *via* the EPR effect [23]. Polydispersity index (≤ 0.28) proved a fairly narrow size distribution for all the formulations. However, empty and T3 liposomes were slightly increased in size after incubation with Lf (126.5 and 103.1 nm), while PI values did not show any significant variation after the Lf attachment. The zeta potential analyses showed that all li-

**Table 1** Composition of empty and T3 loaded-Conventional (Conv-LIPO), Stealth liposomes (Stealth-LIPO) and Lf-modified-Stealth liposomes (Lf-Stealth-LIPO).

| **Formulations** | **Components (μmol)** | | | | | |
|---|---|---|---|---|---|---|
| | T3 | POPC | DDAB | DSPE-PEG | DSPE-PEG-Maleimide | Lactoferrin |
| Conv-LIPO | | 78.94 | 0.63 | - | - | - |
| T3-Conv-LIPO | 10 | 78.94 | 0.63 | - | - | - |
| Stealth-LIPO | - | 78.94 | 0.63 | 2.4 | - | - |
| T3-Stealth-LIPO | 10 | 78.94 | 0.63 | 2.4 | - | - |
| Lf-Stealth-LIPO | - | 78.94 | 0.63 | 2.4 | 0.72 | 0.043 |
| T3-Lf-Stealth-LIPO | 10 | 78.94 | 0.63 | 2.4 | 0.72 | 0.043 |

**Table 2.** Liposomes physicochemical characterization. Average diameter (MD), polydispersity index (PI), zeta potential (ZP) and Encapsulation Efficiency (E%) of freshly prepared liposomal formulations. Values are the means ± standard deviation (n = 3).

| | | **MD (nm)** | **PI** | **ZP (mV)** | **E %** |
|---|---|---|---|---|---|
| Conv-LIPO | empty | 98.1 ± 1.04 | 0.28 ± 0.01 | 5.7 ± 0.22 | |
| | T3 | 86.8 ± 0.66 | 0.28 ± 0.02 | 7.5 ± 2.37 | 91 ± 3.1 |
| Stealth-LIPO | empty | 94.6 ± 1.53 | 0.20 ± 0.03 | 2.5 ± 0.41 | |
| | T3 | 99.4 ± 0.77 | 0.23 ± 0.02 | 1.3 ± 0.03 | 87 ± 4.2 |
| Lf-Stealth-LIPO | empty | 126.5 ± 2.58 | 0.25 ± 0.03 | 1.2 ± 0.55 | |
| | T3 | 103.1 ± 1.16 | 0.17 ± 0.02 | 1.1 ± 0.35 | 90 ± 3.2 |

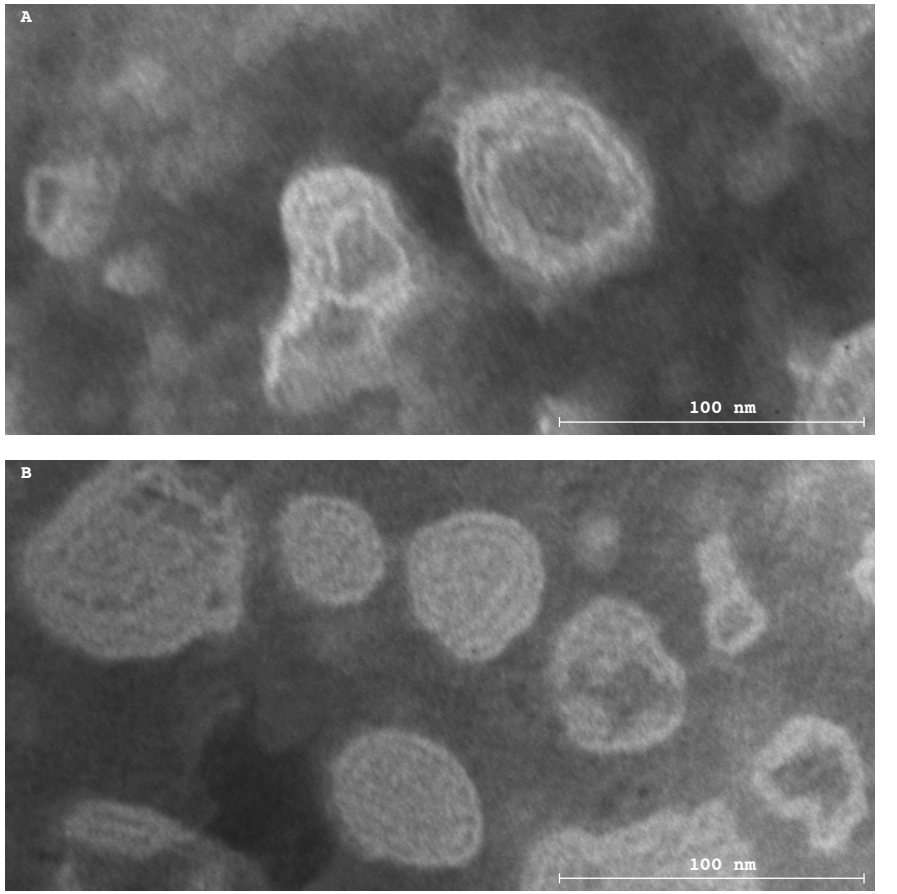


**Figure 7** TEM micrographs of T3-loaded conventional and stealth liposomes: Conv-LIPO (a) and Stealth-LIPO (b)

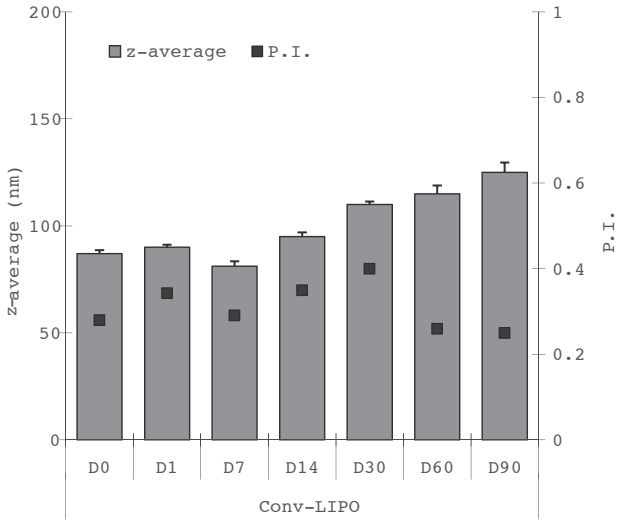


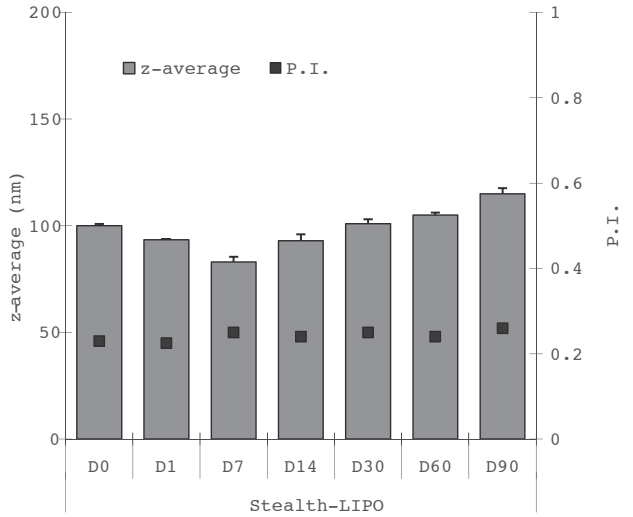


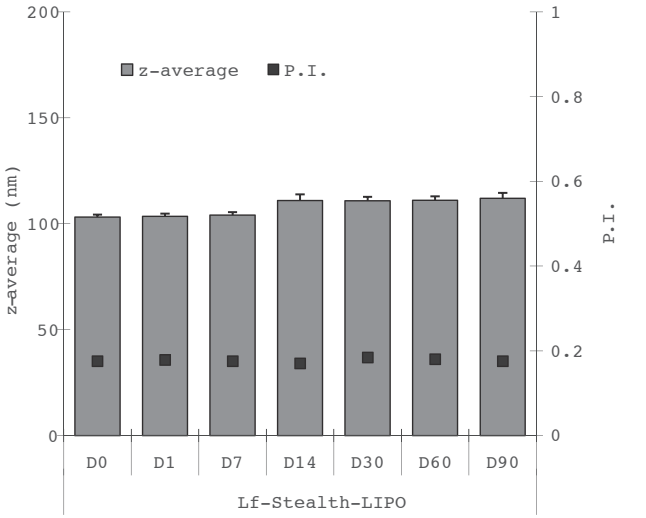


**Figure 8** Average diameter (Z-average) and polydispersity index (PI) of T3 loaded liposomal formulations monitored during 90 days of storage at 4 °C.

posomes possessed nearly neutral surface charges (≤7.5 mV), which could reduce undesirable nonspecific protein adsorption [83]. The encapsulation efficiency (EE) of T3 loaded liposomes was relatively high, approximately 90%, thus demonstrating that the presence of the ligand did not influence the liposome ability to include the drug.
Physical stability is an important parameter for *in vivo* biomedical application of liposomes. In this study the physical stability of drug-loaded liposomes was investigated by monitoring variations in size distribution during time. As shown in Figure 8, all liposomes were stable over 90 days at 4°C and only a slight increase in size was observed for Conv-LIPO and Stealth-LIPO. However, after 90 days the mean diameter of all the studied vesicles was below130 nm.

### 4.2. Cell studies

In this study rat hepatoma, FaO, human hepatocarcinoma, HepG2 and SKHep, cell lines have been chosen as HCC target cells.
First of all, the Thyroid Hormone Receptor β-1 (TRβ) expression has been checked in the selected cell lines. It is known that T3 performs its action through interaction with its nuclear receptors (TRs) among which, TRβ form is predominant in liver and it is responsible for the hepatomitogenic activity of T3 [7].
TRβ expression was analyzed by Western Blot analysis using actin as loading control and densitometric analysis was also performed to quantify TRβ expression. As shown in Figure 9, the TRβ protein expression was observed in all the tested cell lines (Figure 9.a) with the highest expression detected in HepG2 (approximately 4 fold higher than that observed in FaO and SKHep cell lines) (Figure 9.b).

#### 4.2.1. Cell binding and cellular uptakes of liposomes

The internalization of liposomes into the target cells was analyzed by confocal microscopy. To this pur-



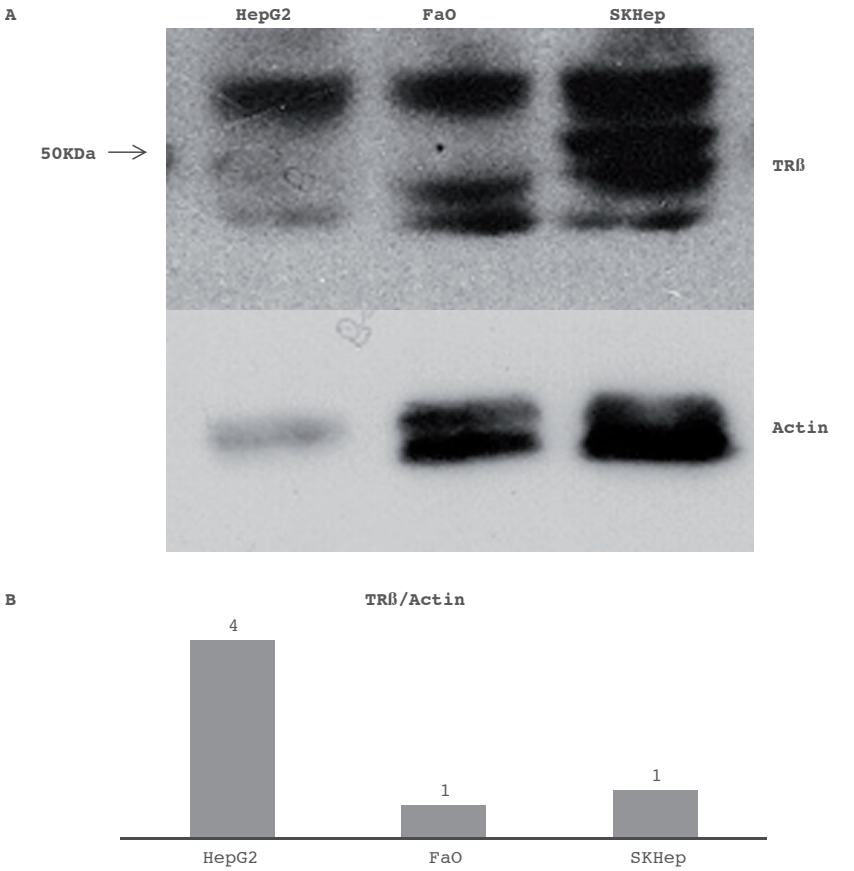


**Figure 9** a)Western blot analysis of TRβ in HepG2, FaO and SKHep cells. Western analysis was performed as described in Materials and Methods. Actin was used as a loading control. b) Densitometric quantification of TRβ in HepG2, FaO and SKHep cells compared to actin (TRβ/Actin)

pose, FaO, HepG2 and SKHep cells were incubated for 1 and 3 hours with Lf-Stealth-LIPO, Conv-LIPO and Stealth-LIPO, containing two fluorescent markers: one lipophilic, rhodamine (0.035 mg/ml Rho) and one hydrophilic, (6)-carboxyfluorescein (0.025 mg/ml, CF). CF was chosen because it is a membrane impermeable probe largely used for investigating membrane integrity and permeability [84,85]. After treatment with liposome formulations, the cells were fixed, and the Hoechst dye, which allows the visualization of the nucleus, was added. The images obtained for each marker were overlapped to simultaneously display the location of each marker inside the cells. Figures 10.a, 10.b, 10.c, 11.a, 11.b, 11.c, 12.a, 12.b, 12.c, show the fluorescence images of FaO, HepG2 and SKHep cells treated with liposomes after 3 hours incubation, in which it is clear that the markers were internalised. In particular, orange fluorescence intensity, due to the merging of red-rhodamine and green-CF, was higher in cells treated with Lf-Stealth-LIPO compared to that detected in FaO, HepG2 and SKhep cells after treatment with Conv-LIPO and Stealth-LIPO. Furthermore, a progressive time-dependent increase of orange fluorescence intensity in all three cell lines after treatment with Lf-Stealth-LIPO was observed (Figures 13, 14, 15). By contrast, this phenomenon does not occur when using conventional or Stealth liposomes. These results suggested that cell binding and cellular uptake of Lf-liposomes and non-targeted liposomes (Conv-LIPO and Stealth-LIPO) were different. Lf-Stealth-LIPO might markedly enhance the specific cell binding and cellular uptake in hepatoma cells due to the mediating of Lf that could bind to multiple receptors on cell surface such as ASGP-R with high affinity [79].



**A**
**Conv-LIPO**

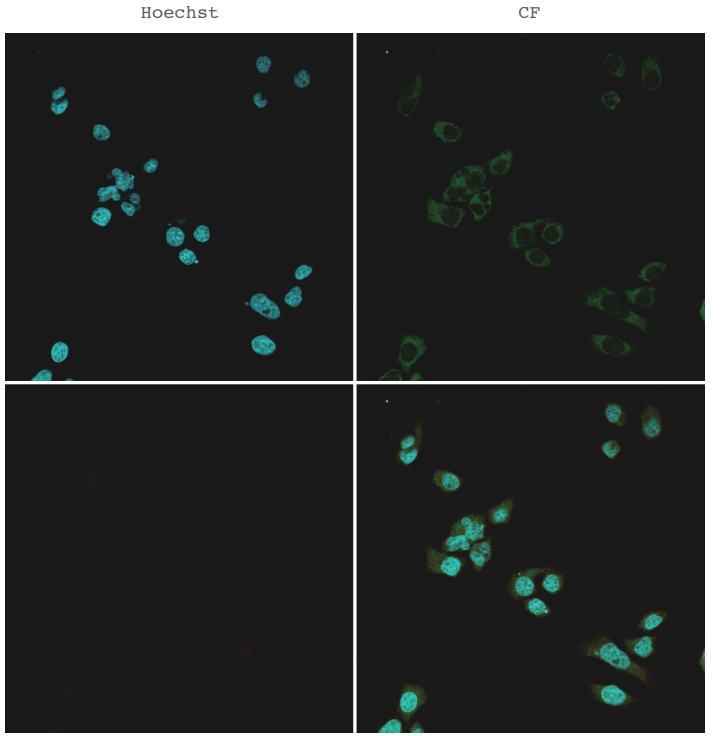


**Figure 10a** Confocal microscopy images of FaO cells treated with Rho and CF loaded liposomal formulations. FaO cells were incubated with Conv-LIPO for 3h at 37 °C. Cell nuclei were stained blue with Hoechst and the localisation and intensity of dyes are displayed in red for Rho, in green for CF.

**A**
**Stealth-LIPO**

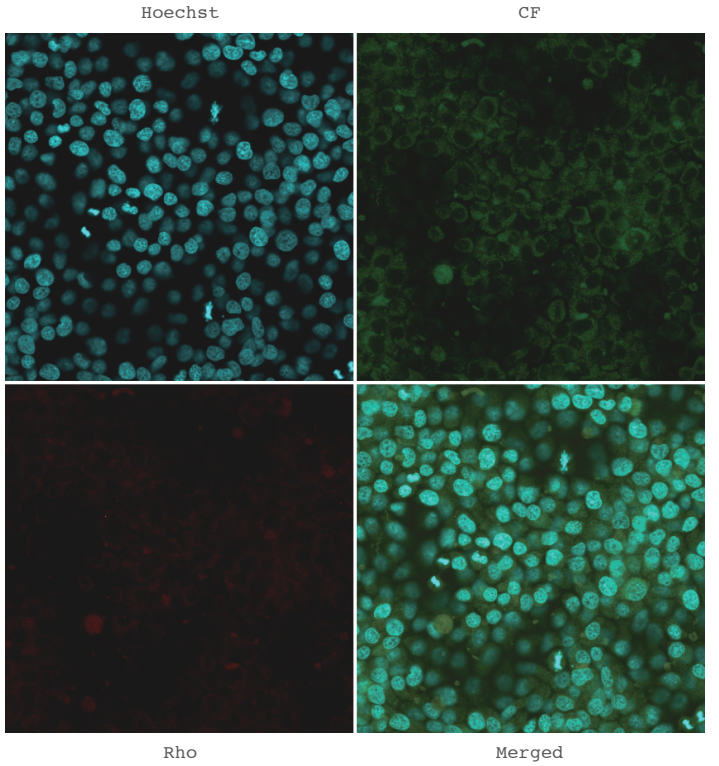


**Figure 10b** Confocal microscopy images of FaO cells treated with Rho and CF loaded liposomal formulations. FaO cells were incubated with Stealth-LIPO for 3h at 37 °C. Cell nuclei were stained blue with Hoechst and the localisation and intensity of dyes are displayed in red for Rho, in green for CF.



**A**
**Lf-Stealth-LIPO**

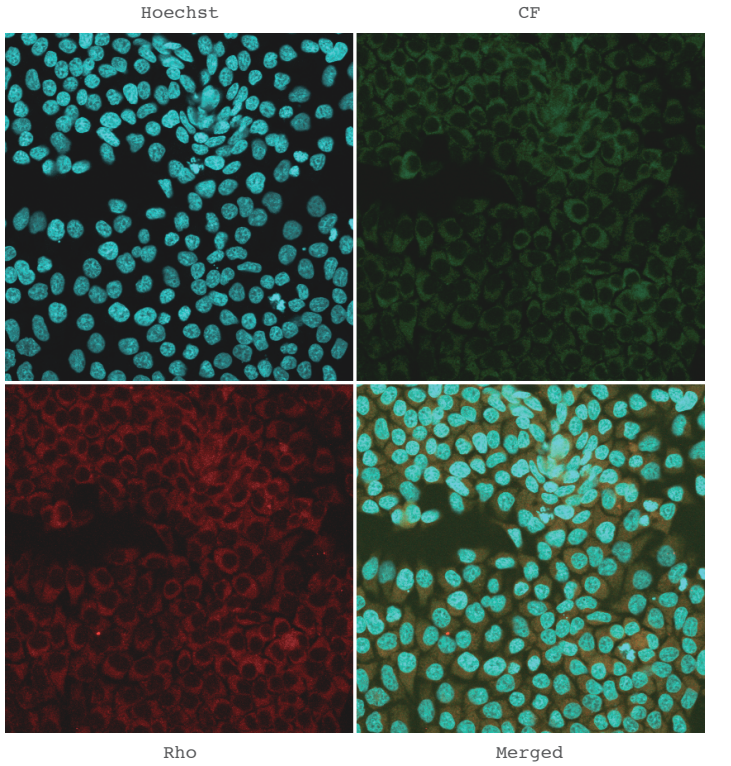


**Figure 10c** Confocal microscopy images of FaO cells treated with Rho and CF loaded liposomal formulations. FaO cells were incubated with Lf-Stealth-LIPO (c) for 3h at 37 °C. Cell nuclei were stained blue with Hoechst and the localisation and intensity of dyes are displayed in red for Rho, in green for CF.

**B**
**Conv-LIPO**

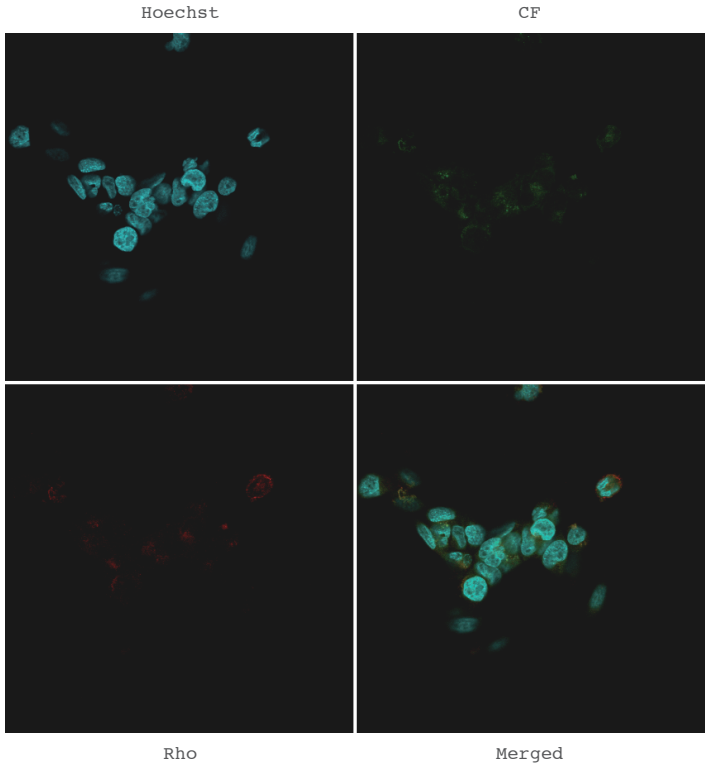


**Figure 11a** Confocal microscopy images of HepG2 cells treated with Rho and CF loaded liposomal formulations. HepG2 cells were incubated with Conv-LIPO for 3h at 37 °C. Cell nuclei were stained blue with Hoechst and the localisation and intensity of dyes are displayed in red for Rho, in green for CF.



**B**
**Stealth-LIPO**

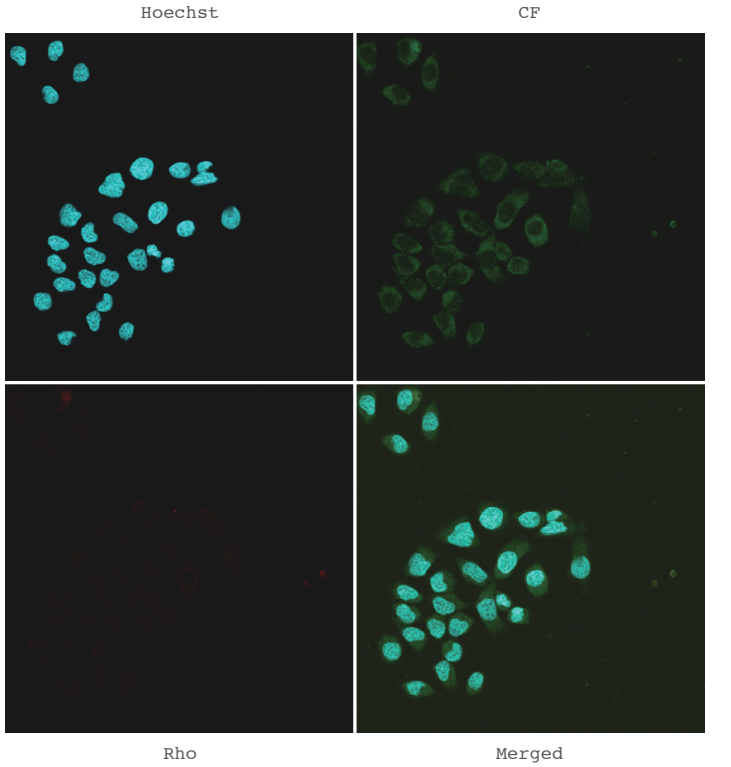


**Figure 11b** Confocal microscopy images of HepG2 cells treated with Rho and CF loaded liposomal formulations. HepG2 cells were incubated Stealth-LIPO for 3h at 37 °C. Cell nuclei were stained blue with Hoechst and the localisation and intensity of dyes are displayed in red for Rho, in green for CF.

**B**
**Lf-Stealth-LIPO**

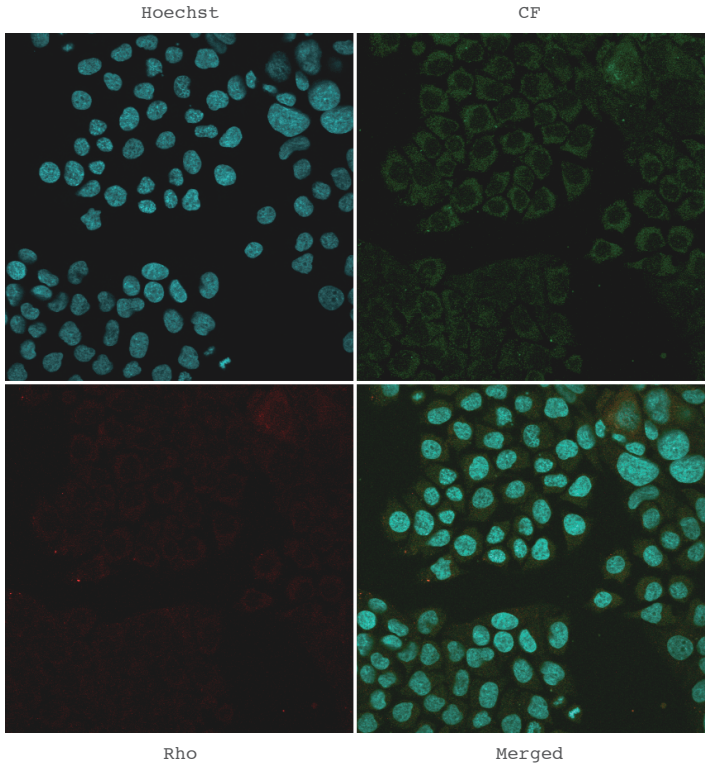


**Figure 11c** Confocal microscopy images of HepG2 cells treated with Rho and CF loaded liposomal formulations. HepG2 cells were incubated with Lf-Stealth-LIPO for 3h at 37 °C. Cell nuclei were stained blue with Hoechst and the localisation and intensity of dyes are displayed in red for Rho, in green for CF



**C**
**Conv-LIPO**

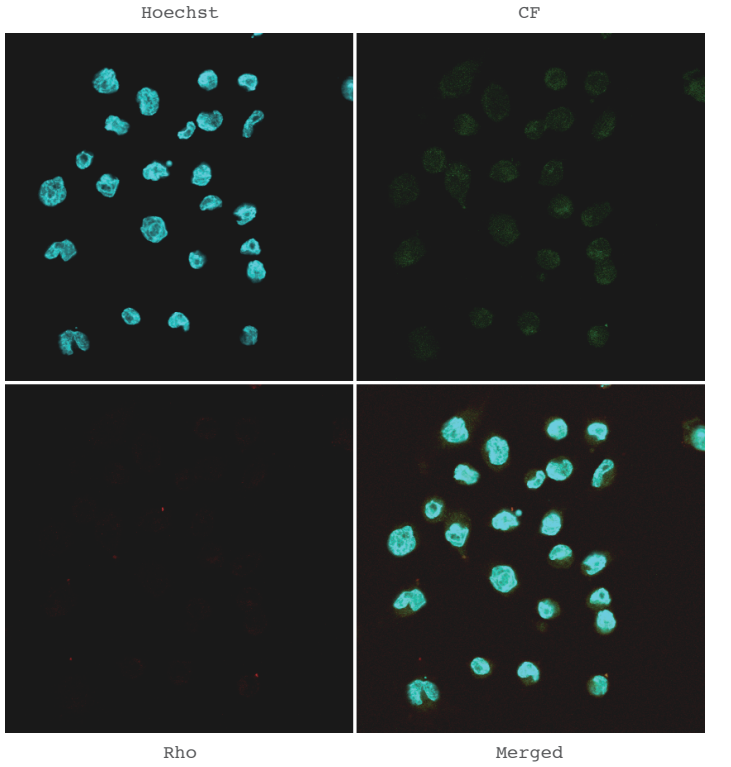


**Figure 12a** Confocal microscopy images of SKHep cells treated with Rho and CF loaded liposomal formulations. SKHep cells were incubated with Conv-LIPO for 3h at 37 °C. Cell nuclei were stained blue with Hoechst and the localisation and intensity of dyes are displayed in red for Rho, in green for CF.

**C**
**Stealth-LIPO**

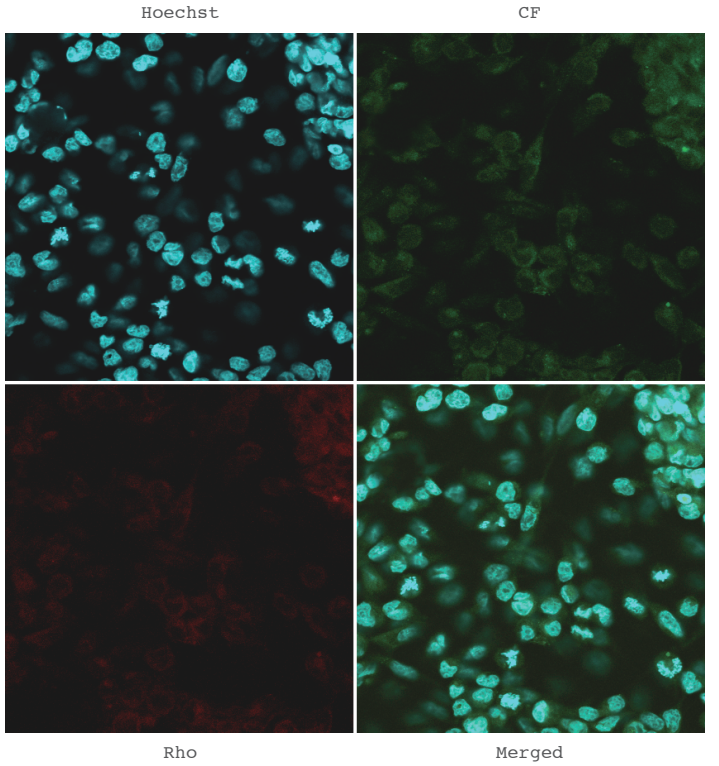


**Figure 12b** Confocal microscopy images of SKHep cells treated with Rho and CF loaded liposomal formulations. SKHep cells were incubated with Stealth-LIPO for 3h at 37 °C. Cell nuclei were stained blue with Hoechst and the localisation and intensity of dyes are displayed in red for Rho, in green for CF



**C**
**Lf-Stealth-LIPO**

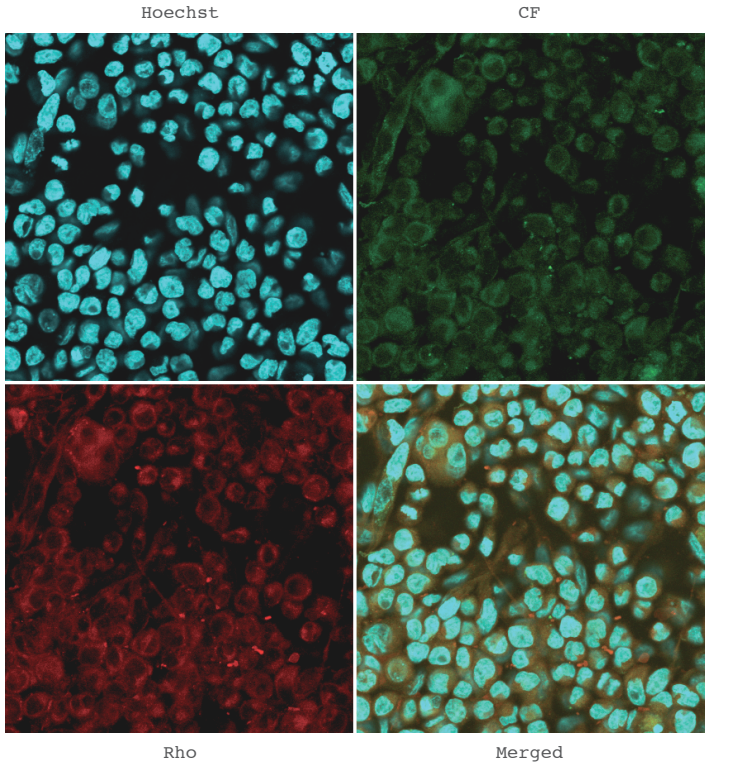


**Figure 12c** Confocal microscopy images of SKHep cells treated with Rho and CF loaded liposomal formulations. SKHep cells were incubated with Lf-Stealth-LIPO (c) for 3h at 37 °C. Cell nuclei were stained blue with Hoechst and the localisation and intensity of dyes are displayed in red for Rho, in green for CF

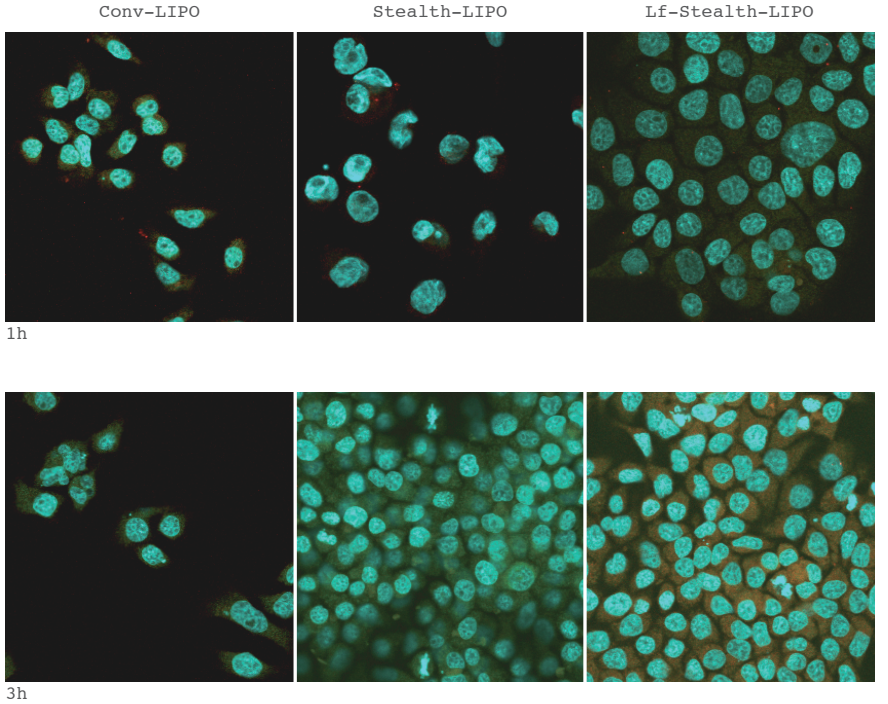


**Figure 13** Confocal microscopy images of FaO cells treated for 1 e 3 hours with fluorescent liposomal formulations: Conv-LIPO (a), Stealth-LIPO (b) and Lf-Stealth-LIPO (c). Cell nuclei were stained blue with Hoechst and the orange fluorescence is due to the overlap of red-Rho and green-CF.



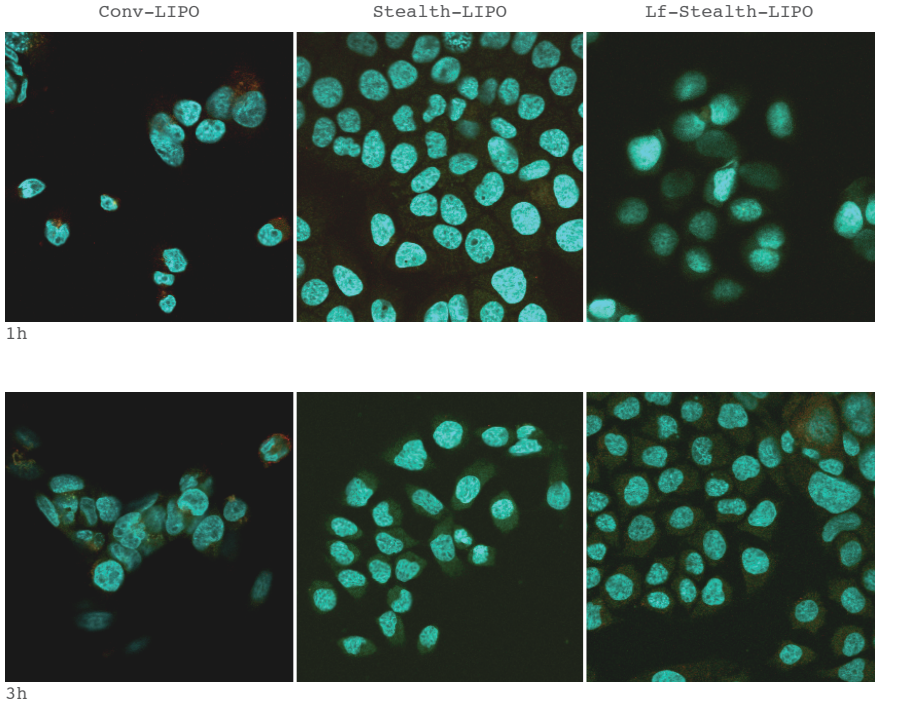


**Figure 14** Confocal microscopy images of HepG2 cells treated for 1 e 3 hours with fluorescent liposomal formulations: Conv-LIPO (a), Stealth-LIPO (b) and Lf-Stealth-LIPO (c). Cell nuclei were stained blue with Hoechst and the orange fluorescence is due to the overlap of red-Rho and green-CF.

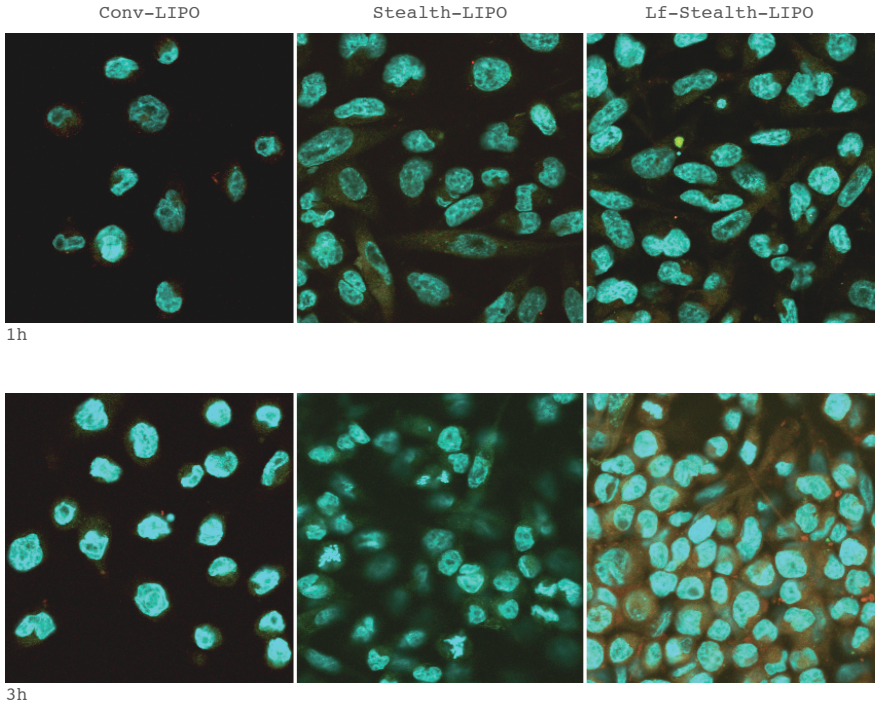


**Figure 15** Confocal microscopy images of SKHep cells treated for 1 e 3 hours with fluorescent liposomal formulations: Conv-LIPO (a), Stealth-LIPO (b) and Lf-Stealth-LIPO (c). Cell nuclei were stained blue with Hoechst and the orange fluorescence is due to the overlap of red-Rho and green-CF.



### 4.2.2. In vitro toxicity studies

In order to investigate the toxicity of the liposome delivery system, target cells (FaO, HepG2 and SKHep cells) were used to evaluate the cell viability via MTT assay. The test is based on the ability of MTT to be metabolised by a mitochondrial enzyme, succinate dehydrogenase. The reduction of MTT leads to the formation of crystals of formazan, a water insoluble blue/violet dye. Since viable cells reduce MTT, the amount of formazan produced is proportional to their number. Cytotoxicity effects strongly depend on different parameters such as phospholipid used, cell line, incubation times, serum-containing/free medium, ect [86]. Therefore, the serum-free conditions were chosen [79] and cells were treated with increasing concentrations of both empty and T3-containing liposomes (Conv-LIPO, Stealth-LIPO, and Lf-Stealth-LIPO) at different incubation time (24, 48 and 72 hours). Outcomes of citotoxicity studies for the empty formulations are summarized in Figures 16, 17, 18. The value obtained for treated cells was expressed as percentage of the value obtained in control cells (untreated). As shown in Figures 16, 17, 18, treatment with different concentrations of empty conventional (Conv-LIPO) and Lf-modified-Stealth liposomes (Lf-Stealth-LIPO) did not induce statistically significant differences in the degree of toxicity in the time interval between 24 and 72 hours in FaO (Figure 16), HepG2 (Figure 17) and SKHep (Figure 18) cells. By contrast, a low but significant loss of viability (~20%) occurred already after 24 hours treatment in the presence of the higher concentration of empty Stealth liposomes (Stealth-LIPO) in all the analyzed cell lines (Figure 16b, Figure 17b, Figure 18b). In conclusion, our results indicated that all the empty liposome formulations tested induced a very low citotoxic effect on hepatoma cell lines suggesting that they are safe carriers.
Afterwards, the effect of T3

incorporated into liposomes was investigated. Figures 19, 20, 21 show the results of the cell viability test performed in hepatoma cells using T3 loaded vesicles or a T3 solution. FaO, HepG2 and SKHep cells were treated with different concentrations (100, 50 and 10 $\mu$M) of T3 solution or T3-containing liposomes (Conv-LIPO, Stealth-LIPO, and Lf-Stealth-LIPO) at different incubation time (24, 48 and 72 hours). The value obtained with treated cells was expressed as percentage of the value obtained whit control cells: untreated cells for T3 solution and cells treated with the empty formulation for T3-containing liposomes. In FaO cells (Figure 19) increasing concentrations of T3 (in solution or loaded liposomes) did not induce any cytotoxic effect since cell viability was statistically similar to that observed for control cells. By contrast, in HepG2 and SKHep cells incubation in the presence of the highest concentration of drug solution led to an increased cell mortality that reached almost 70% after 72 hours (Figures 20.a and 21.a). Instead, T3-incorporated liposomes did not induce loss of cell viability even at the highest concentration (100 $\mu$M) but we observed a significantly increased cell proliferation. In particular, in HepG2 cells (Figure 20b, 20c, 20d) the highest proliferative activity occurs at 72 hours for all three formulations, reaching greater values at lower concentrations.
A similar effect was also seen in SKHep cells (Figure 21b, 21c, 21d) where, for Conv-LIPO, Stealth-LIPO, and Lf-Stealth-LIPO, it was observed a significant increase ($p$ <0.001) in cell viability compared to control (cells treated with the respective empty formulations) after 48 hours; this proliferative effect was maintained up to 72 hours. In SKHep, as well as in HepG2 cells, the proliferative activity was higher at lower concentrations (50 and 10 $\mu$M). Proliferative effect of T3 on hepatoma cells is not surprising. Indeed, it has been hypothesized that the antitumoral effect of T3 is not due to cell death, but T3, by interaction with its TR receptors, negatively influences the carcinogenic process through induction of a differentiation program of preneoplastic hepatocytes. According to this hypothesis, malignant hepatocyte return to a fully differentiated phenotype with loss of the fetal markers GSTP and gamma glutamyl transpeptidase, and reacquisition of the activity of glucose 6-phosphatase and adenosine triphosphatase, two enzymes expressed in normal hepatocytes [11].
All together these findings emphasize that liposomes protect the cells against the cytotoxicity of high concentration of T3, since the liposome delivery system slowly release the drug inside the cells and significantly induce a proliferative effect at low concentrations. At the same time, the employment of lower drug concentrations should allow to reduce the possible side effects on other target cells (e.g. heart).



**5. Conclusions**

In conclusion, this study provides useful information about the great potential of liposomes as suitable carrier for T3 delivery to hepatoma cells. Internalization studies performed using Lf-modified-liposomes labeled with the lipophilic marker Rho-PE and loaded with the hydrophilic probe CF clearly demonstrated the effective internalization of both hydrophilic and lypophilic markers. From our data, emerges that liposome delivery system may insure a specific and sustained drug delivery, a reduced therapeutic dose and, in particular, should avoid deleterious side effects of T3 treatment. Overall, our results showed that liposomes are good candidates as liver delivery system of T3 since cell viability tests performed by using hepatoma cell lines demonstrated a very low toxicity of all three lyposome formulations.
Further studies are needed in order to analyze the effectiveness of this delivery system in *in vivo* models.

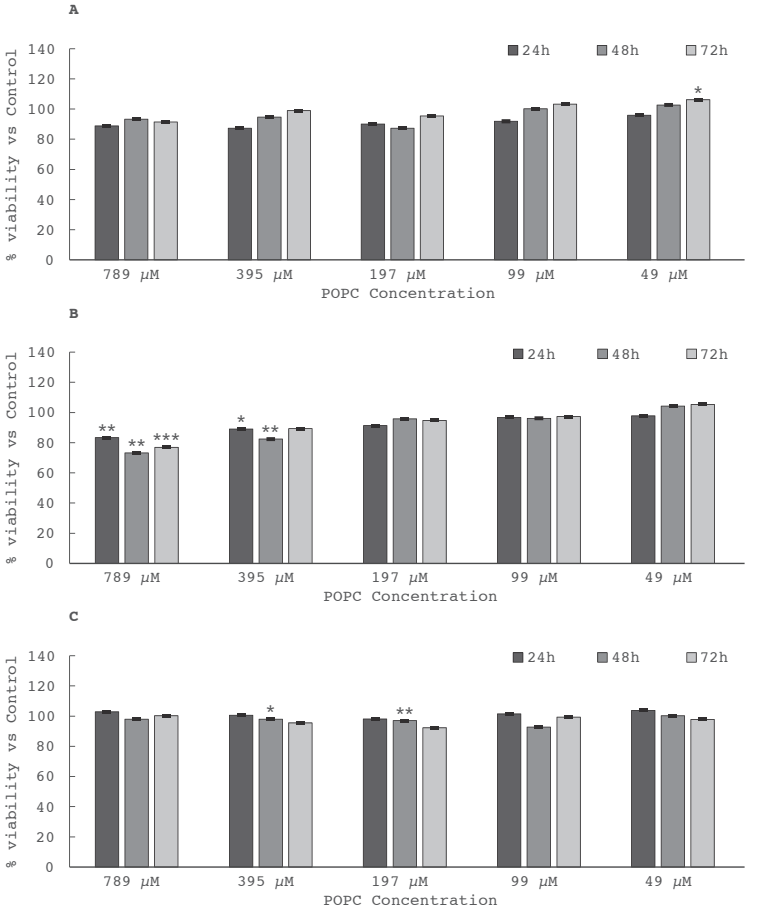


**Figure 16** In vitro cytotoxic effect of increasing concentrations of empty liposome formulations Conv-LIPO (a), Stealth-LIPO (b) and Lf-Stealth-LIPO (c) on FaO cells at different coincubation times (24, 48 and 72h). * p <0.05, ** p <0.01 and *** p <0.001 in comparison with untreated cells (100% viability). Data represented the mean ± SD (n = 3).

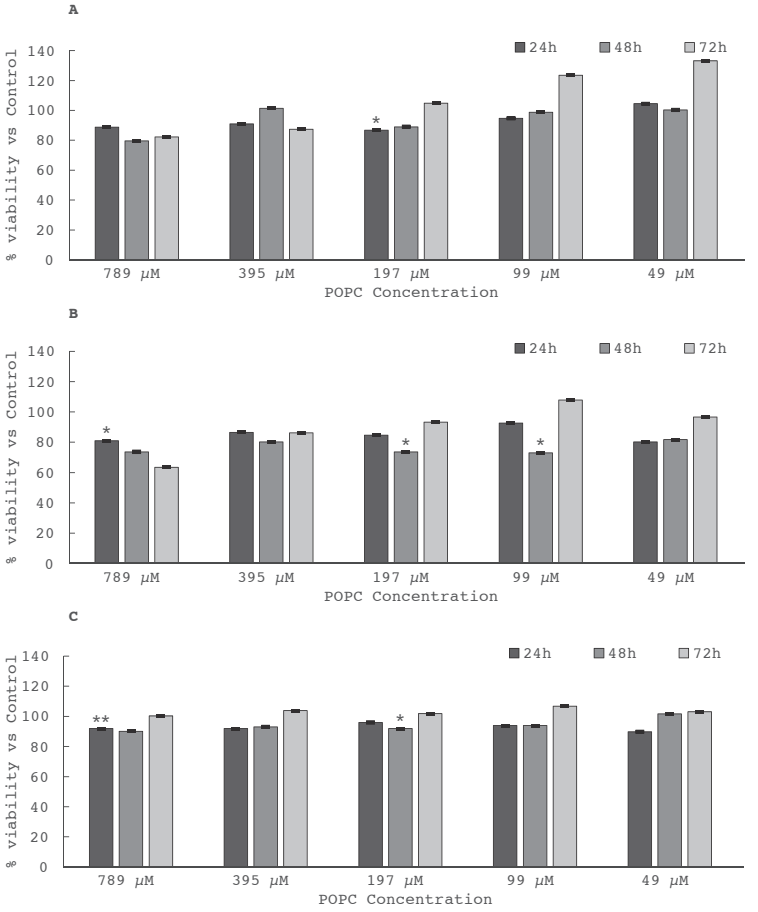


**Figure 17** In vitro cytotoxic effect of increasing concentrations of empty liposome formulations Conv-LIPO (a), Stealth-LIPO (b) and Lf-Stealth-LIPO (c) on HepG2 cells at different coincubation times (24, 48 and 72h). * p <0.05, ** p <0.01 and *** p <0.001 in comparison with untreated cells (100% viability). Data represented the mean ± SD (n = 3).



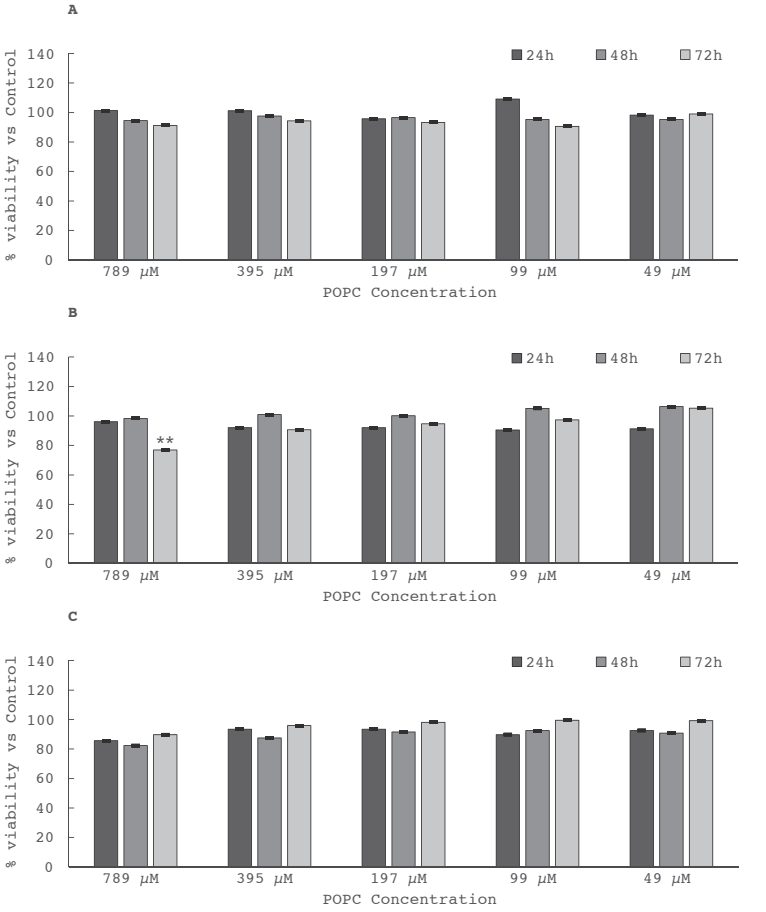


**Figure 18** In vitro cytotoxic effect of increasing concentrations of empty liposome formulations Conv-LIPO (a), Stealth-LIPO (b) and Lf-Stealth-LIPO (c) on SKHep cells at different coincubation times (24, 48 and 72h). * p <0.05, ** p <0.01 and *** p <0.001 in comparison with untreated cells (100% viability). Data represented the mean ± SD (n = 3).

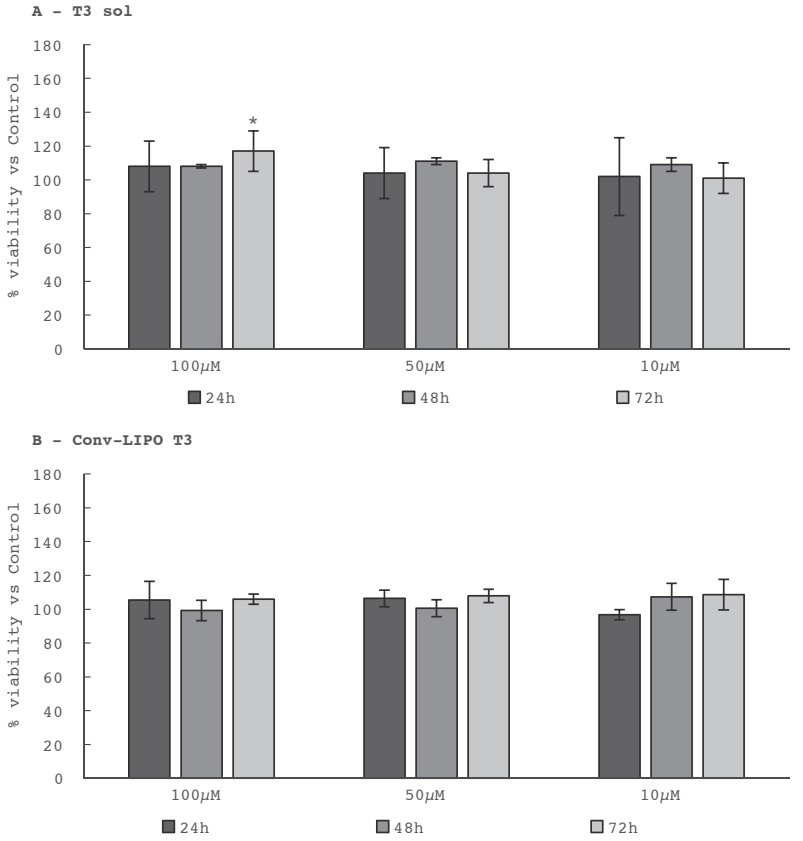


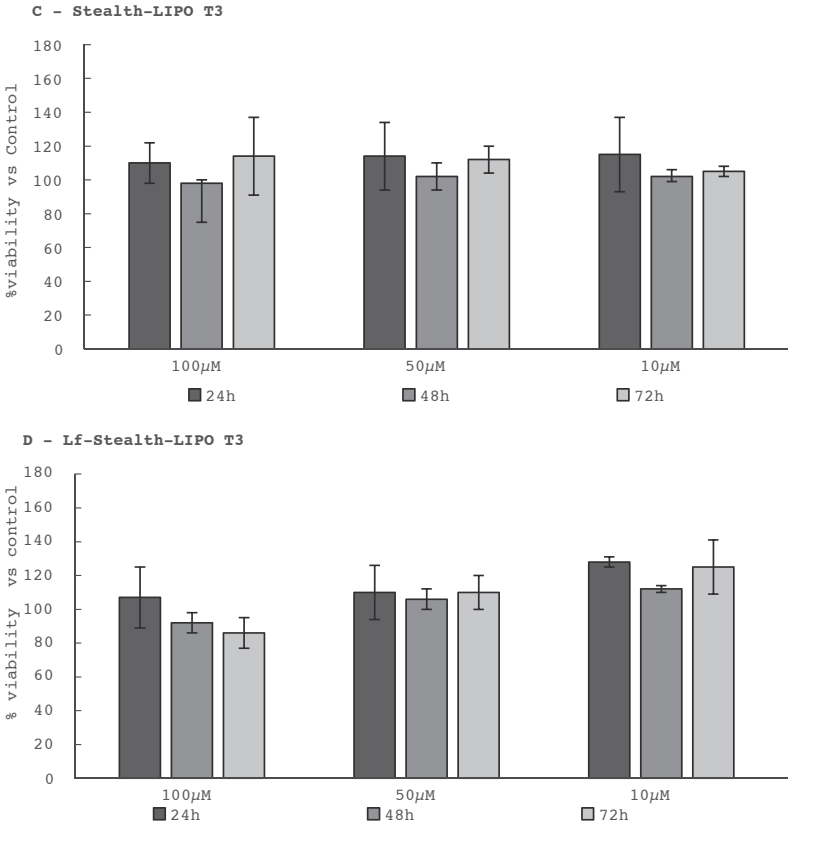


**Figure 19** In vitro cytotoxicity assays: FaO cells incubated with different concentrations of T3 solution (a) or T3-containing liposomes (Conv-LIPO (b), Stealth-LIPO (c) and Lf-Stealth-LIPO (d)) at different incubation time (24, 48 and 72 h). * p <0.05, ** p <0.01 and *** p <0.001 in comparison with control cells (100% viability):untreated cells for T3 solution and cells treated with the empty formulation for T3-containing liposomes Data represented the mean ± SD (n = 3).

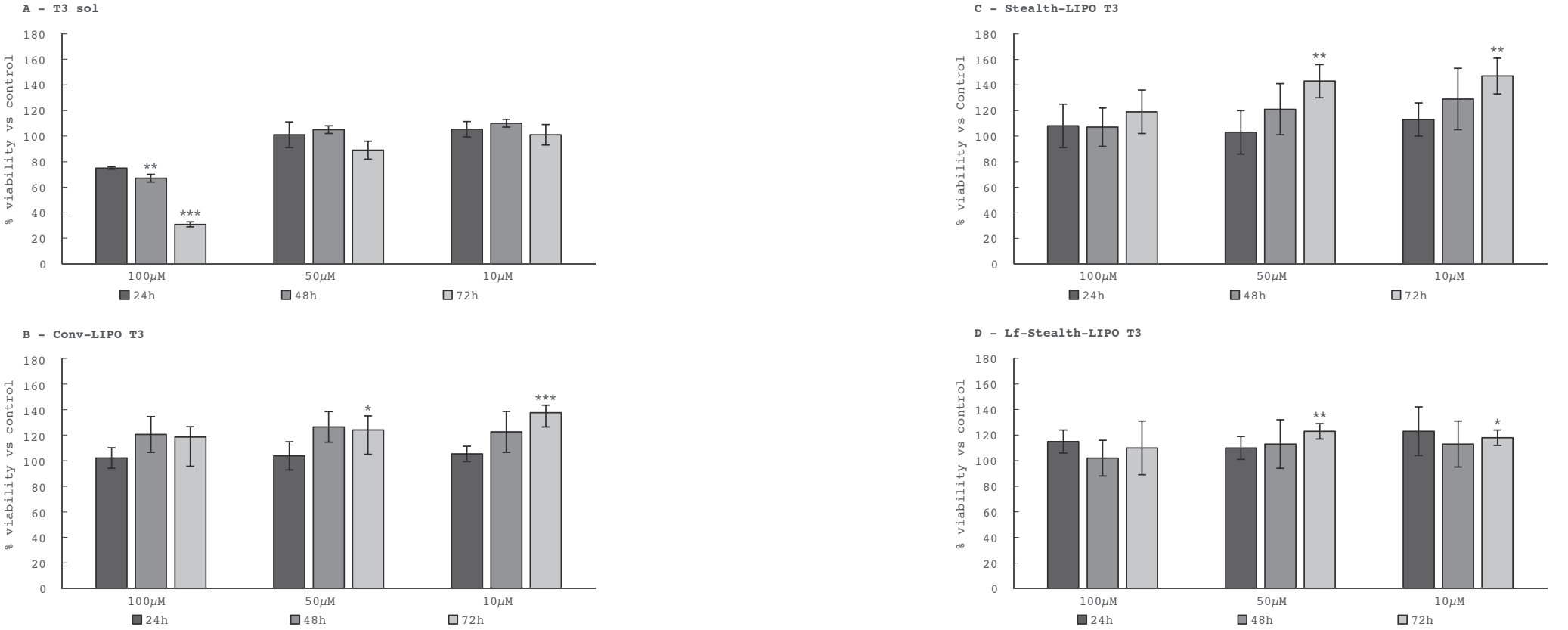


**Figure 20** In vitro cytotoxicity assays: HepG2 cells incubated with different concentrations of T3 solution (a) or T3-containing liposomes (Conv-LIPO (b), Stealth-LIPO (c) and Lf-Stealth-LIPO (d)) at different incubation time (24, 48 and 72 h). * p <0.05, ** p <0.01 and *** p <0.001 in comparison with control cells(100% viability):untreated cells for T3 solution and cells treated with the empty formulation for T3-containing liposomes Data represented the mean ± SD (n = 3).

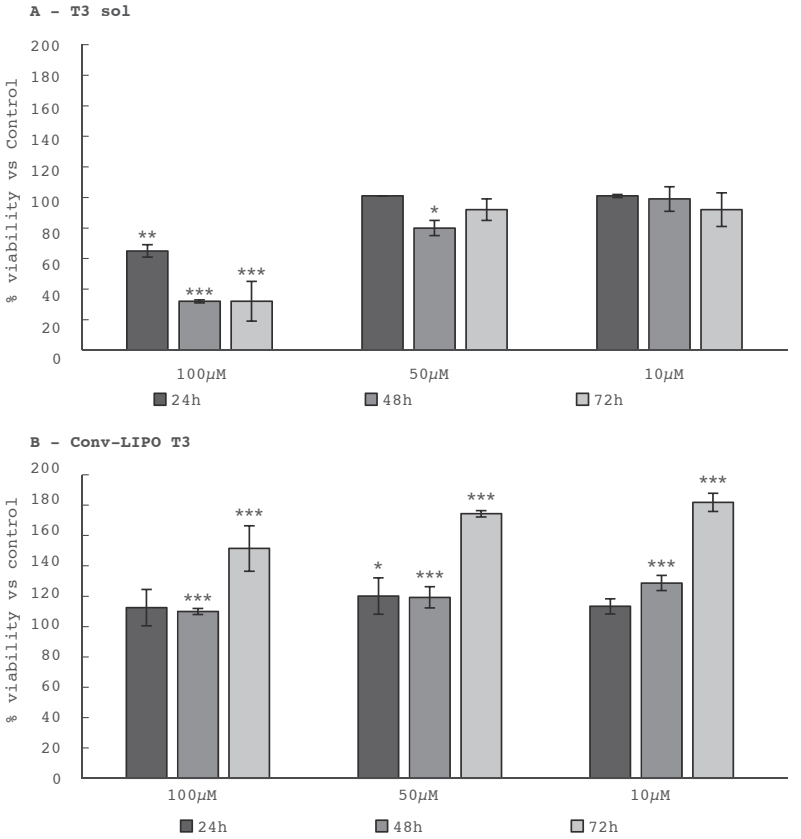


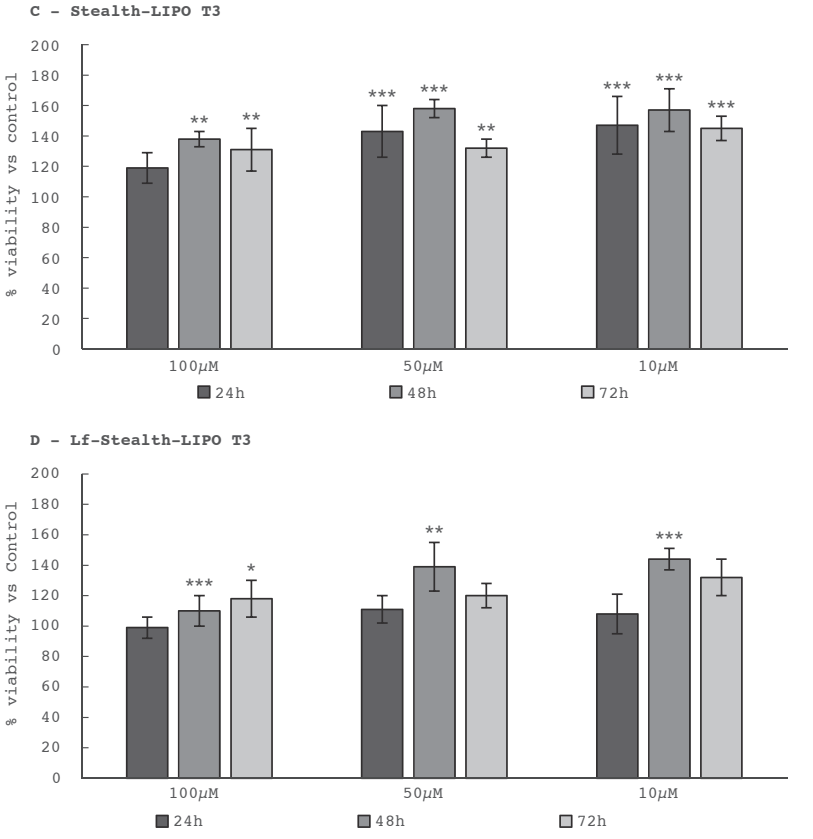


**Figure 21** In vitro cytotoxicity assays: SKHep cells incubated with different concentrations of T3 solution (a) or T3-containing liposomes (Conv-LIPO (b), Stealth-LIPO (c) and Lf-Stealth-LIPO (d)) at different incubation time (24, 48 and 72 h). * p <0.05, ** p <0.01 and *** p <0.001 in comparison with control cells (100% viability):untreated cells for T3 solution and cells treated with the empty formulation for T3-containing liposomes Data represented the mean ± SD (n = 3).

## References

[1] Moradpour D, Blum HE. Pathogenesis of hepatocellular carcinoma. Eur J Gastroenterol Hepatol. 2005;17:477–83.

[2] Yau T, Pang R, Chan P, Poon RT. Molecular targeted therapy of advanced hepatocellular carcinoma beyond sorafenib. Expert Opin Pharmacother. 2010;11:2187–98.

[3] Ahmadzadehfar H, Sabet A, Wilhelm K, Biersack HJ, Risse J. Iodine-131-Lipiodol therapy in hepatic tumours. Methods. 2011;55:246–52.

[4] Yen PM. Physiological and molecular basis of thyroid hormone action. Physiol Rev. 2001;81(3):1097–142.

[5] Epstein FH, Brent GA. The molecular basis of thyroid hormone action. N Engl J Med. 1994;81:1097–142.

[6] Lazar MA. Thyroid Hormone Receptors: Multiple Forms, Multiple Possibilities. Endocr Rev. 1993;14:184–93.

[7] Pascual A, Aranda A. Thyroid hormone receptors, cell growth and differentiation. Biochim Biophys Acta. 2013;1830(7):3908–16.

[8] Forrest D, Vennström B. Functions of thyroid hormone receptors in mice. Thyroid. 2000;10(1):41–52.

[9] Ledda-columbano GM, Perra A, Loi R. Cell Proliferation Induced by Triiodothyronine in Rat Liver Is Associated with Nodule Regression and Reduction of Hepatocellular Carcinomas. Cancer Res. 2000;60:603–9.

[10] Ledda-Columbano GM, Perra a., Concas D, Cossu C, Molotzu F, Sartori C, et al. Different Effects of the Liver Mitogens Triiodo-Thyronine and Ciprofibrate on the Development of Rat Hepatocellular Carcinoma. Toxicol Pathol. 2003;31(1):113–20.

[11] Perra A, Kowalik MA, Pibiri M, Ledda-Columbano GM, Columbano A. Thyroid hormone receptor ligands induce regression of rat preneoplastic liver lesions causing their reversion to a differentiated phenotype. Hepatology. 2009;49(4):1287–96.

[12] Chen R-N, Huang Y-H, Yeh C-T, Liao C-H, Lin K-H. Thyroid hormone receptors suppress pituitary tumor transforming gene 1 activity in hepatoma. Cancer Res. 2008;68(6):1697–706.

[13] Martínez-Iglesias O, García-Silva S, Regadera J, Aranda A. Hypothyroidism enhances tumor invasiveness and metastasis development. PLoS One. 2009;4(7).

[14] Martínez-Iglesias O, Garcia-Silva S, Tenbaum SP, Regadera J, Larcher F, Paramio JM, et al. Thyroid hormone receptor beta1 acts as a potent suppressor of tumor invasiveness and metastasis. Cancer Res. 2009;69(2):501–9.

[15] FH Epstein, I Klein KO. Thyroid hormone and the cardiovascular system. N Engl J Med. 2001;344(7):501–9.

[16] Maeda H, Wu J, Sawa T, Matsumura Y, Hori K. Tumor vascular permeability and the EPR effect in macromolecular therapeutics: A review. J Control Release. 2000;65(1-2):271–84.

[17] Gaumet M, Vargas A, Gurny R, Delie F. Nanoparticles for drug delivery: The need for precision in reporting particle size parameters. Eur J Pharm Biopharm. 2008;69(1):1–9.

[18] Igarashi E. Factors affecting toxicity and efficacy of polymeric nanomedicines. Toxicol Appl Pharmacol. 2008;229(1):121–34.

[19] Owens DE, Peppas N a. Opsonization, biodistribution, and pharmacokinetics of polymeric nanoparticles. Int J Pharm. 2006;307(1):93–102.



[20] Nagayama S, Ogawara KI, Fukuoka Y, Higaki K, Kimura T. Time-dependent changes in opsonin amount associated on nanoparticles alter their hepatic uptake characteristics. Int J Pharm. 2007;342(1-2):215–21.

[21] Hoffman AS. The origins and evolution of “controlled” drug delivery systems. J Control Release. 2008;132(3):153–63.

[22] Vega-Villa KR, Takemoto JK, Yáñez J a., Remsberg CM, Forrest ML, Davies NM. Clinical toxicities of nanocarrier systems. Adv Drug Deliv Rev. 2008;60(8):929–38.

[23] Torchilin VP. Passive and active drug targeting: drug delivery to tumors as an example. Drug Delivery. 2010. p. 3–53.

[24] Bawarski WE, Chidlowsky E, Bharali DJ, Mousa S a. Emerging nanopharmaceuticals. Nanomedicine Nanotechnology, Biol Med. 2008;4(4):273–82.

[25] Qiu L, Jing N, Jin Y. Preparation and in vitro evaluation of liposomal chloroquine diphosphate loaded by a transmembrane pH-gradient method. Int J Pharm. 2008;361(1-2):56–63.

[26] Ning Y-M, He K, Dagher R, Sridhara R, Farrell AT, Justice R, et al. Liposomal doxorubicin in combination with bortezomib for relapsed or refractory multiple myeloma. Oncology. 2007;21:1503–8.

[27] Ogawara KI, Un K, Minato K, Tanaka KI, Higaki K, Kimura T. Determinants for in vivo anti-tumor effects of PEG liposomal doxorubicin: Importance of vascular permeability within tumors. Int J Pharm. 2008;359(1-2):234–40.

[28] Ogawara KI, Un K, Tanaka KI, Higaki K, Kimura T. In vivo anti-tumor effect of PEG liposomal doxorubicin (DOX) in DOX-resistant tumor-bearing mice: Involvement of cytotoxic effect on vascular endothelial cells. J Control Release. 2009;133(1):4–10.

[29] Malam Y, Loizidou M, Seifalian AM. Liposomes and nanoparticles: nanosized vehicles for drug delivery in cancer. Trends Pharmacol Sci.

2009;30(11):592–9.

[30] Mishra N, Yadav NP, Rai VK, Sinha P, Yadav KS, Jain S, et al. Efficient hepatic delivery of drugs: Novel strategies and their significance. BioMed Research International. 2013. p. 1–20.

[31] Smith JS, Xu Z, Byrnes AP. A quantitative assay for measuring clearance of adenovirus vectors by Kupffer cells. J Virol Methods. 2008;147(1):54–60.

[32] Kjeken R, Kindberg GM, Berg T. Distribution of liposome-encapsulated iodixanol in rat liver cells. Biochem Pharmacol. 2000;60:553–9.

[33] Poelstra K, Prakash J, Beljaars L. Drug targeting to the diseased liver. Journal of Controlled Release. 2012. p. 188–97.

[34] Wang H, Thorling C a., Liang X, Bridle KR, Grice JE, Zhu Y, et al. Diagnostic imaging and therapeutic application of nanoparticles targeting the liver. J Mater Chem B. 2015;3(6):939–58.

[35] Rensen PCN, Sliedregt L a JM, Ferns M, Kieviet E, Van Rossenberg SMW, Van Leeuwen SH, et al. Determination of the Upper Size Limit for Uptake and Processing of Ligands by the Asialoglycoprotein Receptor on Hepatocytes in Vitro and in Vivo. J Biol Chem. 2001;276(40):37577–84.

[36] Zhang XQ, Wang XL, Zhang PC, Liu ZL, Zhuo RX, Mao HQ, et al. Galactosylated ternary DNA/polyphosphoramidate nanoparticles mediate high gene transfection efficiency in hepatocytes. J Control Release. 2005;102(3):749–63.

[37] Singh M, Ariatti M. Targeted gene delivery into HepG2 cells using complexes containing DNA, cationized asialoorosomucoid and activated cationic liposomes. J Control Release. 2003;92(3):383–94.

[38] Wu J, Nantz MH, Zern MA. Targeting hepatocytes for drug and gene delivery: emerging novel approaches and applications. Front Biosci. 2002;7:d717–25.



[39] Wu Y-T, Jiaang W-T, Lin K-G, Huang C-M, Chang C-H, Sun Y-L, et al. A New N-Acetylgalactosamine Containing Peptide as a Targeting Vehicle for Mammalian Hepatocytes Via Asialoglycoprotein Receptor Endocytosis. Curr Drug Deliv. 2004;1:119–27.

[40] Di Stefano G, Colonna FP, Bongini A, Busi C, Mattioli A, Fiume L. Ribavirin conjugated with lactosaminated poly-l-lysine. Selective delivery to the liver and increased antiviral activity in mice with viral hepatitis. Biochem Pharmacol. 1997;54(3):357–63.

[41] Di Stefano G, Fiume L, Baglioni M, Bolondi L, Busi C, Chieco P, et al. A conjugate of doxorubicin with lactosaminated albumin enhances the drug concentrations in all the forms of rat hepatocellular carcinomas independently of their differentiation grade. Liver Int. 2006;26(6):726–33.

[42] Fiume L, Bolondi L, Busi C, Chieco P, Kratz F, Lanza M, et al. Doxorubicin coupled to lactosaminated albumin inhibits the growth of hepatocellular carcinomas induced in rats by diethylnitrosamine. J Hepatol. 2005;43(4):645–52.

[43] Duncan R. Development of HPMA copolymer-anticancer conjugates: Clinical experience and lessons learnt. Adv Drug Deliv Rev. 2009;61(13):1131–48.

[44] D'Souza AA, Devarajan P V. Asialoglycoprotein receptor mediated hepatocyte targeting – Strategies and applications. J Control Release. 2015;203:126–39.

[45] Zhu L, Mahato RI. Targeted delivery of siRNA to hepatocytes and hepatic stellate cells by bioconjugation. Bioconjug Chem. 2010;21(11):2119–27.

[46] Nie C, Liu C, Chen G, Dai J, Li H, Shuai X. Hepatocyte-targeted psiRNA Delivery Mediated by Galactosylated Poly(Ethylene Glycol)-Graft-Polyethylenimine In Vitro. J Biomater Appl. 2011;26(3):255–75.

[47] Hyodo I, Mizuno M, Yamada G, Tsuji A. Distribution of asialoglycopro-

tein receptor in human hepatocellular carcinoma. Liver. 1993;13(2):80–5.

[48] Seymour LW, Ulbrich K, Wedge SR, Hume IC, Strohalm J, Duncan R. N-(2-hydroxypropyl)methacrylamide copolymers targeted to the hepatocyte galactose-receptor: pharmacokinetics in DBA2 mice. Br J Cancer. 1991;63(6):859–66.

[49] Julyan PJ, Seymour LW, Ferry DR, Daryani S, Boivin CM, Doran J, et al. Preliminary clinical study of the distribution of HPMA copolymer-doxorubicin bearing galactosamine. J Cont Rel. 1999;57:281–90.

[50] Fiume L, Di Stefano G. Lactosaminated human albumin, a hepatotropic carrier of drugs. Eur J Pharm Sci. 2010;40(4):253–62.

[51] Fiume L, Baglioni M, Busi C, Manerba M, Di Stefano G. The enhancement of interstitial transport of a doxorubicin-lactosaminated albumin conjugate by imatinib: In rat hepatocellular carcinoma it is not preferentially higher than that in liver and bone marrow. Eur J Pharm Biopharm. 2009;72(3):630–1.

[52] Merwin JR, Noell GS, Thomas WL, Chiou HC, DeRome ME, McKee TD, et al. Targeted delivery of DNA using YEE(GalNAcAH)3, a synthetic glycopeptide ligand for the asialoglycoprotein receptor. Bioconjug Chem. 1994;5(6):612–20.

[53] Maruyama K, Iwasaki F, Takizawa T, Yanagie H, Niidome T, Yamada E, et al. Novel receptor-mediated gene delivery system comprising plasmid/protamine/sugar-containing polyanion ternary complex. Biomaterials. 2004;25(16):3267–73.

[54] Cheng M, He B, Wan T, Zhu W, Han J, Zha B, et al. 5-Fluorouracil Nanoparticles Inhibit Hepatocellular Carcinoma via Activation of the p53 Pathway in the Orthotopic Transplant Mouse Model. PLoS One. 2012;7(10):1–12.

[55] Li X, Xu H, Dai X, Zhu Z, Liu B, Lu X. Enhanced in vitro and in vivo therapeutic efficacy of codrug-loaded nanoparticles against liver cancer. Int J Nanomedicine. 2012;7:5183–90.



[56] Zhou X, Zhang M, Yung B, Li H, Zhou C, James Lee L, et al. Lactosylated liposomes for targeted delivery of doxorubicin to hepatocellular carcinoma. Int J Nanomedicine. 2012;7:5465–74.

[57] Zhang X, Zhang X, Yu P, Han Y, Li Y, Li C. Hydrotropic polymeric mixed micelles based on functional hyperbranched polyglycerol copolymers as hepatoma-targeting drug delivery system. J Pharm Sci. 2013;102:145–53.

[58] Mohr L, Yeung A, Aloman C, Wittrup D, Wands JR. Antibody-directed therapy for human hepatocellular carcinoma. Gastroenterology. 2004;127(SUPPL.):225–31.

[59] Zhu AX, Stuart K, Blaszkowsky LS, Muzikansky A, Reitberg DP, Clark JW, et al. Phase 2 study of cetuximab in patients with advanced hepatocellular carcinoma. Cancer. 2007;110(3):581–9.

[60] Asnacios A, Fartoux L, Romano O, Tesmoingt C, Louafi S S, Mansoubakht T, et al. Gemcitabine plus oxaliplatin (GEMOX) combined with cetuximab in patients with progressive advanced stage hepatocellular carcinoma: Results of a multicenter phase 2 study. Cancer. 2008;112(12):2733–9.

[61] Liu X, Tian P, Yu Y, Yao M, Cao X, Gu J. Enhanced antitumor effect of EGF R-targeted p21WAF-1 and GM-CSF gene transfer in the established murine hepatoma by peritumoral injection. Cancer Gene Ther. 2002;9:100–8.

[62] Lee TK, Han JS, Fan ST, Liang ZD, Tian PK, Gu JR, et al. Gene delivery using a receptor-mediated gene transfer system targeted to hepatocellular carcinoma cells. Int J Cancer. 2001;93(3):393–400.

[63] Wolschek MF, Thallinger C, Kursa M, Rössler V, Allen M, Lichtenberger C, et al. Specific systemic nonviral gene delivery to human hepatocellular carcinoma xenografts in SCID mice. Hepatology. 2002;36(5 II):1106–14.

[64] Liu X, Tian P-K, Ju D-W, Zhang M-H, Yao M, Cao X-T, et al. Systemic ge-

netic transfer of p21WAF-1 and GM-CSF utilizing of a novel oligopeptide-based EGF receptor targeting polyplex. Cancer Gene Ther. 2003;10(7):529–39.

[65] Maeda H, Bharate GY, Daruwalla J. Polymeric drugs for efficient tumor-targeted drug delivery based on EPR-effect. Eur J Pharm Biopharm. 2009;71(3):409–19.

[66] Iwamaru Y, Shimizu Y, Imamura M, Murayama Y, Endo R, Tagawa Y, et al. Lactoferrin induces cell surface retention of prion protein and inhibits prion accumulation. J Neurochem. 2008;107(3):636–46.

[67] Suzuki Y a., Lopez V, Lönnerdal B. Mammalian lactoferrin receptors: Structure and function. Cell Mol Life Sci. 2005;62(22):2560–75.

[68] Ward PP, Uribe-Luna S, Conneely OM. Lactoferrin and host defense. Biochem Cell Biol. 2002;80(1):95–102.

[69] De Luca MA, Lai F, Corrias F, Caboni P, Bimpisidis Z, Maccioni E, et al. Lactoferrin- and antitransferrin-modified liposomes for brain targeting of the NK3 receptor agonist senktide : Preparation and in vivo evaluation. Int J Pharm. 2015;479:129–37.

[70] Huang R, Ke W, Liu Y, Jiang C, Pei Y. The use of lactoferrin as a ligand for targeting the polyamidoamine-based gene delivery system to the brain. Biomaterials. 2008;29(2):238–46.

[71] Chen H, Tang L, Qin Y, Yin Y, Tang J, Tang W, et al. Lactoferrin-modified procationic liposomes as a novel drug carrier for brain delivery. Eur J Pharm Sci. 2010;40(2):94–102.

[72] Meilinger M, Haumer M, Szakmary K a, Steinböck F, Scheiber B, Goldenberg H, et al. Removal of lactoferrin from plasma is mediated by binding to low density lipoprotein receptor-related protein/alpha 2-macroglobulin receptor and transport to endosomes. FEBS Lett. 1995;360(1):70–4.

[73] Crawford SE, Borensztajn J. Plasma clearance and liver uptake of chylomicron remnants generated by hepatic lipase lipolysis: evidence for a



lactoferrin-sensitive and apolipoprotein E-independent pathway. J Lipid Res. 1999;40(5):797–805.

[74] Bennatt DJ, McAbee DD. Identification and isolation of a 45-kDa calcium-dependent lactoferrin receptor from rat hepatocytes. Biochemistry. 1997;36(27):8359–66.

[75] Bennatt DJ, Ling YY, McAbee DD. Isolated rat hepatocytes bind lactoferrins by the RHL-1 subunit of the asialoglycoprotein receptor in a galactose-independent manner. Biochemistry. 1997;36(27):8367–76.

[76] Baker EN. Lactoferrin: A multi-tasking protein par excellence. Cell Mol Life Sci. 2005;62(22):2529–30.

[77] Strickland DK, Gonias SL, Argraves WS. Diverse roles for the LDL receptor family. Trends Endocrinol Metab. 2002;13(2):66–74.

[78] McAbee DD, Jiang X, Walsh KB. Lactoferrin binding to the rat asialoglycoprotein receptor requires the receptor’s lectin properties. Biochem J. 2000;348:113–7.

[79] Wei M, Xu Y, Zou Q, Tu L, Tang C, Xu T, et al. Hepatocellular carcinoma targeting effect of PEGylated liposomes modified with lactoferrin. Eur J Pharm Sci. 2012;46(3):131–41.

[80] Pathak A. Nano-vectors for effi cient liver specifi c gene transfer. Nucleic Acids Res. 2008;3(1):31–49.

[81] Gijsens A, Derycke A, Missiaen L, De Vos D, Huwyler J, Eberle A, et al. Targeting of the photocytotoxic compound AlPcS4 to Hela cells by transferrin conjugated PEG-liposomes. Int J Cancer. 2002;101(1):78–85.

[82] Bradford MM. A rapid and sensitive method for the quantitation of microgram quantities of protein utilizing the principle of protein-dye binding. Anal Biochem. 1976;72:248–54.

[83] Xiao K, Li Y, Luo J, Lee JS, Xiao W, Gonik AM, et al. The effect of surface charge on in vivo biodistribution of PEG-oligocholic acid based micellar nanoparticles. Biomaterials. 2011;32(13):3435–46.

[84] Manconi M, Isola R, Falchi A. Intracellular distribution of fluorescent probes delivered by vesicles of different lipidic composition. Colloids Surfaces B …. 2007;57:143–51.

[85] Manca M, Cassano R. Isoniazid-gelatin conjugate microparticles containing rifampicin for the treatment of tuberculosis. J Pharm …. 2013;1302–11.

[86] Kirchner C, Liedl T, Kudera S, Pellegrino T, Gaub HE, Sto S, et al. Cytotoxicity of Colloidal CdSe and CdSe / ZnS Nanoparticles. Nano Lett. 2005;5:331–8.

# II. Nanosuspensions

# 2. Nanosuspensions



## 1. Introduction

The number of poorly water-soluble molecules with potential therapeutic activity has progressively increased in the last years. As reported in literature, more than 40% of the new chemical entities in the pipeline and about 70% of drug coming directly from discovery programs are poorly soluble [1]. These molecules are very often characterized by a highly variable bioavailability, in particular too low oral bioavailability and erratic absorption profiles due to their low dissolution velocity and saturation solubility.

Different strategies including the use of salts, co-solvents [2], solubilizing agents [3], co-crystal formulations [4], pH adjustment [5], solid dispersions [6], lipid based formulations [7] (e.g. liposomes and microemulsions) [8], incorporation into inclusion complexing agents (cyclodextrins) [9], have been used to enhance drug solubility. However, most of these strategies have limited success because they can be applied only for drugs exhibiting special features, such as solubility in specific organic solvents or molecular structures fitting in the cyclodextrin rings.

For many years, micronization has also been used as general and simple approach to increase dissolution velocity of poorly water-soluble compounds [10]. In the micronization process (jet milling or wet milling) coarse drug powders are disintegrated in ultrafine powders characterized by drug crystal average diameters typically in the range of 2-5 $\mu$m. The reduction of crystal drug diameter enlarges the surface area thus increasing the dissolution velocity, as described by the Nerst-Brunner/Noyes-Whitney equations [11].

However, for drug with very low saturation solubility, micronization is not sufficient to achieve an adequate bioavailability. Consequently, the next step was the production of nanocrystals.

Nanocrystals can be defined as nanoparticles of pure drug without any matrix material

with an average diameter below 1 μm (typically in the range of 200-500 nm) [12,13]. Nanocrystals can be prepared in both water and non-water media as colloidal suspension (referred to as nanosuspensions) stabilized using surfactants (ionic or non-ionic) or polymers.

Compared to micronized powders, the reduction of the drug crystal average diameter below 1 μm not only increases the particle surface area but also decreases the diffusion layer thickness, as described by the Prandtl equation, further increasing the dissolution velocity [14]. In addition, as described by the Freundlich–Ostwald equation, nanocrystals are characterize by an increased saturation solubility not observed with micronized crystals [15].

Nanocrystals can be prepared using two different approaches: the bottom up and the top down technologies or a combination of two (Figure 1) [16]. In the bottom up technology, the low water soluble drugs are (molecularly) dissolved in a solvent and then precipitated in different ways as nanocrystals in a surfactant solution [17]. The top down technology is based on particle disintegration techniques including beads wet milling [18–21].

The drug absorption through the gastro intestinal tract (GIT) is basically characterized by two distinct steps: the drug dissolution into the GIT fluids and the drug transport across the GI membranes. Normally, in oral administration, the dissolution step is the rate limiting the absorption process. Poorly water-soluble drugs, belonging to class II and IV of the biopharmaceutical classification system (BCS) which absorption is limited by the low dissolution velocity, are characterized by no reproducible oral absorption, low bioavailability and absorption variation in the fed or fast state.

One of the first article describing the potential use of nanosuspension for oral administration was published by Merisko-Liversidge et al. [22]. The authors demonstrated the ability of nanosuspensions to improve the bioavailability of the poorly water soluble gonadotropin inhibitor Danazol in fasted male beagle dogs. At a dose of 200 mg danazol nanocrystals with a mean diameter of about 169 nm showed an absolute bioavailability of 82.3%, 16 times greater than that obtained using danazol marketed microsuspension (5.2%). Furthermore, the Cmax (maximum plasma concentration) was increased by 15 times and the Tmax (time to maximum plasma concentration) was reduced. Ever since, the ability of nanocrystals to increase the dissolution velocity and saturation solubility *in vitro* [23] and the oral biovailability *in vivo* has been extensively demonstrated in different animal models [24–26]. Formulation of poorly soluble drugs in nanosuspension has already achieved resounding success as also confirmed by the five oral and one parenteral medicinal products already on the market [27].

Interesting, nanocrystals dispersed in orally disintegrating tablets or polymer orodispersible films have been also studied for buccal administration of several drugs such as pyroxicam, quercetin and herpetrione as model drugs [28–30]. Overall, outcomes from these studies indicated a great amelioration of the dissolution velocity *in vitro* when the drugs are formulated in nanocrystal form.

Furthermore, intravenous injection of nanosuspension formulations has been extensively studied and several articles and reviews concerning this route of administration have been published [31–34]. Basically, intravenous injected nanocrystals or immediatly dissolve in the blood (very small nanocrystal or drug having an high intrinsic solubility), or slowly dissolve and accumulate in liver, lungs and spleen after recognition by the mononuclear phagocyte system (larger nanocrystals of drugs having very low water solubility).

Besides they have been especially studied for oral and parenteral administration,

nanocrystals have showed a great potential also for topical delivery through alternative routes such as the dermal, pulmonary and ocular route, which have not been intensely reviewed in literature.
For these reasons, in this thesis the use of nanocrystals for enhance dermal bioavailability of poorly soluble drugs was investigated.

### 1.1. Methods of production

Fundamentally, there are two approaches to produce drug nanocrystals the top down and the bottom up technologies as well as a combination thereof (Figure 1).

#### 1.1.1. Top down technologies

Top down process consists in reducing large drug crystal particles (micro range) into smaller crystals (nanometer range) by using different wet milling techniques such as media milling, microfluidization and high pressure homogenization. These technologies do not make use of aggressive solvents and, thus, are considered suitable for formulations as nanocrystals of all insoluble drugs including "brick dust drugs" (drugs insoluble in any solvent) (Figure 1).

*Wet ball media milling*

In the first 1990s, for the first time, Gary Liversidge and his coworkers of the company Sterling Drug Inc./Eastman Kodak, adapted a wet media-based milling technique used in the photographic industry to reduce the particle size of poorly water-soluble drugs [35]. Few years later, this milling technology was registered with the trade name NanoCrystal® by the company Elan Pharma International Ltd. Since then, wet ball media milling (WBM, known as pearl milling or bead milling) was developed demonstrating to be a very effective top-down process and, hence, becoming quickly the referential technology in nanosuspension pharmaceutical industry [36–38]. At present, WBM technology is represented in the market with five products (Rapamune® (Wyeth), Emend® (Merck), TriCor® (Abbott Laboratories), Triglide®



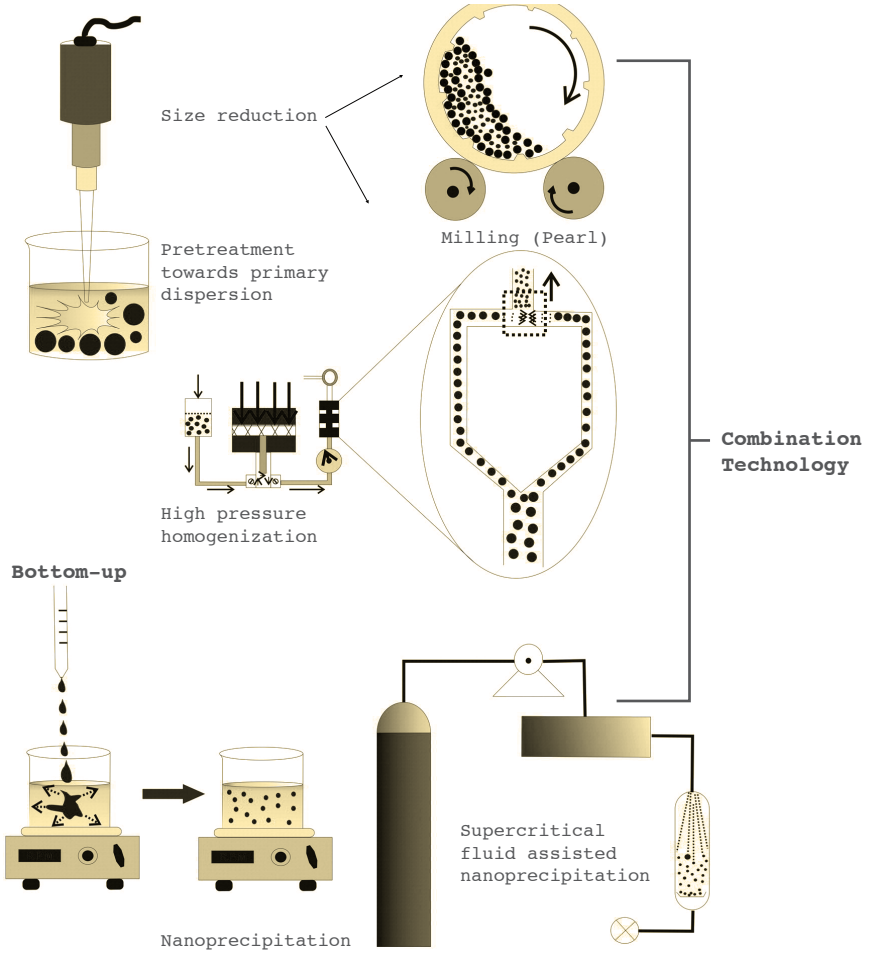


**Figure 1.** Schematic representation of the main nanocrystals production methods. Adapted from Ref. [16].

(Skye Pharma) and Megace ES® (Bristol-Myers Squibb) [39]. The milling procedure is very simple, achievable in almost all laboratories and universally applicable to most drug candidates or, more in general, to all solid materials [21]. On the whole, WBM technology can be divided in two different energetic processes: a low energy and a high energy wet ball milling.

In the former method, a drug coarse aqueous suspension containing stabilizers (polymers and/or surfactants) is mixed with the media milling (beads) in a jar or in a becker by using a stirrer at very high speeds (becker) or a roller plate or a mixer (jar). Continuous strong collisions between the micron-sized drug particles and the beads lead to a combination of cleavage, abrasion and fractures and consequently to a size reduction of the crystals down to the nanometer size range [40]. Surfactants or polymers are usually added to avoid aggregation phenomena of the newly formed nanocrystals as well as to minimize crystal growth on storage [41,42]. Unfortunately, although this technique produces very small and homogeneous nanometer-particles, the low energy supplied normally leads to very long milling times that can even reach several days [35,43]. On the contrary, the patented NanoCrystal® technology is based on a high energy WBM performed using specific equipment [44] . The higher power density supplied to the drug suspension allows to reduce significantly the production time needed to obtain nanosuspensions (30—120 min) of the desired size [45]. For this reason, today, the high energy WBM is considered the procedure of choice in the production of nanosuspensions. An important drawback of this technique was highlighted: nanosuspension contamination phenomena caused by abrasion of both milling media or parts of the equipment material, especially when glass or zirconium beads were used [46,47]. However, this problem has been overcome when new, more deformable beads made of zirconium alloy, stabilized with yttrium or polystyrene, were introduced [38,42]. Nowadays, equipments capable of producing small quantities of nanosuspensions or different types of nanosuspensions at the same time are available, thus, making this WBM technology a very scalable method as well as the most versatile top down process [48,49]. Indeed, all poor soluble drugs can be milled and, consequently, reduced in size by using this technique [50].

*High pressure homogenization*

High pressure homogenization (HPH) is considered the second most important process to produce drug nanocrystals. When the first nanosuspensions were formulated by using this technique, various types of homogenizers (both at high or low pressure) had already been employed in food field, while pharmaceutical industry employed this technique for the first time in 1990 in the preparation of liposomes and different emulsions [51,52].

Basically, there are three main approaches to produce nanosuspensions by HPH: insoluble drug delivery technology (IDD®) also referred as Microfluidizer technology (Microfluidizer®, Microfluidics Inc.), the piston-gap homogenization in water or, alternatively, in water-reduced/non-aqueous media [53,54].

Historically, the first HPH patented technique is the IDD® technology, developed in 1992 by the Research Triangle Pharmaceuticals company (now SkyePharma, Canada). IDD® is based on the use of a jet stream homogenizer, known as microfluidizer. In the microfludizer, the drug coarse suspension moves at high pression and speed through two different homogenization chambers. In the first chamber (the so called “Z” chamber), the coarse particles change quickly their flow direction randomly, therefore, colliding each other. On the ”Y” chamber (the second one), suspension flow is divided in two leading to a frontal collision of the new two generated flows. In both chambers, particle collision, shear and cavitation forces lead to the

desired particle size reduction. Unfortunately, this technique requires too long preparation times due to the high number of passes through the homogenizer. Moreover, it generally leads to a modest size reduction with hard drug nanosuspensions often containing a relatively large fraction of microparticles, and a consequent drop of the typical nanosuspensions advantages. However, Triglide® (fenofibrate) is an example of a marketed formulation produced using the microfluidizer.
In 1994, an alternative technology based on piston gap high pressure homogenization was developed by Müller and his team to produce small and homogeneous drug nanocrystals. Due to the cubic form of the obtained crystals (in contrast to spherical amorphous drug nanoparticles produced by IDD®), the trade name of this new method was DissoCubes® [55]. As for IDD® technology, in 1999 Dissocubes® was acquired by SkyePharma. In this technology, the coarse drug suspended in an aqueous surfactant solution is pushed several times by a piston under high pressure (from 1500-2000 bar up to 4000 bar) through a tiny gap (5—20 $\mu$m). The consequent high flow speed of the coarse suspension and the drastic reduction in the diameter from the cylindrical deposit (about 3 cm) to the tiny gap lead to an increased dynamic pressure. At the same time, static pressure falls below the vapor pressure of the external phase (water) compensating the increased dynamic pressure in the system: the water boils and the newly formed bubbles collapse quickly when the suspension escapes from the gap. The turbulence caused by these phenomena (cavitation) generates drug macrocrystal fragmentation in nanocrystals.
In general, the pressure inside the homogenizer gradually increases from 10% to 100% as pre-milling. Normally, to prevent a possible obstruction of the tight homogenizer gap, the coarse suspension is previously submitted to a de-agglomeration phase using high-speed stirrers. It must be underlined that here, cavitation forces play a fundamental role in drug crystal reduction but other factors are also involved, i.e. shear forces, and crystal against crystal and crystal against homogenizer wall collisions [56]. Moreover, several homogenization cycles are needed to obtain the desired crystal size using the Microfluidizer technique. Three main factors are considered to affect drug nanocrystals size obtained by the HPH technology: type and power density of the homogenizer, number of homogenization cycles, drug hardness and size of the starting material.
While coarse suspension moves through the homogenizer gap under pressure, particles start to crash nearby crumbly points becoming (after each cycle) smaller, more homogeneous, compact and, obviously, also more difficult to be further reduced. Thus, both the choice of the homogenizer equipment (the greater the equipment power density the easier the reduction process of crystal dimension) and the number of cycles to perform (more cycles mean more probability to break “survived crystals” at the following cycle) appears crucial factors. Furthermore, the softer the drug the lower is the system energy required to reduce crystals size and vice versa. Drug hardness can also affect another important aspect in any production process: erosion phenomena of the internal surfaces of the equipment and subsequent steel contamination of the final product. Normally, high pressure homogenization is less inclined in generating process impurities as a consequence of abrasion and wearing of the equipment if compared to WBM (below 1 ppm after 20 cycles at 1500 bar) [57]. However, after a certain time of usage or when extremely hard material is processed, the tip of the homogenization valve can show some signs of wear due to cavitation and particle impact, so the default smooth surface will appear scratched.
In 1999, starting from Dissocubes® technology, the Ger-

man company PharmaSol GmbH (now Abbott Laboratories) developed an alternative piston gap homogenization process registered with the trade name of Nanopure® technology (pure nanocrystals) [58]. This technology uses, as primary dispersion medium, non-aqueous liquids, oils, liquid and solid (melted) PEG, or water reduced media (glycerol, water, ethanol or water mixtures). As highlighted above, the first patent of DissoCubes® is based on the dominating role of cavitation in the homogenization process. In contrast to water, oils and oily fatty acids have a very low vapour pressure at room temperature, so cavitation takes place partially or not at all. Therefore, when water shows cavitation, the oil will not. Even without cavitation, the size reduction is sufficient because of the shear forces, particle collisions and turbulences. Nanopure® technology is especially suitable for the formulation of oral dosage forms. Production of drug nanocrystals in a mixture of water and water-miscible liquids has some process advantages, for example in case of spray-drying or lyophilisation. In addition, it allows the production of isotonic drug nanosuspensions for i.v. administration in a one-step production process (homogenization in an isotonic glycerol–water mixture). In conclusion, high pressure homogenization represents an efficient method to produce nanocrystals, especially for relatively soft drugs, although the obtained nanosuspension seems to be less homogeneous if compared with that obtained with the *wet ball milling process*. Moreover, HPH is a scalable method (used in pharmaceutical, food and cosmetics fields) and applicable both in laboratory and industrial production [20,59].

On the contrary, the choice of the stabilizer seems to be a less determining factor since, in nanosuspension technology, the stabilizers do not affect either crystal reduction or crystal form but only play a role in preventing aggregation phenomena of the new obtained nanocrystals, i.e. in long-term stability.



**1.1.2. Bottom-up technologies**

In the bottom-up technology, also termed as nanoprecipitation, the process starts from a supersaturated drug solution, where the molecules grow and precipitate in the form of nanocrystals. Precipitation can be induced by processes that further increase the supersaturation, such as reduction of temperature, evaporation of the solvent or by mixing it with an antisolvent (Figure 1). At a higher extent of supersaturation, the nucleation rate increases, and, then, the crystal size decreases. Crucial in this process is it to control the structure of the particles (amorphous versus crystalline) and to avoid growth of the crystals to the μm size range. The first traditional precipitation method used to obtain drug nanocrystals was the so-called Hydrosol technique invented by List and Sucker in 1988 [60]. In this technique, also called liquid solvent-antisolvent (LAS) precipitation, the drug is first solubilized in a suitable solvent, preferably water miscible (e.g. acetone, ethanol, methanol, isopropanol (IPA), N-methylpyrrolidone (NMP)) and then mixed with an antisolvent (water, in most of the cases), which must be miscible with the solvent phase. Mixing of the organic solution and the anti-solvent should be performed rapidly to guarantee a fast nucleation and, thereby, small particles. To stabilize the nanocrystals, a stabilizing agent can be dissolved in the aqueous phase. Hereafter, the solvents can be removed by evaporation or lyophilization to obtain a dry nanocrystalline drug product. The use of this technique for drug nanocrystal preparation was reported in several research studies [61–64].

In order to obtain nanocrystals with a smaller particle size or narrower particle size distribution (PSD), modified LAS precipitation methods are reported in literature. The

lower particle size obtained by these modified methods is a result of either faster mixing to affect the nucleation stage or by blocking particle growth. Additional external energy, such as ultrasounds, has been demonstrated to enhance a rapid mixing [65]. However, sonoprecipitation has been employed only for very few drugs [66–71]. Alternatively, precipitation can be carried out in combination with centrifugation (High gravity antisolvent precipitation) [72–74]. Another modified solvent-antisolvent precipitation method is the evaporative precipitation into aqueous solution (EPAS). In the EPAS process, the drug precipitates due to evaporation of the organic solvent close or above the boiling point [75–77].

Supercritical fluid (SCF) technologies have been proposed as alternatives to liquid solvent-antisolvent processes. The most relevant SCF methods include rapid expansion of supercritical solutions (RESS) and supercritical antisolvent process (SAS). The RESS technique was described for the first time in 1999 by Pace et al. in the preparation of drug nanocrystals [78]. In this process, the supercritical fluid, such as supercritical carbon dioxide, acts as a solvent. The drug solution rapidly expand across an orifice or a capillary nozzle into ambient air. The fast pressure reduction in the expansion is characterized by high degrees of supersaturation, resulting in the homogeneous nucleation and, thereby, the formation of well-dispersed particles. A modified method called rapid expansion of supercritical solution with solid cosolvent (RESS–SC) was used for drugs with low solubility in the SCF [79,80]. In addition, further modifications of the RESS technique led to processes called, respectively, rapid expansion of a supercritical solution into a liquid solvent (RESOLV) and rapid expansion from supercritical to aqueous solution (RESAS). RESOLV and RESAS technologies were later used for preparing nanoparticles of various other compounds as well [58,81–83].

In contrast, in the SAS process the supercritical fluid acts as an anti-solvent. An organic drug solution is mixed with the supercritical antisolvent leading to a precipitation of nanometer-sized drug particles, which are collected in various ways. A solution of the drug in an organic solvent is saturated with supercritical fluid, thus, decreasing the solubility of the drug in the solvent and causing consequently the drug precipitation. Several examples of using SAS method for nanosized drug particle production are shown in the literature [53,84] . Depending on process conditions and mixing types, various process variants exist: gas antisolvent process (GAS) [85], solution-enhanced dispersion by supercritical fluids (SEDS) [86], aerosol supercritical extraction system (ASES) [85,87] and SAS with enhanced mass transfer (SAS–EM)[88,89].

More recently, bottom-up techniques, such as controlled crystallization during freeze drying (CCDF) [90], spray-freezing into liquid [91] or nanoprecipitation in microfluidic reactors [92,93], were developed to prepare drug nanocrystals. In CCDF, a drug solution in an organic solvent is mixed with an aqueous solution of a cryoprotectant and, then, immediately frozen and lyophilized. Freeze-drying is performed at a relatively high temperature (above the glass transition temperature of the maximally freeze-concentrated fraction) to allow the drug and matrix to crystallize. Faster freezing rate and lower water content induce higher nucleation rate, which reduces the size of the solvent crystals and, thereby, the interstitial spaces among them. Smaller interstitial spaces limit the growth of the drug crystals. However, this method is only suitable for drugs with low glass transition temperature ($T_g$). To scale up this method for large scale production, the mixing step was modified by using a 3-way nozzle (for solvent, antisolvent

and atomizing air) [94]. The fine droplets of solvent and antisolvent, generated by atomizing air, mix one another as soon as they leave the nozzle, and the mixture directly enter into the liquid nitrogen for freezing.
Spray-freezing into liquid (SFL), which consists of similar process steps as CCDF, was first proposed by Hu et al [91]. The drug can be dissolved either in a mixture of aqueous/organic solvent or in pure organic solvent, with or without stabilizer, and then sprayed into liquid nitrogen for immediate precipitation of amorphous particles in a nanometer size [95]. The SFL process has several advantages in comparison with other precipitation methods that use spray technique, i.e. EPAS. Indeed, the SFL process leads to highly porous, amorphous and smaller size nanostructured particles in the form of solid solution. On the contrary, the EPAS process produces particles relatively larger and, furthermore, the miscibility of the polymer and the drug is low. This results in higher dissolution rates of the particles prepared by SFL if compared to the EPAS process [54].
Bottom-up processes are low energy processes, require simple instruments, are less expensive and can be operated at a low temperature, making them particularly suitable for thermolabile drugs. However, a basic disadvantage of many precipitation processes is the use of organic solvents, which need to be removed, leading to high cost of production. Particularly, in case of low soluble drug in water and organic solvent, large solvent volumes are required. Moreover, advanced techniques like processing with supercritical fluid are more expensive. Hence, in the pharmaceutical industry, the bottom up processes are not employed for the production of marketed drugs [17].

### 1.1.3. Combination technologies

The combination of a pre-treatment step with following high energy step have been introduced to overcome limitations and to improve the particle size reduction effectiveness of the single “bottom-up” or “top-down” strategies (Figure 1). The patent combination technologies are, for example, Nanoedge® and smartCrystal® technologies.
The Nanoedge® technology by Baxter consists of a bottom-up step (micro-precipitation) followed by a top-down step (high-pressure homogenization). The drug is dissolved, e.g. in a water-miscible, non-aqueous media and precipitates in form of a suspension consisting of fragile drug particles This suspension is then further processed to nanosuspension by means of high-pressure homogenization. In the presence of high energy, the unstable form of the drug particles is converted to a stable crystalline particle [96].
On the contrary, SmartCrystal® technology is considered as the second generation of drug nanocrystals and it is owned by Abbott and marketed by its drug delivery company Soliqs in Ludwigshafen/ Germany. This approach consists of a family of various combination processes, where a pre-treatment step is followed by a high pressure homogenization (HPH) step to accelerate nanocrystal production and/or obtain small nanocrystal size below 100 nm. Several processes, such as the CT (combination technology) process (pearl milling followed by high pressure homogenization)[97], the H 69 technology (cavi-precipitation followed by high pressure homogenization) [98,99], the H 96 technology (freeze-drying followed by high pressure homogenization)[100] and the H 42 technology (spray-drying followed by high pressure homogenization)[101] belong to this family. Literature provides many examples where combinational technologies have produced stabilized nanocrystals [93,102–105].
Recently, a novel tri-combination technology, the so called “Precipitation-lyophilization-homogenization (PLH) method” has been proposed for preparing nanocrystals [106]. Here, the solvent-antisolvent precip-

itation process is used to reduce the starting particle size prior to homogenization. Then, a lyophilization step follows, thus, allowing the solvent to be completely removed and providing porous and friable drug particles. Finally, the application of high pressure homogenization may facilitate the reduction of drug crystals to the nanometer size range.
In addition to this combinational methods, ultrasonic sound was used as pre-treatment step followed by high pressure homogenization [107] as well as a high energy step to reduce the particle size after precipitation [108].

### 1.2. Dermal delivery

The skin represents an important site for non-invasive and painless delivery of therapeutic agents with possibility to control their release and to avoid the first-pass metabolism [109]. After dermal absorption drugs can reach different target sites and exert topical, regional, or systemic effects. For these reasons, delivery of drugs through the skin has been considered an attractive as well as a challenging research area [110,111]. The primary challenge is overcoming the unusually impermeability of the skin barrier. The skin (Figure 2) is a complex structure that protects the human body preventing invasion of pathogens and fending off chemical and physical assaults and controls essential processes like thermal regulation. It is made up of several anatomically distinct layers, namely the stratum corneum (SC), the viable epidermis and the dermis [112]. The physical barrier is mainly localized in the SC and consists of protein-enriched dead cells (corneocytes with cornified envelope and cytoskeletal elements, as well as corneodesmosomes) and lipid-enriched intercellular domains which are organized as multiple lipid bilayers (lamellar sheets composed of approximately equimolar concentrations of free fatty acids, cholesterol, and long chain ceramides) [113]. The nucleated epidermis also contributes to the



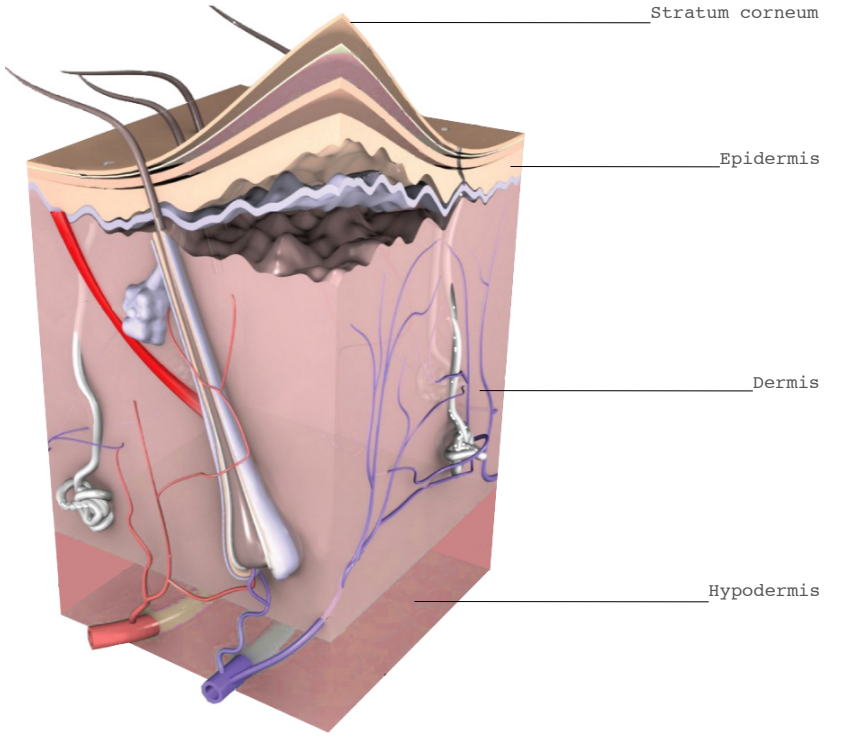


**Figure 2 Schematic representation of skin layers.**

barrier through tight, gap and adherent junctions, as well as through desmosomes and cytoskeletal elements. Therefore, the skin barrier function is not only dependent on one single component but on its total architecture [114]. Appendages such as sweat glands, pilosebaceous units, and hair follicles are structures originate either from the dermis or the subcutaneous fat tissue which penetrate the skin thus forming important discontinuities in this compact structure [115]. Drugs applied to the skin surface enter the skin by a passive diffusion process through two pathways such as the transappendegeal and the transepidermal routes (Figure 3). The skin appendages present an alternative pathway for drug delivery into the skin, raising the possibility of avoiding the difficulty of delivering drug through the SC. This route was traditionally considered of minor importance because of the relatively small area, but recent results on follicular penetration have emphasize that the hair follicles pathway may plays a major role as skin penetration pathway and reservoir of topically applied molecules. Moreover, the hair follicles and sebaceous glands are associated with various dermatological disorders such as acne, alopecia, and several skin tumors [115]. Through the epidermis, there are two different routes by which a molecule can cross this barrier: the transcellular, across the corneocytes and the intercellular across the lipid domains between the corneocytes. Although it is generally accepted that the intercellular route provides the principal pathway for the permeation of drugs, also this route is severely limited by the inability of the large majority of drugs to cross the skin at therapeutic rates due to the great barrier imposed by the outer SC layer [109,110,114]. To increase skin permeability, a number of different approaches has been studied, ranging from chemical enhancers to soft matter nanocarriers such as liposomes, which oppor-



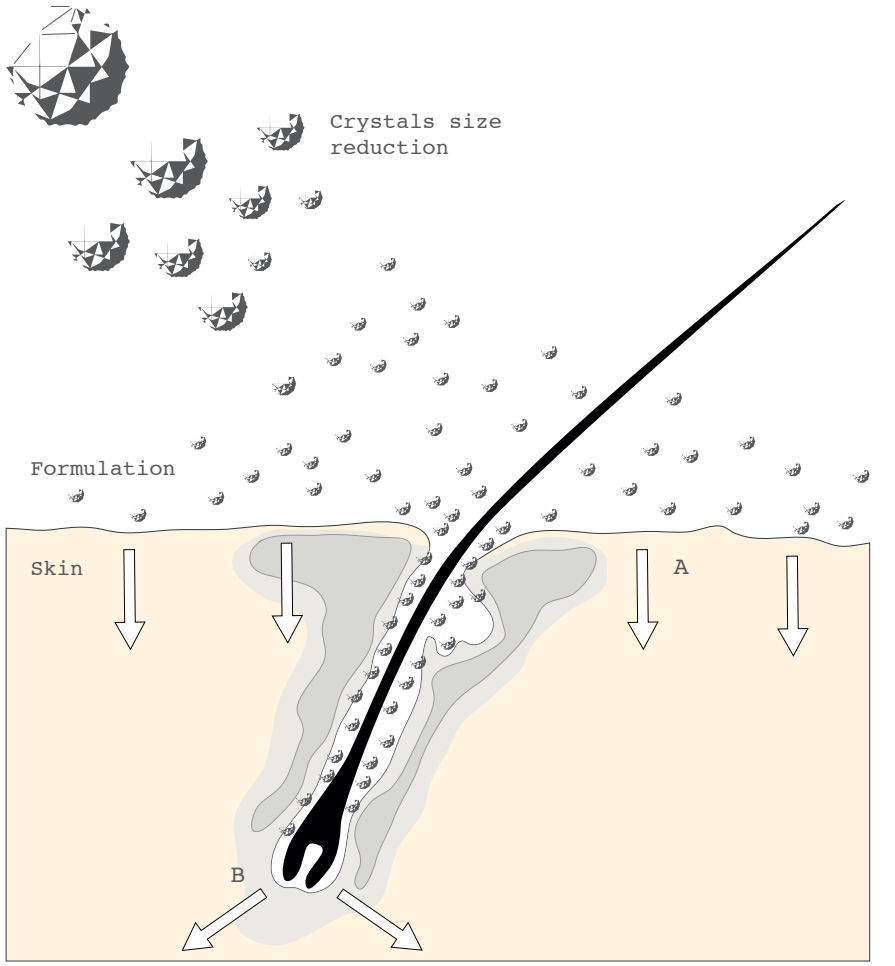


**Figure 3.** Proposed mechanism of increased dermal penetration of drug actives formulated as nanocrystals via (A) increased penetration into skin surface (epidermis) and (B) localization of nanocrystals in the hair follicles. Adapted from Ref. [120].

tunely formulated might have the potential to meet the demands [116,117]. Among the various strategy for enhancing dermal application, nanocrystals can be considered a rather new but highly interesting approach [13,118]. Despite several nanosuspension products have become very fast available in the last 10 years, with most of them intended for oral administration, only few research has been dedicated to the study of skin permeation and accumulation of drugs formulated as nanosuspension. However, the few published results clearly indicate that this technology could be very effective for improving dermal bioavailability of actives with both poor and more recently, medium solubility. Indeed, besides the increased saturation solubility and dissolution rate, nanocrystals also exhibit the property of increased adhesiveness to the skin thus facilitating the dermal delivery [12,13]. The interest towards this technology for dermal application has been raising since 2007, when the first anti-aging and skin-protective cosmetic products based on nanosuspensions of poorly soluble antioxidants rutin and hesperidin have been introduced to the market [119]. Rutin nanocrystals were produced by a combination process of low energy pearl milling followed by high pressure homogenization. When applied on the skin of human volunteers, a nanosuspension with 5% rutin as non-dissolved nanocrystals showed a 500-fold higher antioxidant activity compared with a 5% solution of a water soluble rutin-glycoside derivative. Due to the higher solubility of active rutin as a nanocrystal, there is an increased concentration gradient between dermal formulation and skin, which leads to a higher penetration when compared to large drug crystals. Rutin penetrated into the skin is immediately replaced by fast dissolving molecules from the nanocrystals. Moreover, compared to the hydrophilic rutin-glucoside, the original lipophilic molecule rutin can better penetrate into the skin where it is believed to have a higher affinity to the sites of action than the synthetically modified derivative [12,119]. As a consequence of these positive outcomes, several research focused on nanosuspensions of antioxidant molecules have been reported in literature since 2007 [120–123]. First, Mishra et al. produced nanocrystals of hesperetin, the aglycone of hesperidin, which has not only antioxidative but also anti-inflammatory properties and, therefore, is thought to be a very effective anti-aging compound. As these authors state, there is no difference in the procedure for producing nanocrystals for oral, intravenous or dermal application. The only difference in the formulations is the choice of the stabilizers. Hence, in this study nanosuspensions of hesperetin were produced by high-pressure homogenization employing four different stabilizers suitable for dermal use such as Poloxamer 188, Inutec SP1, Tween 80 and Plantacare 2000, possessing different mechanisms of stabilization. Interestingly, as predicted from the zeta potential measurements, Inutec and Plantacare stabilized nanosuspensions were stable with no change in mean diameter size. Slight increases in size were found for Poloxamer and Tween stabilized nanosuspensions, which is not considered to impair their use in dermal formulations [121].

In 2011, Kobierski et al chose the anti-oxidant resveratrol as an ideal candidate to be used as nanocrystal in dermal cosmetic formulations such as creams, lotions and gels. Since preservation is essential for dermal formulations, resveratrol nanosuspensions were produced by a high pressure homogenization process and the effects of preservatives on physical stability were monitored as a function of cycle numbers [122]. The same year, Mitri et al prepared a lutein nanosuspension by means of high pressure homogenization to enhance dissolution velocity and saturation solubility, which are major factors determining

oral bioavailability and penetration into the skin [123]. Lutein is a well-known antioxidant and anti-free radical used in cosmetic, nutraceutical industry with potential application in pharmaceutics as supportive antioxidant. The main results from this study indicated that lutein nanocrystals significantly increased drug saturation solubility (26.3 fold) as well as permeation through cellulose nitrate membranes (14 fold), compared to coarse powder. Moreover, no permeation through pig ear skin occurred, which supports the fact that lutein rather penetrates into the skin and remains there where it should act as antioxidant [123].

A solid in oil nanosuspension of diclofenac sodium was the first pharmaceutical formulations in which nanosuspension technology was applied to topical application of a poorly soluble therapeutic agent [124]. In this study, Piao et al successfully dispersed diclofenac sodium into isopropylmiristate (oil phase) as a nanosized suspension via complex formation with sucrose ester surfactant. The drug flux across the Yucatan micropig skin model was increased up to approximately 4 fold compared with a coarse oil suspension used as control. In a more recent paper, nanosuspension gel formulations were studied as suitable formulation approach for improving the skin permeability of a poorly soluble molecule such as ibuprofen, a non-steroidal anti-inflammatory drug used for the treatment of acute and chronic arthritic conditions [125]. Since the ibuprofen oral administration can cause gastric mucosal damage which may result in ulceration, its topical delivery can overcomes many side effects such as gastric complications. In this study, tocopherylpolyethyleneglycol 1000 succinate (TPGS) and hydroxylpropylmethylcellulose (HPMC) were used as the basic components in nanoparticle ibuprofen formulations. TPGS was used to enhance the drug permeability (tested in both porcine and human skin) and to stabilize the system by hydrophobic interactions, while HPMC was used as a steric stabilizer to inhibit crystal growth of the drug in the formulation. Results of experiments clearly indicated that the overall skin permeation enhancement process strongly depended on the solubilizer as well the particle size of the drug crystals. These factors resulted in higher drug release due to the formation of supersaturated solution around the crystals and thus a high concentration gradient was produced between the drug crystals and skin surface. Authors conclude that a number of factors including the particle size of the drug crystals, surface properties of the carrier, interaction of drug molecule with the stabilizer needed to be considered while designing a suitable dermal formulation for poorly soluble compounds. In 2013, Lai et al tested nanosuspensions prepared by simple precipitation method as a tool to improve cutaneous targeting and photostability of tretinoin, a poor water soluble and instable molecule, commercially formulated in cream and gel forms for the treatment of acne vulgaris [64]. Drug skin permeation and deposition were studied *in vitro* by diffusion experiments through new born pig skin while TRA photostability was investigated by irradiating samples with UV light. As an appropriate comparison, an O/W nanoemulsion was also prepared and tested. Indeed, nanoemulsions have shown to be particularly useful as vehicle for dermal and transdermal delivery of hydrophobic compounds for pharmaceutical, cosmetic, and chemical industry applications. During 8 h percutaneous experiments, the nanosuspension was able to localize the drug into the pig skin with a very low transdermal drug delivery (which is responsible of systemic side effects of this drug), whereas the nanoemulsion greatly improved drug permeation. Therefore, also this work demonstrated the high potentiality of nanosuspensions in dermal drug delivery. It is worth to notice that nanosuspensions are al-

most exclusively composed of the drug nanoparticles with small amounts of biocompatible and safe surfactants, such as the soy lecithin used in this work and although only few toxicological data are available at the moment, no side effects are known or expected from nanocrystal topically applied. Indeed, as suggested by Muller et al., each solid macro/micro-particle applied on the skin will convert to nanocrystals during its dissolution process and, up to now, no intolerability has been reported [12]. As already reported above, also in this research paper authors justified the increased drug dermal delivery as a consequence increased of concentration gradient between the dermal formulation and the skin. More specifically, they claimed that finely divided and uniformly suspended tretinoin nanocrystals possess an increased dissolution rate due to their large surface area and increased saturation solubility. Solid drug dissolves in the vehicle, diffuses through the vehicle to the skin, establishes local phase equilibrium with the outer layer of skin and finally thanks to the larger concentration gradient penetrates the skin forming a depot in the lipophilic SC from which it diffuses. Furthermore, the topical application of tretinoin nanocrystals has the advantage of increasing the drug photostability, in comparison with the control nanoemulsion.

In the last two years, the application of nanocrystal technology have been extended to medium soluble compounds and a new mechanism by which nanocrystals can improve dermal delivery has been proposed, in addition to the simple increase of concentration gradient between formulation and skin [120]. This second mechanism involve the hair follicles. Nanocrystals with an appropriated size (approximately 700nm) can accumulated into these shunts, which act as a depot from which the drug can diffuse into the surrounding cells for prolonged release [126,127]. In a novel interesting paper, Zhai et al produce nanocrystals with the aim of increasing the skin penetration of a medium soluble active such as caffeine [128]. Moreover, they developed a specific production process, namely a low energy milling in low dielectric constant dispersion media and a selected stabilizer, which allowed to overcome crystal growth and fiber formation caused by supersaturation and re-crystallization effects, typical with medium soluble compounds. The novel concept introduced by Zhai et, consisted of formulating nanocrystals from medium soluble actives, and applying a dermal formulation containing additionally nanocrystals, which should act as fast dissolving depot, increase saturation solubility and accumulate in the hair follicles, to further enhance skin penetration. For this purpose, they produced caffeine nanocrystals with varied size ranging from 660 nm (optimal for hair follicle accumulation) to 250 nm (optimal for fast dissolution), by pear milling process in ethanol/propylene glycol 3:7 with 2% carbopol. As state by authors, selected formulations are currently being tested *in vivo* in a human study.

## References

[1] Muller RH, Benita S, Bohm B. Emulsions and Nanosuspensions for the Formulation of Poorly Soluble Drugs. Stuttgart: CRC Press; 1998.

[2] Rubino JT. Encyclopedia of Pharmaceutical Technology: Volume 20 - Supplement 3. Swarbrick J, Boylan JC, editors. New York, Basel: Marcel Dekker, Inc.; 2000.

[3] Nema S, Brendel RJ. Excipients and their role in approved injectable products: current usage and future directions. PDA J Pharm Sci Technol. 2011;65(3):287–332.

[4] Friščić T, Jones W. Benefits of cocrystallisation in pharmaceutical materials science: an update. J Pharm Pharmacol. 2010;62(11):1547–59.

[5] Li P, Zhao L. Developing early formulations: practice and perspective. Int J Pharm. 2007;341(1-2):1–19.

[6] Newman A, Knipp G, Zografi G. Assessing the performance of amorphous solid dispersions. J Pharm Sci. 2012;101(4):1355–77.

[7] O'Driscoll CM, Griffin BT. Biopharmaceutical challenges associated with drugs with low aqueous solubility--the potential impact of lipid-based formulations. Adv Drug Deliv Rev. 2008;60(6):617–24.

[8] Nakano M. Places of emulsions in drug delivery. Adv Drug Deliv Rev. 2000;45(1):1–4.

[9] Davis ME, Brewster ME. Cyclodextrin-based pharmaceutics: past, present and future. Nat Rev Drug Discov. 2004;3(12):1023–35.

[10] Rasenack N, Müller D (hon)Bernd W. Micron-Size Drug Particles: Common and Novel Micronization Techniques. Informa UK Ltd UK; 2004;

[11] Noyes AA, Whitney WR. The rate of solution of solid substances in their own solutions. J Am Chem Soc. ACS Publications; 1897;19(12):930–4.

[12] Müller RH, Gohla S, Keck CM. State of the art of nanocrystals--special features, production, nanotoxicology aspects and intracellular delivery. Eur J Pharm Biopharm. 2011;78(1):1–9.

[13] Rabinow BE. Nanosuspensions in drug delivery. Nat Rev Drug Discov. 2004;3(9):785–96.

[14] Mosharraf M, Nyström C. The effect of particle size and shape on the surface specific dissolution rate of microsized practically insoluble drugs. Int J Pharm. 1995;122(1-2):35–47.

[15] Müller RH, Peters K. Nanosuspensions for the formulation of poorly soluble drugs. Int J Pharm. 1998;160(2):229–37.

[16] Pawar VK, Singh Y, Meher JG, Gupta S, Chourasia MK. Engineered nanocrystal technology: in-vivo fate, targeting and applications in drug delivery. J Control Release. 2014;183:51–66.

[17] Sinha B, Müller RH, Möschwitzer JP. Bottom-up approaches for preparing drug nanocrystals: Formulations and factors affecting particle size. Int J Pharm. Elsevier B.V.; 2013;453(1):126–41.

[18] Ghosh I, Schenck D, Bose S, Ruegger C. Optimization of formulation and process parameters for the production of nanosuspension by wet media milling technique: Effect of Vitamin e TPGS and nanocrystal particle size on oral absorption. Eur J Pharm Sci. 2012;47:718–28.

[19] Merisko-Liversidge E, Liversidge GG, Cooper ER. Nanosizing: a formulation approach for poorly-water-soluble compounds. Eur J Pharm Sci Off J Eur Fed Pharm Sci. 2003;18(2):113.

[20] Keck CM, Müller RH. Drug nanocrystals of poorly soluble drugs produced by high pressure homogenisation. Eur J Pharm Biopharm. 2006;62(1):3–16.



[21] Müller R., Jacobs C, Kayser O. Nanosuspensions as particulate drug formulations in therapy. Adv Drug Deliv Rev. 2001;47(1):3–19.

[22] Liversidge GG, Cundy KC. Particle size reduction for improvement of oral bioavailability of hydrophobic drugs: I. Absolute oral bioavailability of nanocrystalline danazol in beagle dogs. Int J Pharm. 1995;125(1):91–7.

[23] Lai F, Sinico C, Ennas G, Marongiu F, Marongiu G, Fadda AM. Diclofenac nanosuspensions: influence of preparation procedure and crystal form on drug dissolution behaviour. Int J Pharm. 2009;373(1-2):124–32.

[24] Mou D, Chen H, Wan J, Xu H, Yang X. Potent dried drug nanosuspensions for oral bioavailability enhancement of poorly soluble drugs with pH-dependent solubility. Int J Pharm. 2011;413(1-2):237–44.

[25] Vergote G., Vervaet C, Van Driessche I, Hoste S, De Smedt S, Demeester J, et al. In vivo evaluation of matrix pellets containing nanocrystalline ketoprofen. Int J Pharm. 2002;240(1-2):79–84.

[26] Li X, Gu L, Xu Y, Wang Y. Preparation of fenofibrate nanosuspension and study of its pharmacokinetic behavior in rats. Informa UK Ltd London, UK; 2009;

[27] Möschwitzer JP. Drug nanocrystals in the commercial pharmaceutical development process. Int J Pharm. 2013;453:142–56.

[28] Lai F, Pini E, Angioni G, Manca ML, Perricci J, Sinico C, et al. Nanocrystals as tool to improve piroxicam dissolution rate in novel orally disintegrating tablets. Eur J Pharm Biopharm. Elsevier B.V.; 2011;79(3):552–8.

[29] Lai F, Franceschini I, Corrias F, Sala MC, Cilurzo F, Sinico C, et al. Maltodextrin fast dissolving films for quercetin nanocrystal delivery. A feasibility study. Carbohydr Polym. 2015;121:217–23.

[30] Shen B, Shen C, Yuan X, Bai J, Lv Q, Xu H, et al. Development and characterization of an orodispersible film containing drug nanoparticles. Eur J Pharm Biopharm. 2013;85(3 Pt B):1348–56.

[31] Gao Y, Li Z, Sun M, Li H, Guo C, Cui J, et al. Preparation, characterization, pharmacokinetics, and tissue distribution of curcumin nanosuspension with TPGS as stabilizer. Drug Dev Ind Pharm. Informa Healthcare New York; 2010;36(10):1225–34.

[32] Rabinow B, Kipp J, Papadopoulos P, Wong J, Glosson J, Gass J, et al. Itraconazole IV nanosuspension enhances efficacy through altered pharmacokinetics in the rat. Int J Pharm. 2007;339(1-2):251–60.

[33] Gao L, Zhang D, Chen M, Duan C, Dai W, Jia L, et al. Studies on pharmacokinetics and tissue distribution of oridonin nanosuspensions. Int J Pharm. 2008;355(1-2):321–7.

[34] Ganta S, Paxton JW, Baguley BC, Garg S. Formulation and pharmacokinetic evaluation of an asulacrine nanocrystalline suspension for intravenous delivery. Int J Pharm. 2009;367(1-2):179–86.

[35] Liversidge GG, Conzentino P. Drug particle size reduction for decreasing gastric irritancy and enhancing absorption of naproxen in rats. Int J Pharm. 1995;125(2):309–13.

[36] Bhakay A, Merwade M, Bilgili E, Dave RN. Novel aspects of wet milling for the production of microsuspensions and nanosuspensions of poorly water-soluble drugs. Drug Dev Ind Pharm. Informa Healthcare New York; 2011;37(8):963–76.

[37] Joseph A. Bruno, Brian D. Doty, Evan Gustow, Kathleen J. Illig, Nats Rajagopalan PS. Method of grinding pharmaceutical substances US5518187 A. 1996.

[38] Merisko-Liversidge E, Liversidge GG, Cooper ER. Nanosizing: a formulation approach for poorly-water-soluble compounds. Eur J Pharm Sci. 2003;18(2):113–20.



[39] Junghanns J-UAH, Müller RH. Nanocrystal technology, drug delivery and clinical applications. Int J Nanomedicine. 2008;3(3):295–309.

[40] Hennart SLA, van Hee P, Drouet V, Domingues MC, Wildeboer WJ, Meesters GMH. Characterization and modeling of a sub-micron milling process limited by agglomeration phenomena. Chem Eng Sci. 2012;71:484–95.

[41] Ghosh I, Bose S, Vippagunta R, Harmon F. Nanosuspension for improving the bioavailability of a poorly soluble drug and screening of stabilizing agents to inhibit crystal growth. Int J Pharm. 2011;409(1-2):260–8.

[42] Kesisoglou F, Panmai S, Wu Y. Nanosizing--oral formulation development and biopharmaceutical evaluation. Adv Drug Deliv Rev. 2007;59(7):631–44.

[43] Merisko-Liversidge E, Sarpotdar P, Bruno J, Hajj S, Wei L, Peltier N, et al. Formulation and Antitumor Activity Evaluation of Nanocrystalline Suspensions of Poorly Soluble Anticancer Drugs. Pharm Res. Kluwer Academic Publishers-Plenum Publishers; 1996;13(2):272–8.

[44] Merisko-Liversidge EM, Liversidge GG. Drug nanoparticles: formulating poorly water-soluble compounds. Toxicol Pathol. 2008;36(1):43–8.

[45] Merisko-Liversidge E, Liversidge GG. Nanosizing for oral and parenteral drug delivery: A perspective on formulating poorly-water soluble compounds using wet media milling technology. Adv Drug Deliv Rev. 2011;63:427–40.

[46] Hennart SLA, Domingues MC, Wildeboer WJ, van Hee P, Meesters GMH. Study of the process of stirred ball milling of poorly water soluble organic products using factorial design. Powder Technol. 2010;198(1):56–60.

[47] Juhnke M, Märtin D, John E. Generation of wear during the production of drug nanosuspensions by wet media milling. Eur J Pharm Biopharm. 2012;81(1):214–22.

[48] Juhnke M, Berghausen J, Timpe C. Accelerated Formulation Development for Nanomilled Active Pharmaceutical Ingredients Using a Screening Approach. Chem Eng Technol. 2010;33(9):1412–8.

[49] Van Eerdenbrugh B, Stuyven B, Froyen L, Van Humbeeck J, Martens JA, Augustijns P, et al. Downscaling drug nanosuspension production: processing aspects and physicochemical characterization. AAPS PharmSciTech. 2009;10(1):44–53.

[50] Cooper ER. Nanoparticles: A personal experience for formulating poorly water soluble drugs. J Control Release. 2010;141(3):300–2.

[51] Brandl M, Bachmann D, Drechsler M, Bauer KH. Liposome Preparation by a New High Pressure Homogenizer Gaulin Micron Lab 40. Drug Dev Ind Pharm. Informa UK Ltd UK; 1990;16(14):2167–91.

[52] Collins-Gold LC, Lyons RT, Bartholow LC. Parenteral emulsions for drug delivery. Adv Drug Deliv Rev. 1990;5(3):189–208.

[53] Müller, R.H., Becker, R., Kruss KP. Pharmaceutical nanosuspensions for medicament administration as systems with increased saturation solubility and rate of solution. US Patent 5858410. 1992;

[54] Müller, R.H., Krause, K., Mäder K. Method for controlled production of ultrafine microparticles and nanoparticles. WO/2001/003670. 2001;

[55] R.H. Muller, Jacobs C, Kayser O. Modified-Release Drug Delivery Technology. Marcel Dek. Rathbone MJ, Hadgraft J, Roberts MS, editors. 2003.

[56] Pharmaceutical nanosuspensions for medicament administration as systems with increased saturation solubility and rate of solution. 1999.

[57] Krause KP, Kayser O, Mäder K, Gust R, Müller RH. Heavy metal contamination of nanosuspensions produced by high-pressure homogenisation. Int J Pharm. 2000;196(2):169–72.



[58] Radtke M. NanopureTM pure drug nanoparticles for the formulation of porly soluble drugs. New Drugs. 2001;3:62–8.

[59] Dumay E, Chevalier-Lucia D, Picart-Palmade L, Benzaria A, Gràcia-Julià A, Blayo C. Technological aspects and potential applications of (ultra) high-pressure homogenisation. Trends Food Sci Technol. 2013;31(1):13–26.

[60] List M, Sucker H. GB 2200048 - Pharmaceutical colloidal hydrosols for injection. 1988.

[61] Yadav D, Kumar N. Nanonization of curcumin by antisolvent precipitation : Process development , characterization , freeze drying and stability performance. Int J Pharm. 2014;477:564–77.

[62] Dong Y, Ng WK, Hu J, Shen S, Tan RBH. A continuous and highly effective static mixing process for antisolvent precipitation of nanoparticles of poorly water-soluble drugs. Int J Pharm. 2010;386(1-2):256–61.

[63] Hu J, Ng WK, Dong Y, Shen S, Tan RBH. Continuous and scalable process for water-redispersible nanoformulation of poorly aqueous soluble APIs by antisolvent precipitation and spray-drying. Int J Pharm. 2011;404(1-2):198–204.

[64] Lai F, Pireddu R, Corrias F, Fadda AM, Valenti D, Pini E, et al. Nanosuspension improves tretinoin photostability and delivery to the skin. Int J Pharm. 2013;458:104–9.

[65] Dalvi S V., Rajesh ND. Controlling Particle Size of a Poorly Water-Soluble Drug Using Ultrasound and Stabilizers in Antisolvent Precipitation. Ind Eng Chem Res. 2009;48:7581–93.

[66] Dhumal RS, Biradar S V., Yamamura S, Paradkar AR, York P. Preparation of amorphous cefuroxime axetil nanoparticles by sonoprecipitation for enhancement of bioavailability. Eur J Pharm Biopharm. 2008;70(1):109–15.

[67] Moorthi C, Kathiresan K. Fabrication of highly stable sonication as-

sisted curcumin nanocrystals by nanoprecipitation method. Drug Invent Today. 2013;5(1):66–9.

[68] Tran TT, Tran PH, Ngoc M, Nguyen U, Thi K, Tran M, et al. Amorphous isradipine nanosuspension by the sonoprecipitation method. Int J Pharm. 2014;474:146–50.

[69] Zhang X, Xia Q, Gu N. Preparation of All-Trans Retinoic Acid nanosuspensions using a modified precipitation method. Drug Dev Ind Pharm. 2006;32(7):857–63.

[70] He S, Yang H, Zhang R, Li Y, Duan L. Preparation and in vitro-in vivo evaluation of teniposide nanosuspensions. Int J Pharm. 2014;478(1):131–7.

[71] Dalvi S V, Yadav MD. Effect of ultrasound and stabilizers on nucleation kinetics of curcumin during liquid antisolvent precipitation. Ultrason Sonochem. 2015;24:114–22.

[72] Chiou H, Li L, Hu T, Chan HK, Chen JF, Yun J. Production of salbutamol sulfate for inhalation by high-gravity controlled antisolvent precipitation. Int J Pharm. 2007;331(1):93–8.

[73] Chen JF, Zhang JY, Shen ZG, Zhong J, Yun J. Preparation and characterization of amorphous cefuroxime axetil drug nanoparticles with novel technology: High-gravity antisolvent precipitation. Ind Eng Chem Res. 2006;45(25):8723–7.

[74] Zhang Z-L, Le Y, Wang J-X, Zhao H, Chen J-F. Development of stabilized itraconazole nanodispersions by using high-gravity technique. Drug Dev Ind Pharm. 2012;38:1512–20.

[75] Chen, X.a, Benhayoune, Z.a, Williams III, R.O.b , Johnston KP. Rapid dissolution of high potency itraconazole particles produced by evaporative precipitation into aqueous solution. J Drug Deliv Sci Technol. 2004;14:299–304.



[76] Chen X, Vaughn JM, Yacaman MJ, Williams RO, Johnston KP. Rapid dissolution of high-potency danazol particles produced by evaporative precipitation into aqueous solution. J Pharm Sci. 2004;93(7):1867–78.

[77] Sinswat P, Gao X, Yacaman MJ, Williams RO, Johnston KP. Stabilizer choice for rapid dissolving high potency itraconazole particles formed by evaporative precipitation into aqueous solution. Int J Pharm. 2005;302(1-2):113–24.

[78] Pace GW, Vachon MG, Mishra AK, Henrikson IB, Krukonis V. Processes to generate submicron particles of waterinsoluble compounds. US6177103 B1. 1999. p. 0–7.

[79] Thakur R, Gupta RB. Formation of phenytoin nanoparticles using rapid expansion of supercritical solution with solid cosolvent (RESS-SC) process. Int J Pharm. 2006;308(1-2):190–9.

[80] Thakur R, Gupta RB. Rapid expansion of supercritical solution with solid cosolvent (RESS-SC) process: formation of griseofulvin nanoparticles. Ind Eng Chem Res. 2005;44:7380–7.

[81] Pathak P, Meziani MJ, Desai T, Sun YP. Formation and stabilization of ibuprofen nanoparticles in supercritical fluid processing. J Supercrit Fluids. 2006;37(3):279–86.

[82] Young TJ, Mawson S, Johnston KP, Henriksen IB, Pace GW, Mishra A. Rapid Expansion from Supercritical to Aqueous Solution to Produce Submicron Suspensions of Water-Insoluble Drugs. Biotechnol Prog. 2000;16(3):402–7.

[83] Pathak P, Meziani MJ, Desai T, Foster C, Diaz JA, Sun Y-P. Supercritical Fluid Processing of Drug Nanoparticles in Stable Suspension. J Nanosci Nanotechnol. 2007;7:2542–5.

[84] Kim MS, Jin SJ, Kim JS, Park HJ, Song HS, Neubert RHH, et al. Preparation, characterization and in vivo evaluation of amorphous atorvastatin

calcium nanoparticles using supercritical antisolvent (SAS) process. Eur J Pharm Biopharm. 2008;69(2):454–65.

[85] Thiering R, Dehghani F, Foster NR. Current issues relating to anti-solvent micronisation techniques and their extension to industrial scales. J Supercrit Fluids. 2001;21(2):159–77.

[86] York P. Strategies for particle design using supercritical fluid technologies. Pharm Sci Technol Today. 1999;2(11):430–40.

[87] Foster N, Mammucari R, Dehghani F, Barrett A, Bezanehtak K, Coen E, et al. Processing pharmaceutical compounds using dense gas technology. Ind Eng Chem Res. 2003;42:6476–93.

[88] Chattopadhyay P, Gupta RB. Production of antibiotic nanoparticles using supercritical CO2 as antisolvent with enhanced mass transfer. Ind Eng Chem Res. 2001;40(16):3530–9.

[89] Thote AJ, Gupta RB. Formation of nanoparticles of a hydrophilic drug using supercritical carbon dioxide and microencapsulation for sustained release. Nanomedicine Nanotechnology, Biol Med. 2005;1(1):85–90.

[90] De Waard H, Hinrichs WLJ, Frijlink HW. A novel bottom-up process to produce drug nanocrystals: Controlled crystallization during freeze-drying. J Control Release. 2008;128:179–83.

[91] Hu J, Rogers TL, Brown J, Young T, Johnston KP, Williams RO. Improvement of dissolution rates of poorly water soluble APIs using novel spray freezing into liquid technology. Pharm Res. 2002;19(9):1278–84.

[92] Ali HSM, York P, Blagden N. Preparation of hydrocortisone nanosuspension through a bottom-up nanoprecipitation technique using microfluidic reactors. Int J Pharm. 2009;375(1-2):107–13.

[93] Ali HSM, York P, Ali AM a, Blagden N. Hydrocortisone nanosuspensions



for ophthalmic delivery: A comparative study between microfluidic nanoprecipitation and wet milling. J Control Release. 2011;149(2):175–81.

[94] De Waard H, Grasmeijer N, Hinrichs WLJ, Eissens AC, Pfaffenbach PPF, Frijlink HW. Preparation of drug nanocrystals by controlled crystallization: Application of a 3-way nozzle to prevent premature crystallization for large scale production. Eur J Pharm Sci. 2009;38:224–9.

[95] Hu J, Johnston KP, Williams RO. Spray freezing into liquid (SFL) particle engineering technology to enhance dissolution of poorly water soluble drugs: Organic solvent versus organic/aqueous co-solvent systems. Eur J Pharm Sci. 2003;20(3):295–303.

[96] Kipp JEW, Joseph CT, Doty MJ, Rebbeck CL. Microprecipitation method for preparing submicron suspensions. US Patent 6869617. 2001.

[97] Petersen R. Nanocrystals for use in topical formulations and method of production thereof. PCT/EP2007/009943. 2006.

[98] Möschwitzer J, Müller RH. Method and device for producing very fine particles and coating such particles, DE102005053862A1, PCT/EP2006/009930. 2005.

[99] Müller RH, Möschwitzer J. Methods and device for producing very fine particles and coating such particles, Patent, U.S., 20090297565. 2009.

[100] Möschwitzer J, Lemke A. Method for carefully producing ultrafine particle suspensions and ultrafine particles and use thereof. WO/2006/108637 (WIPO), DE102005017777A1 (German Patent). 2005.

[101] Möschwitzer J. Method for the production of ultra-fine submicron suspensions, DE102005011786A1, EP 1868573A2, W02006/094808. 2005.

[102] Salazar J, Müller RH, Möschwitzer JP. Application of the combinative particle size reduction technology H 42 to produce fast dissolving gliben-

clamide tablets. Eur J Pharm Sci. Elsevier B.V.; 2013;49(4):565–77.

[103] Li Y, Wang Y, Yue P-F, Hu P-Y, Wu Z-F, Yang M, et al. A novel high-pressure precipitation tandem homogenization technology for drug nanocrystals production — a case study with ursodeoxycholic acid. Pharm Dev Technol. 2014;19:662–70.

[104] Xu L-M, Zhang Q-X, Zhoub Y, Zhao H, Wang J-X, Chen J-F. Engineering drug ultrafine particles of beclomethasone dipropionate for dry powder inhalation. Int J Pharm. 2012;436:1–9.

[105] Shelar DB, Pawar SK, Vavia PR. Fabrication of isradipine nanosuspension by anti-solvent microprecipitation–high-pressure homogenization method for enhancing dissolution rate and oral bioavailability. Drug Deliv Transl Res. 2013;3:384–91.

[106] Morakul B, Suksiriworapong J, Leanpolchareanchai J, Junyaprasert VB. Precipitation-lyophilization-homogenization (PLH) for preparation of clarithromycin nanocrystals: Influencing factors on physicochemical properties and stability. Int J Pharm. 2013;457(1):187–96.

[107] Liu Y, Sun C, Hao Y, Jiang T, Zheng L, Wang S. Mechanism of dissolution enhancement and bioavailability of poorly water soluble celecoxib by preparing stable amorphous nanoparticles. J Pharm Pharm Sci. 2010;13(4):589–606.

[108] Liu D, Xu H, Tian B, Yuan K, Pan H, Ma S, et al. Fabrication of Carvedilol Nanosuspensions Through the Anti-Solvent Precipitation–Ultrasonication Method for the Improvement of Dissolution Rate and Oral Bioavailability. AAPS PharmSciTech. 2012. p. 295–304.

[109] Foldvari M. Non-invasive administration of drugs through the skin: challenges in delivery system design. Pharm Sci Technolo Today. 2000;3(12):417–25.

[110] Paudel KS, Milewski M, Swadley CL, Brogden NK, Ghosh P, Stinchcomb AL.



Challenges and opportunities in dermal/transdermal delivery. Ther Deliv. Future Science Ltd London, UK; 2010;1(1):109–31.

[111] Mitragotri S, Burke PA, Langer R. Overcoming the challenges in administering biopharmaceuticals: formulation and delivery strategies. Nat Rev Drug Discov. Nature Publishing Group, a division of Macmillan Publishers Limited. All Rights Reserved.; 2014;13(9):655–72.

[112] Proksch E, Brandner JM, Jensen J-M. The skin: an indispensable barrier. Exp Dermatol. 2008;17(12):1063–72.

[113] Van Smeden J, Janssens M, Gooris GS, Bouwstra JA. The important role of stratum corneum lipids for the cutaneous barrier function. Biochim Biophys Acta. 2014;1841(3):295–313.

[114] Bouwstra JA, Ponec M. The skin barrier in healthy and diseased state. Biochim Biophys Acta. 2006;1758(12):2080–95.

[115] Knorr F, Lademann J, Patzelt A, Sterry W, Blume-Peytavi U, Vogt A. Follicular transport route--research progress and future perspectives. Eur J Pharm Biopharm. 2009;71(2):173–80.

[116] Schoellhammer CM, Blankschtein D, Langer R. Skin permeabilization for transdermal drug delivery: recent advances and future prospects. Informa UK, Ltd. London; 2014;

[117] Sinico C, Fadda AM. Vesicular carriers for dermal drug delivery. Expert Opin Drug Deliv. Informa UK Ltd London, UK; 2009;6(8):813–25.

[118] Shegokar R, Müller RH. Nanocrystals: Industrially feasible multifunctional formulation technology for poorly soluble actives. Int J Pharm. 2010;399:129–39.

[119] Petersen RD. Nanocrystals for use in topical cosmetic formulations and method of production thereof. European Patent EP2099420, 2008.

[120] Romero GB, Chen R, Keck CM, Müller RH. Industrial concentrates of dermal hesperidin smartCrystals(®) - production, characterization & long-term stability. Int J Pharm. 2014;

[121] Mishra PR, Al Shaal L, Müller RH, Keck CM. Production and characterization of Hesperetin nanosuspensions for dermal delivery. Int J Pharm. 2009;371(1-2):182–9.

[122] Kobierski S, Ofori-Kwakye K, Müller RH, Keck CM. Resveratrol nanosuspensions for dermal application--production, characterization, and physical stability. Pharmazie. 2009;64(11):741–7.

[123] Mitri K, Shegokar R, Gohla S, Anselmi C, Müller RH. Lutein nanocrystals as antioxidant formulation for oral and dermal delivery. Int J Pharm. 2011;420(1):141–6.

[124] Piao H, Kamiya N, Hirata A, Fujii T, Goto M. A novel solid-in-oil nanosuspension for transdermal delivery of diclofenac sodium. Pharm Res. 2008;25:896–901.

[125] Ghosh I, Michniak-Kohn B. Influence of critical parameters of nanosuspension formulation on the permeability of a poorly soluble drug through the skin--a case study. AAPS PharmSciTech. 2013;14(3):1108–17.

[126] Patzelt A, Richter H, Knorr F, Schäfer U, Lehr C-M, Dähne L, et al. Selective follicular targeting by modification of the particle sizes. J Control Release. 2011;150(1):45–8.

[127] Lademann J, Richter H, Teichmann A, Otberg N, Blume-Peytavi U, Luengo J, et al. Nanoparticles--an efficient carrier for drug delivery into the hair follicles. Eur J Pharm Biopharm. 2007;66(2):159–64.

[128] Zhai X, Lademann J, Keck CM, Müller RH. Dermal nanocrystals from medium soluble actives - physical stability and stability affecting parameters. Eur J Pharm Biopharm. 2014;88(1):85–91.

# 3.Novel nanosized formulations of two diclofenac acid polymorphs to improve topical bioavailability



## 1. Introduction

Diclofenac (DCF) (Figure 1) is one of the most commercially successful non-steroidal anti-inflammatory drugs (NSAIDs), which was launched by Ciba–Geigy as a sodium salt oral formulation in 1973. As all NSAIDs, DCF exerts anti-inflammatory, analgesic and anti-pyretic actions via inhibition of the cyclooxygenase I (COX 1) and cyclooxygenase II (COX II) enzymes [1]. However, recent research indicates that the pharmacologic activity of DCF goes beyond COX inhibition and includes multimodal and, in some instances, novel mechanisms of action, such as inhibition of the thromboxane-prostanoid receptors or inhibition of lipoxygenase enzymes and activation of the nitric oxide-cyclic guanosine monophosphate pathway [2]. DCF is widely prescribed for the treatment of a variety of localized pain and inflammatory conditions including arthritis and soft tissue injuries. Although it is one of the best-tolerated NSAIDs, several systemic drawbacks often appear following chronic oral administration [3]. Therefore, a topical DCF formulation with improved skin permeation may be useful in the treatment of not only local skin inflammation but also inflammation and pain involving deeper structures such as bones, joints and muscles.

Since 1973, several pharmaceutical preparations have been developed for DCF application to the skin, and a variety of DCF salt products are currently available on the market. By contrast, because of its low water solubility, no DCF acid based commercial product exists. Indeed, even though this molecule possesses a good permeation rate due to its high lipophilicity, poor solubility causes a slow release rate from the formulation which in turn limits the penetration and permeation of an effective drug concentration into and through the skin. The final result is low dermal drug bioavailability. In order to overcome the slow dissolution rate of such drugs, various approaches have been studied such as the

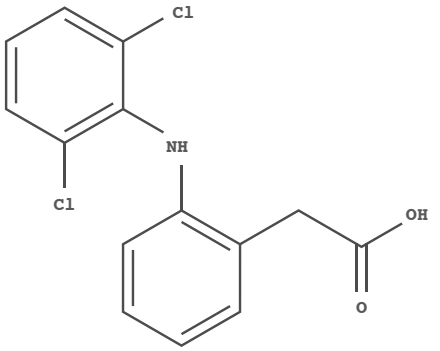


**Figure 1** Diclofenac acid (DCF) structure



use of surfactants, co-solvents, inclusion and complexation compounds. These approaches have been related to different side effects including skin irritation and can be only used for drugs having specific characteristics (sufficient solubility in lipophilic excipients, appropriate shape and molecular size for incorporation in cyclodextrin etc.) [4].

An alternative to such methods is the nanonization of pure drug crystals with the preparation of the so-called nanocrystals (100-1000 nm), one of the most interesting drug delivery technologies of the last twenty years.

Nanocrystals are prepared as a suspension (nanosuspension) in an outer liquid phase, usually water but also water miscible liquids or non-aqueous media. Nanosuspensions are stabilized using ionic stabilizers (sodium dodecyl sulfate, lecithin, etc.) or non-ionic surfactants (Pluronic® surfactants, polyethylene glycol, Tween 80, polyvinylpyrrolidone, cellulose polymers, etc.).

Fundamentally, nanosuspensions can be prepared by bottom up or top down technologies or by a combination of both [5]. In the bottom up technology, the low water soluble drugs are (molecularly) dissolved in a solvent and then precipitated in different ways as nanocrystals in a surfactant solution [6]. The top down technology is based on particle disintegration techniques including beads wet milling (Ghosh et al., 2012; Merisko-Liversidge et al., 2003) and high pressure homogenization [10,11].

Nanosuspensions have been studied for different routes of administration; however, the oral one has been the most studied because of the improved clinical efficacy, the main advantages being enhanced bioavailability, reduced fed/fasted state and subject variability. Therefore, the currently approved and marketed nanocrystal based products are mainly for oral administration [12].

Until now, the use of nanocrystals for dermal applications has not been inten-

sively studied and only a few articles regarding this topic have been published [13–16]. However, this technology could be very effective for improving dermal bioavailability of lipophilic substances with good skin permeability, such as DCF acid.

The aim of the present investigation was to study the ability of nanocrystal technology to improve the dermal bioavailability of the poorly water-soluble drug DCF acid. In order to investigate the role of the nanocrystal polymorphic structure in cutaneous bioavailability, two different DCF acid polymorphic forms (HD1 and HD2) were used to prepare nanosuspensions using a wet media milling technique with poloxamer 188 as a stabilizer.

Characterization of DCF nanosuspensions was carried out by different techniques: scanning electron microscopy (SEM), differential scanning calorimetry (DSC), X-ray powder diffractometry and photon correlation spectroscopy (PCS). The efficacy of the nanocrystals in improving dermal drug bioavailability was evaluated by *in vitro* skin penetration and permeation studies using Franz diffusion vertical cells and newborn pig skin, in comparison with DCF coarse suspension and a commercial topical formulation containing diclofenac sodium.

## 2. Experimental

### 2.1 Materials

Diclofenac sodium salt (DCF-Na) was purchased from Galeno (Comeana, Italy). Lutrol® F68 (Poloxamer 188) was a gift from BASF AG (Ludwigshafen, Germany). DCFNa commercial formulation, Diclofenac Sandoz® gel 1% is produced by Sandoz S.p.a. (Origgio, Varese, Italy). All the other compounds were of analytical grade and used as received from Sigma–Aldrich (Milan, Italy).

### 2.2. Preparation of DCF acid crystal forms

HD2 DCF acid crystal form was obtained following the procedure reported in a previous work [17]. Briefly, a saturated aqueous solution of diclofenac sodium salt was acidified with diluited HCl until a white precipitate of DCF acid was observed. The precipitate was filtered, washed with bidistilled water to remove residual HCl and dried at 40°C overnight. Starting from HD2 DCF satured solution in dimethyl sulfoxide (DMSO), HD1 DCF acid crystal form was obtained by precipitation with bidistillated water. The precipitate was washed with the minimum amount of bidistilled water and after several cycles of centrifugation was dried at 40 °C overnight.



### 2.3. Preparation of coarse suspensions

Coarse drug suspensions were prepared dispersing HD1 or HD2 DCF acid bulk powder in Poloxamer 188 bidistilled water solution using an Ultra Turrax T25 basic (IKA, Werke) for 2 min at 6500 rpm. DCF acid coarse suspensions were prepared using both the same drug amount of the commercial gel formulation (0.0031 mol/100g, CS HD1 I and CS HD2 I) and the double amount (0.0062 mol/100g, CS HD1 II and CS HD2 II). Drug/surfactant ratio (w/w) was 2:1 (Table 1).

### 2.4. Preparation of nanosuspensions

Nanosuspensions were prepared using a wet media milling technique. Drug bulk powder (HD1 or HD2) was dispersed in aqueous Poloxamer 188 solution using an Ultra Turrax T25 basic for 5 min at 6500 rpm (Table 1)This coarse suspension was divided in 1.5 ml conical microtubes containing about 0.4 g of 0.1-0.2 mm yttrium-stabilized zirconia-silica beads (Silibeads® Typ ZY Sigmund Lindner, Germany). The microtubes were oscillated at 3000 rpm for different times using a beads-milling cell disruptor equipment (Disruptor Genie®, Scientific Industries, USA). The obtained nanosuspensions of each microtubes were gathered and then separated from the milling beads by sieving.

DCF acid nanosuspensions were prepared using both the same drug amount of the commercial gel formulation (0.0031 mol/100g, NS HD1 I and NS

HD2 I) and the double amount (0.0062 mol/100g, NS HD1 II and NS HD2 II). Drug/surfactant ratio (w/w) was 2:1 (Table 1).

**2.5. Solubility studies**

DCF acid solubility was measured for both HD1 and HD2 bulk powders, coarse suspensions and nanosuspensions. Formulations were kept under constant stirring for 48 h in a thermostated bath at 37 °C. At preselected time intervals, samples were withdrawn and centrifuged. 0.2 ml of the clear supernatant was diluted with methanol and analyzed by HPLC for DCF content. Solubility studies were performed in triplicate.

**2.6. HPLC analysis**

DCF content was quantified at 280.4 nm using a chromatograph Alliance 2690 (Waters, Milan, Italy), equipped with a photodiode array detector and a computer integrating apparatus (Empower 3). The column was a SunFire C18 (3.5 $\mu$m, 4.6 mm × 100 mm, Waters), and the mobile phase was a mixture of 30% water and 70% acetonitrile (v/v), delivered at a flow rate of 0.7 ml/min.
A standard calibration curve was built up by using working standard solutions. Calibration graphs were plotted according to the linear regression analysis, which gave a correlation coefficient value (R2) of 0.999.

**2.7. Particle size analysis**

Average diameter and polydispersity index (PI, as a measure of the size distribution width) of the samples were determined by photon correlation spectroscopy (PCS) using a Zetasizer nano (Malvern Instrument, Worcestershire, United Kingdom). Samples were backscattered by a helium-neon laser (633 nm) at an angle of 173° and a constant temperature of 25°C. Zeta potential was estimated using the Zetasizer nano by means of the M3-PALS (Phase Analysis Light Scattering) technique. Just before the analysis, DCF nanosuspensions were diluted with distilled water. Nanocrystals average diameter and PI were monitored over 90 days storage at room temperature to check nano formulation physical stability.



**2.8. Differential scanning calorimetry**

Differential scanning calorimetry (DSC) was performed with PerkinElmer DSC7 instrument, under a pure argon flux and with a heating rate of 10 °C/min in the temperature range from 30 °C to 190 °C. Each sample was accurately weighted (1–2 mg) in an aluminum pan, crimped and sealed. Temperature calibration was obtained using palmitic acid and indium before and after each measurement. At least three different measurements were made for each sample and average values of Tpeak (peak maximum) and Tonset (extrapolated onset temperature) were reported.

**2.9. X-ray powder diffractometry**

X-ray diffraction powder (XRDP) patterns were collected with a SeifertX3000 diffractometer operating at 35 mA and 40 kV using Cu Ka radiation and equipped with a graphite monochromator on the diffracted beam. XRDP patterns were recorded in step scan mode in the range 3° ≤2J ≤45° with step size 0.05 2J degree, collecting at least 1000 counts for each step. The divergence and receiving slits were chosen in order to ensure a high resolution mode for the crystalline phases. Attention was paid in the sample preparation in order to minimize preferred orientation. Average crystalline size was estimated by Scherrer equation where the integral breadth was corrected for instrumental broadening. The instrumental profile broadening was derived from the fitting of XRDP data obtained from standard samples.

**2.10. Scanning electron microscopy (SEM)**

The morphology of pure HD1 and HD2 bulk powder and nanosuspensions was evaluated using scanning electron microscopy (SEM) (S-4100, HITACHI). The samples were fixed on a brass stub using carbon double-sided, coated with gold blazers SCD 004 sputter coater for 2 minutes and observed under an

excitation voltage of 10 kV.

**2.11. *In vitro* skin penetration and permeation studies**

Experiments were performed on newborn pig skin using Franz vertical cells with an effective diffusion area of 0.785 $cm^2$, under non-occlusive conditions. One-day-old Goland–Pietrain hybrid pigs (~1.2 kg) were provided by a local slaughterhouse. The skin, stored at –80 °C, was pre-equilibrated in saline (0.9% w/v of NaCl) at 25 °C. Skin specimens (n = 6 per formulation) were sandwiched between donor and receptor compartments. The receptor was filled with 5.5 ml of saline, continuously stirred and thermostated at 37 ± 1 °C to reach the physiological skin temperature (i.e. 37 ± 1°C). HD1 and HD2 nanosuspensions, coarse suspensions and the commercial gel formulation (Diclofenac Sandoz® gel 1%) were placed onto the skin surface. Experiments were carried out using DCF acid nanosuspensions and coarse suspensions with both the same drug amount of the commercial gel formulation (3.1 μmoles) and the double amount (6.2 μmoles). At regular intervals, up to 8 h, the receiving solution was entirely withdrawn, replaced with pre-thermostated (37 °C) fresh saline to ensure sink conditions and analysed by HPLC for drug content. After 8 h, the skin surface was gently washed (3 times) with 1 ml of distilled water, then dried with filter paper. The stratum corneum (SC) was removed by stripping with adhesive tape Tesa®AG (Hamburg, Germany). Each piece of the adhesive tape was firmly pressed on the skin surface and rapidly pulled off with one fluent stroke. Epidermis was separated from dermis with a surgical scalpel. Tape strips, epidermis and dermis were cut, placed each in a flask with methanol and sonicated for 4 min in an ice bath to extract the drug. The tapes and tissue suspensions were filtered out and assayed for drug content by HPLC.

**2.12 Statistical analysis of data**



Data analysis was carried out with the software package R, version 2.10.1. Results are expressed as the mean ± standard deviation. Multiple comparisons of means (Tukey test) were used to substantiate statistical differences between groups, while Student's t-test was used for comparison between two samples. Significance was tested at the 0.05 level of probability (p).

**3. Results and Discussion**

**3.1. Preparation and characterization of DCF acid nanosuspensions**

In this study, four different DCF acid nanosuspensions were prepared, characterized and tested as (trans)dermal drug delivery systems in comparison with the corresponding coarse suspensions and a commercial cream containing diclofenac sodium.

As shown in Table 1, the nanosuspension formulations, which were prepared by the wet media milling process, contained both DCF acid crystal forms, HD1 or HD2, at two different concentrations. These DCF acid concentrations, 0.92% and 1.84% (w/w), were selected in order to obtain coarse suspensions and nanosuspensions with the same (0.0031 mol/100g) or double (0.0062 mol/100g) the DCF molarity of the DCFNa commercial formulation used as control. Poloxamer 188 was chosen as the stabilizer since it is a generally recognized as safe (GRAS) excipient, biocompatible and, therefore, suitable for dermal applications. The drug/stabilizer ratio was kept constant at 2:1 w/w, which, according to our previous research [17], had shown high stability when nanosuspension formulations were prepared with this drug/poloxamer 188 ratio.

Preliminary tests were carried out to determine the appropriate operative conditions for nanosuspension preparation. In particular, average diameter and PI modifications were studied as a function of the milling time. As shown in Figure 2, after 10 minutes of milling at 3000 rpm, the mean size of all formulations significantly decreased, reach-

**Table 1** Composition of HD1 and HD2 coarse suspension (CS HD2 II, CS HD2 I, CS HD1 II, CS HD1 I) and nanosuspension formulations (NS HD2 II, NS HD2 I, NS HD1 II, NS HD1 I

| Components (% w/w) | Formulations | | | |
|---|---|---|---|---|
| | NS HD1 I (CS HD1 I) | NS HD1 II (CS HD1 II) | NS HD2 I (CS HD 2 I) | NS HD2 II (CS HD2 II) |
| HD1 | 0.92 | 1.84 | - | - |
| HD2 | - | - | 0.92 | 1.84 |
| Poloxamer 188 | 0.46 | 0.92 | 0.46 | 0.92 |
| Water | 98.62 | 97.24 | 98.62 | 97.24 |

**Table 2** Average diameter (Z-AVE), polydispersity index (PI) and Zeta potential (ZP) of HD1 and HD2 freshly prepared nanosuspensions. Each value is the mean ± standard deviation of at least six experimental determinations.

| | Z-AVE (nm) | PI | ZP (mV) |
|---|---|---|---|
| NS HD1 I | 315± 5 | 0.25 ± 0.10 | -35 |
| NS HD1 II | 284 ± 6 | 0.20 ± 0.04 | -35 |
| NS HD2 I | 279 ± 8 | 0.17 ± 0.01 | -35 |
| NS HD2 II | 304 ± 4 | 0.23 ± 0.04 | -39 |



ing a mean diameter below 1 μm. By increasing the milling duration, all formulations showed both size and PI values reduction. In particular, formulations containing 0.92% (w/w) DCF (either HD1 or HD2) required 60 minutes to reach the minimal value in mean diameter and an acceptable homogeneity.

When the concentration of the drug was doubled (1.84% w/w), the milling time required to reach the smallest size was 70 minutes. Increasing the milling time further did not result in additional reduction of the nanocrystal size. In light of these results, nanosuspensions were prepared using the following operating conditions: 60 or 70 minutes of milling time at 3000 rpm for 0.92% (0.0031 mol/100g) or 1.84% (0.0062 mol/100g) drug concentration, respectively.

Table 2 reports the PCS measurements of the freshly prepared HD1 and HD2 nanosuspensions. No significant differences were found between average particle diameters in formulations prepared with the two polymorphic forms, thus indicating that this factor did not influence the particle dimensions of the studied nanosuspensions. Freshly prepared formulations exhibited a mean diameter ranging between 279 e 315 nm and a PI lower than 0.25. Formulation NS HD2 I (HD2, 0.0031 mol/100g) showed the lowest mean size and PI values (279 nm and 0.17 PI). The zeta potential values were highly negative (-35 mV).

The stability of the nanosuspension was evaluated by monitoring the size distribution during 90 days of storage at room temperature (~25 C). As shown in Figure 3, particle size and PI values of all the studied nanosuspensions increased after 90 days of storage, except NS HD2 I. An increase in size of ~40%, ~50% and ~60% was observed for formulation NS HD1 I, NS HD1 II and NS HD2 II, respectively. By contrast, formulation NS HD2 I, with the smallest initial values, retained similar mean diameter and PI values during the 90 days of storage (~315 nm and 0.19 PI). The morphological changes of HD1

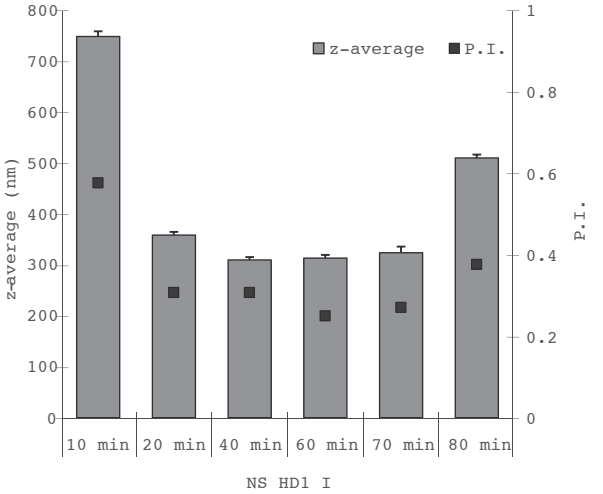


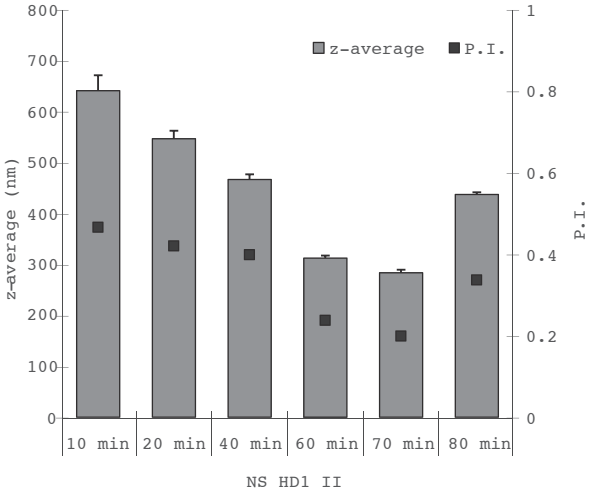


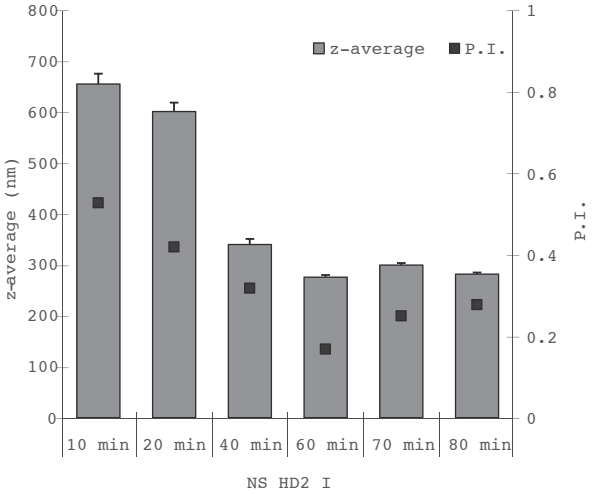


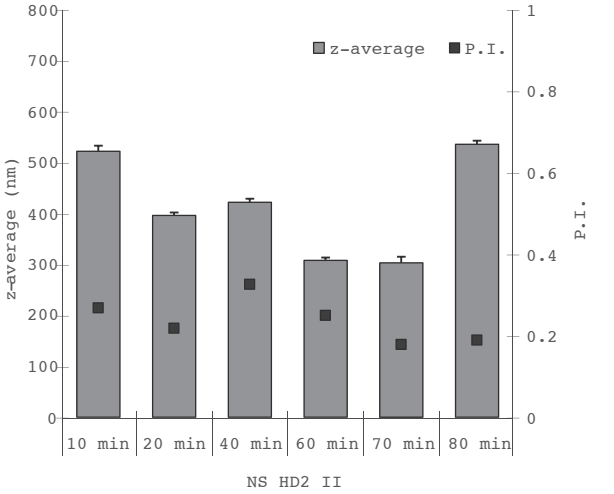


**Figure 2** Average diameter (Z-average) and polydispersity index (PI) of nanosuspension formulations as function of milling time.

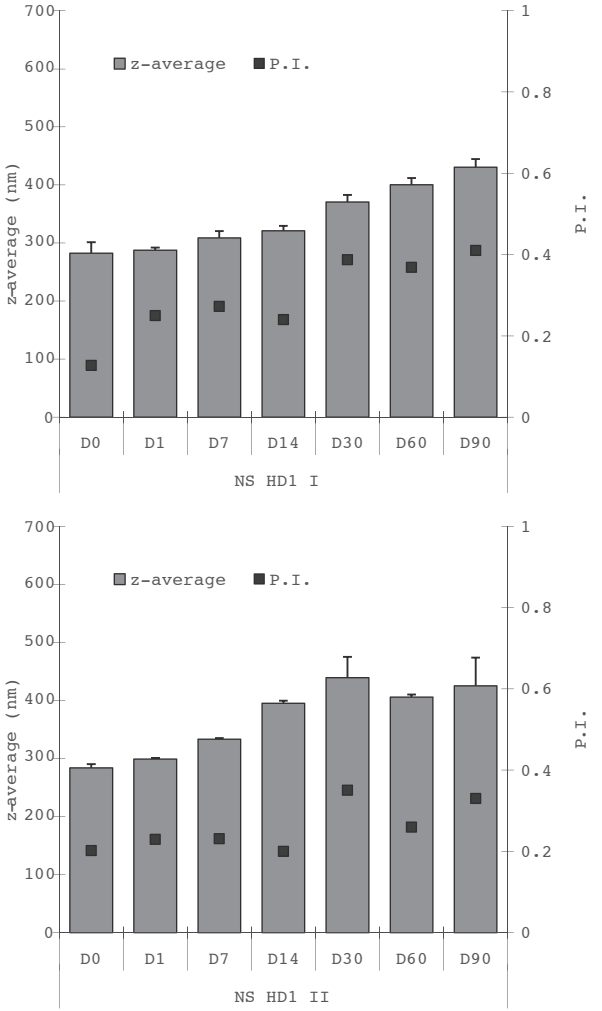


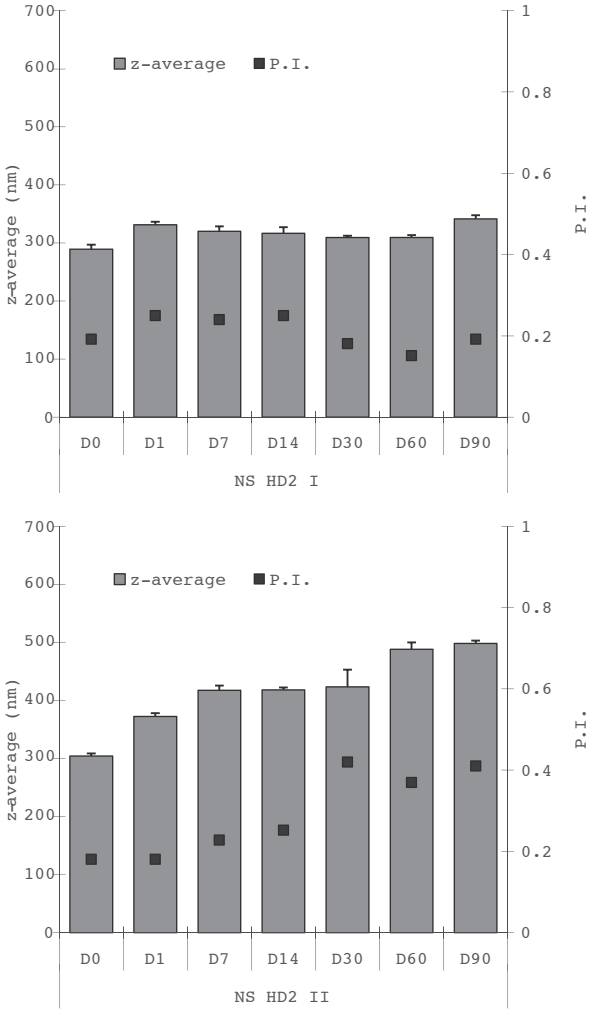


**Figure 3** Average diameter (Z-average) and polydispersity index (PI) of nanosuspension formulations monitored during 90 days of storage at room temperature.

and HD2 crystals after the milling process were evaluated by SEM imaging. As seen in Figure 4, the milling process modified both the shape and size of HD1 and HD2 crystals. In the milling process, high shear forces are generated during collision of the drug crystals with the yttrium-stabilized zirconia-silica beads and with the wall of the tubes, which provide the energy to break the drug crystals down to the nanometer range. Before milling, raw drug material (Figure 4a) had large crystals with a regular elongated shape. After milling, in the presence of stabilizers, the large HD1/HD2 crystals were reduced into nanocrystals, with angular surfaces much smoother and rounded (Figure 4b-c). The size of the nanocrystals shown in the SEM images are well in accordance with the results obtained by PCS, which demonstrated that the particle size of the nanosuspensions were approximately 100 times smaller (0.3-0.5 $\mu$m) than that of HD1 or HD2 coarse powders (10-50 $\mu$m).

X-ray diffraction powder (XRDP) spectra of yttrium-stabilized zirconia-silica beads, poloxamer 188, bulk HD1 and bulk HD2 are reported in Figure 5. The diffraction pattern of poloxamer 188 is typical of crystalline polymeric materials and is characterized by a peak around 19° 2$\theta$ and a second broader peak centered at 23° 2$\theta$ (Figure 5). XRDP spectra of yttrium-stabilized zirconia-silica beads exhibit Bragg peaks due to the crystalline yttrium and zirconium oxide mixtures with the strongest lines centered around 30.25° and 26.72° 2$\theta$ degree. The X-ray powder diffraction patterns of bulk HD1 and HD2, are those expected on the base of their structures: monoclinic P21/c and monoclinic C2/c crystal structures, respectively [18]. No peaks due to HD1 are present in the HD2 spectrum and vice versa. Peaks with Miller index (111/012), (111) (102), and (200) are used as fingerprints to characterize this phase. Moreover, no peaks due to HD3 polymorphic form are detectable in both HD1 and



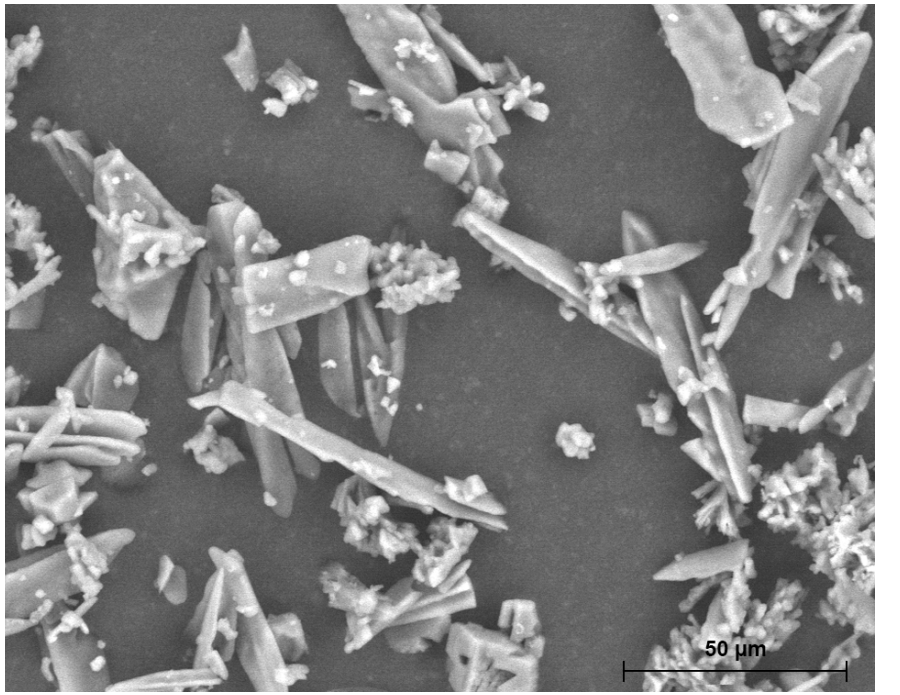


**Figure 4.a.** SEM images of HD1 raw material.

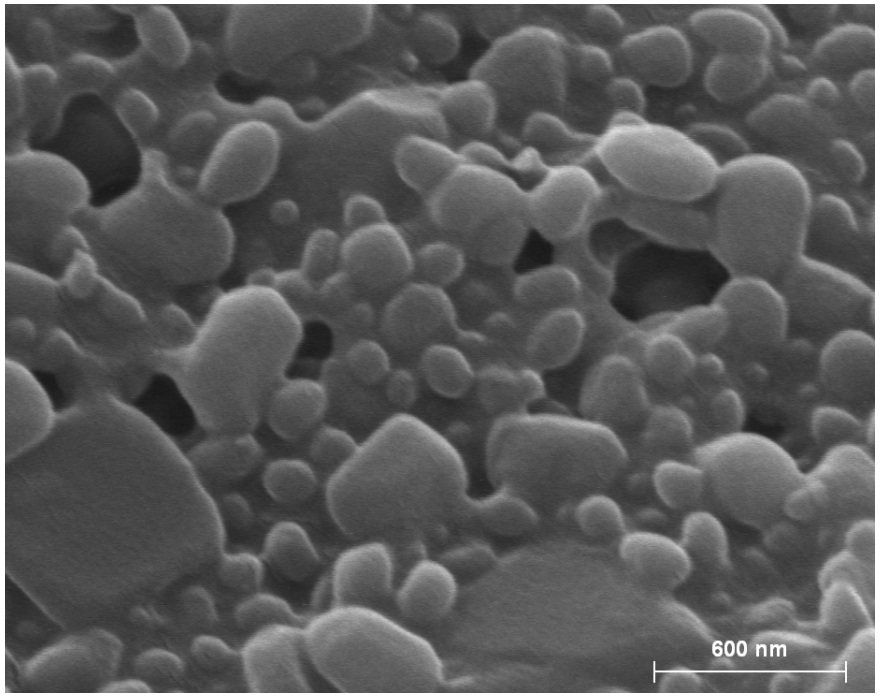


**Figure 4.b.** SEM images of HD1 nanosuspension.



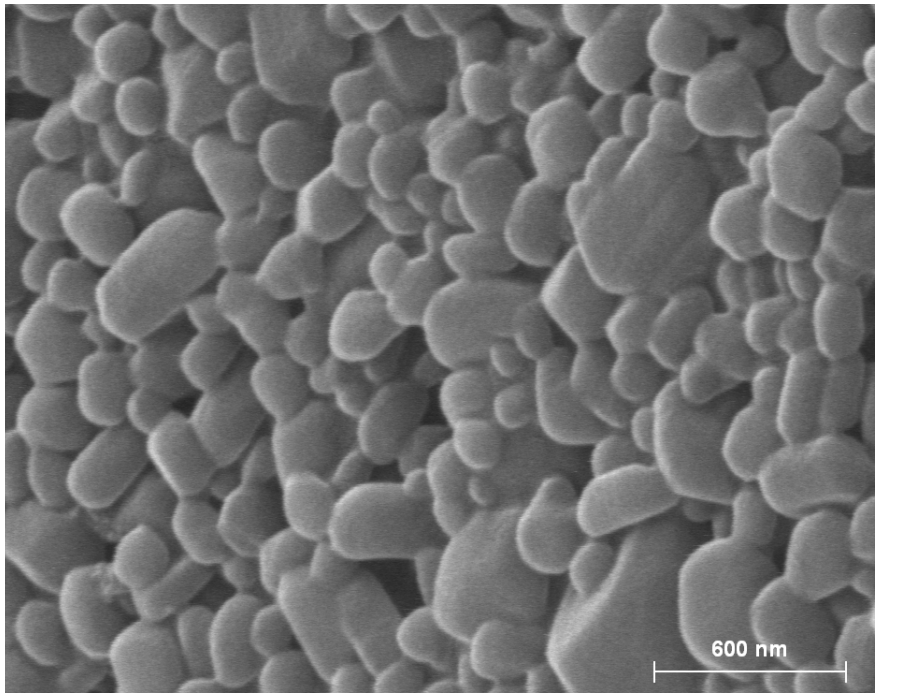


**Figure 4.c.** SEM images of HD2 nanosuspension.

HD2 spectra, thus, indicating that the media milling process does not modify the DCF polymorphic form.

In the XRDP spectra of HD1 and HD2 nanosuspensions, typical peaks due to poloxamer 188 are visible (peaks around 19° and 23° 2θ) while no peaks due to yttrium-stabilized zirconia-silica are present. Therefore, this is a clear sign that no trace of yttrium-stabilized zirconia-silica beads contaminated the nanosuspension during the preparation process. Moreover, in all these spectra, relative peak intensities show the same trend of bulk samples (Figure 5b) even if the peaks are broader as a result of the lower particle size. Indeed, the average diameter values, calculated according to the Scherrer equation [19], are in the range of 65–90 nm. Nevertheless, we cannot exclude a partial contribution of structural disorder as the cause of the peak broadening. In more detail, XRDP spectra of the HD1 nanosuspensions show that peaks due to HD1 phase are slightly wide, hence, indicating crystalline size around 90 nm. On the other hand, the spectra of the HD2 nanosuspensions show that the HD2 phase peaks are wider than those of the HD1 nanosuspensions, thus, indicating a narrower crystalline size around 65 nm.

In conclusion, the XRDP analysis confirmed that the different HD1 and HD2 bulk powder retain their polymorphic form in the prepared nanosuspensions.

Differential scanning calorimetry (DSC) thermograms of the different components and formulations are reported in Figure 6. Bulk HD2 and HD1 thermograms are characterized by a sharp endothermic peak followed by sample decomposition (Figure 6) [20]. In the thermograms of all nanosuspensions, the poloxamer endothermic melting peak, around 50°C, is always present. Tpeak and Tonset values of the bulk polymorphs and nanosuspension formulations are reported in Table 3. Bulk HD2 sample melted at a temperature slightly lower (Tpeak 177.9 °C) than that of the bulk HD1 (Tpeak 179.0 °C). Thermograms



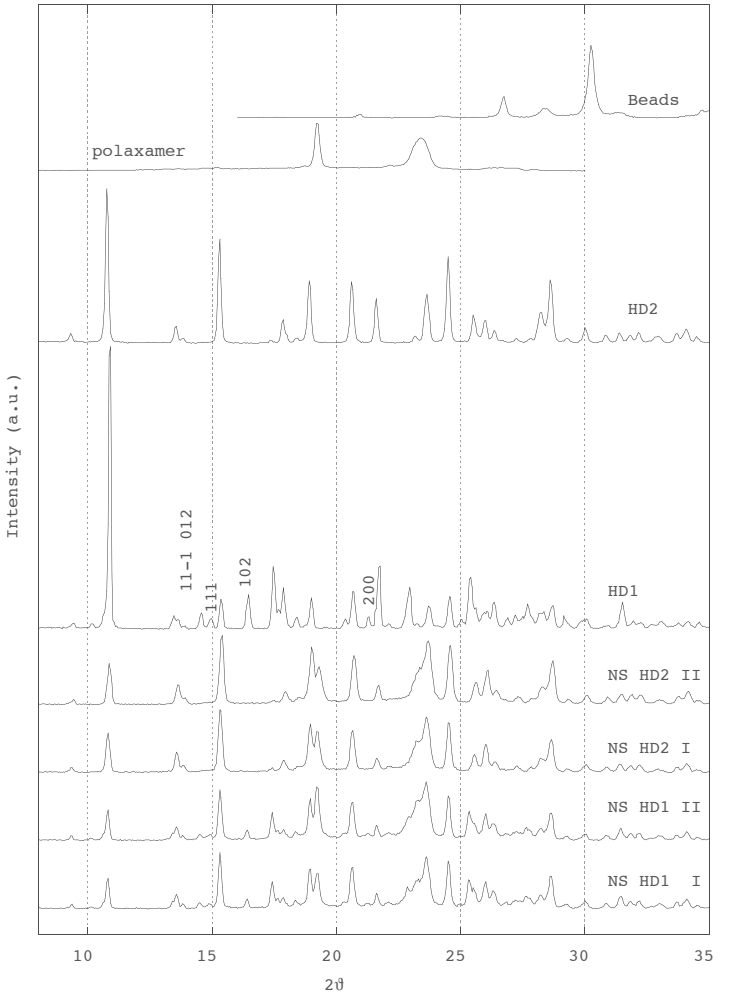


**Figure 5** XRD spectra of Yttrium-stabilized zirconia-silica beads (beads), poloxamer, bulk HD2 and HD1 and nanosuspensions (NS HD2 II, NS HD2 I, NS HD1 II, NS HD1 I).

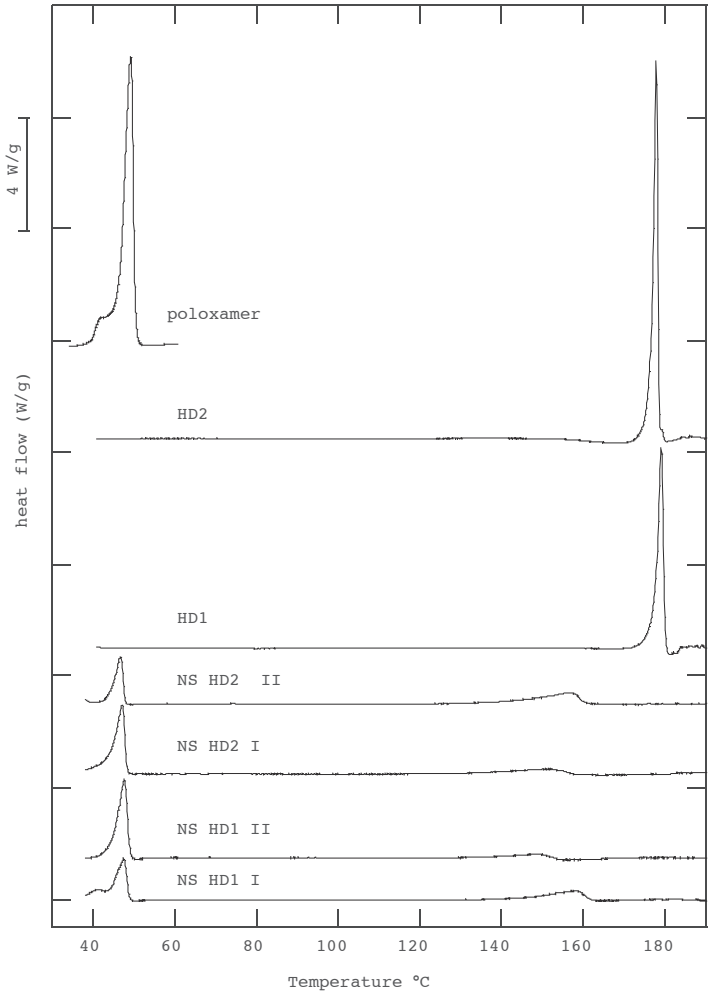


**Figure 6** DSC thermograms of poloxamer, bulk HD2 and HD1 and nanosuspensions (NS HD2 II, NS HD2 I, NS HD1 II, NS HD1 I).



of the four nanosupensions are very similar and they are all characterized by a broad peak with Tpeak centered around 148-158°C. This behavior, lower Tpeak and broader peak compared to that of bulk powders, is in agreement with the Van't Hoff equation [21] and is expected for mixtures like nanosuspensions. Slight differences in Tpeak (and Tonset) of the nanosuspension formulations can be due to the slight differences in the average particle size and PI, in agreement with the XRDP results.

### 3.2. *In vitro* skin penetration and permeation studies

To evaluate the effect of the reduced crystal size on dermal and transdermal delivery of DCF, *in vitro* penetration and permeation studies through newborn pig skin were carried out in non occlusive conditions using Franz diffusion cells. Coarse suspensions of both DCF crystal forms (HD1 and HD2) and a commercial gel formulation were used as control. Figure 7 shows the % of DCF moles delivered to and accumulated in the skin strata for nanosuspensions, coarse suspensions and commercial formulation prepared using the same DCF molar concentration (0.0031 mol/100g), after an 8 h experiment. As shown in Table 4, nanosuspensions enhanced DCF skin delivery compared to the coarse suspension and commercial gel formulation, which showed the lowest drug delivery into and through the newborn pig skin. In particular, nanosuspensions enhanced DCF skin accumulation by a factor of 12 over DCFNa commercial gel formulation (Table 4).
Indeed, as reported in Figure 7, after application of the gel formulation, drug deposition into the skin was only 1.38% in the stratum corneum, 1.15% in the epidermis and 0.31% in the dermis. Also, the application of nanosuspensions and coarse suspensions always gave the higher accumulation of DCF in the stratum corneum. In particular, HD1 and HD2 nanosuspensions produced a drug accumulation in the SC approximately 16 times higher than the commercial gel and 7

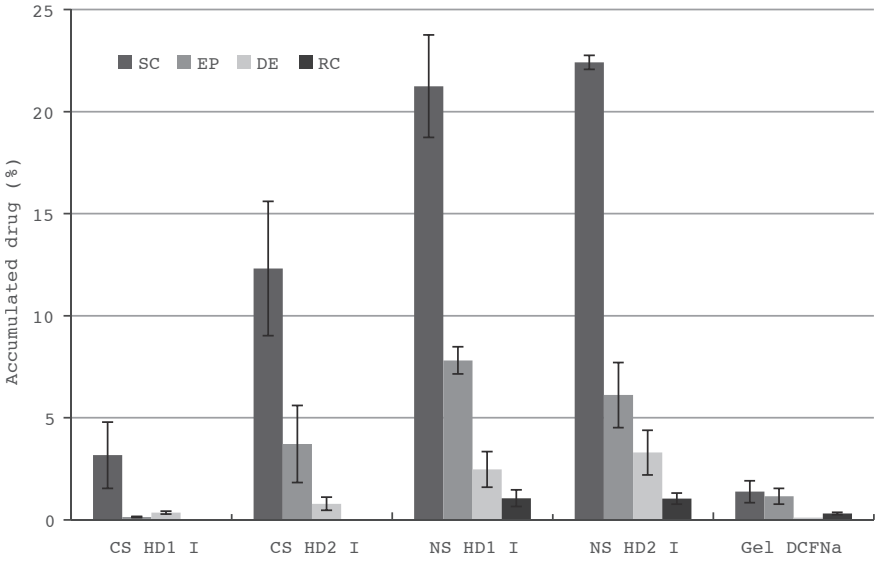


**Figure 7** Cumulative amount of DCF retained into and permeated through pig skin layers after 8 h application of HD1 and HD2 nanosuspensions (NS, 0.0031 mol/100g) in comparison with HD1 and HD2 coarse suspensions (CS, 0.0031 mol/100g) and Diclofenac Sandoz® gel 1% (0.0031 mol/100g). SC, stratum corneum; Ep, epidermis; D, dermis; and RC, receptor compartment.



**Table 4** Amount of accumulated and permeated drug ($\mu$mol/cm$^2$), total drug delivered (%), Local Accumulation Efficiency (LAC) values: drug accumulated into the skin/drug delivered through the skin ratio, steady-state flux (J $\mu$mol/cm$^2$/h), lag time (h) after 8 h in vitro diffusion experiments of DCF nanosuspensions in comparison with DCF coarse suspensions and Diclofenac Sandoz® gel 1%. Values are the means ± standard deviation (n = 6).

| Sample | Accumulated drug ($\mu$mol/cm$^2$±SD) | Permeated drug ($\mu$mol/cm$^2$±SD) | Total drug delivered (%) | LAC | Lag time (h) | J ($\mu$mol/cm$^2$/h±SD) |
|---|---|---|---|---|---|---|
| Gel $DCF_{Na}$ | 0.11±0.038 | 0.01±0.002 | 2.9 | 8.6 | 2.3 | 0.002±0.0003 |
| CS HD1 I | 0.16±0.074 | - | 3.7 | - | - | - |
| CS HD1 II | 0.24±0.043 | - | 2.8 | - | - | - |
| CS HD2 I | 0.72±0.167 | - | 16.8 | - | - | - |
| CS HD2 II | 0.72±0.224 | - | 8.37 | - | - | - |
| NS HD1 I | 1.05±0.134 | 0.04±0.014 | 33.6 | 27.3 | 2.0 | 0.005±0.0017 |
| NS HD1 II | 1.16±0.060 | 0.03±0.003 | 16.0 | 42.9 | 2.0 | 0.003±0.0004 |
| NS HD2 I | 1.16±0.111 | 0.04±0.010 | 32.9 | 30.4 | 2.2 | 0.005±0.0012 |
| NS HD2 II | 1.15±0.092 | 0.03±0.008 | 15.9 | 42.4 | 2.5 | 0.003±0.0009 |

and 2 times higher than the corresponding coarse suspensions. In addition, nanosuspensions were able to improve DCF deposition, with respect to coarse suspensions, in the epidermis and dermis, where they reached 7.8% (NS HD1 I) and 6.1% (NS HD2 I) in the epidermis and 2.5% (NS HD1 I HD1) and 3.3% (NS HD2 I) in the dermis.

These outcomes indicate that DCF crystal size plays an important role in the ability of the drug to penetrate the stratum corneum barrier, due to the increased saturation solubility and dissolution rate of the nanocrystals, according to the Kelvin and Noyes–Whitney equations [22]. This leads to an increased concentration gradient between formulation and skin, thus enhancing drug penetration in comparison with the coarse suspension. DCF acid solubility values of HD1 and HD2 raw material, coarse and nanosuspension are reported in Table 5. HD1 and HD2 raw material showed a similar solubility value of approximately 20 $\mu$g/ml. The presence of the surfactant increased the water solubility of both HD1 and HD2 in the coarse suspension (~35 $\mu$g/ml). The size reduction from DCF coarse crystals to nanocrystals further increased the DCF water solubility that increased to approximately 90 $\mu$g/ml.

In this study, the results of the transdermal experiments emphasize the influence of drug solubility on the ability of a poorly soluble drug to cross the skin and accumulate in the deeper skin layers.

In particular, we found that a reduction of approximately 100 times in size and an increase of approximately 3 times in solubility were obtained by producing nanocrystals, which led to a total skin accumulation of DCF 4 times higher than the coarse suspensions.

When coarse DCF is transformed into nanocrystals, drug saturation solubility increases, namely the DCF acid molecules in solution in equilibrium with the solid phase increases. These molecules are more lipophilic than the hydrophilic derivative (DCF-Na) and, therefore, afford increased penetration into the skin. DCF molecules dissolve quickly from the nanocrystals, which act as a depot in the water phase, and rapidly replace the DCF molecules penetrated from the water phase into the skin.

Furthermore, Table 4 and Figure 7 show that the two DCF crystal forms, HD1 and HD2, display different behavior when applied as large crystals (coarse suspension). In fact, HD2 coarse suspensions (CS HD2 I) resulted in a higher accumulation into the skin strata compared with the HD1 coarse suspension (CS HD1 I). By contrast, the release profiles and the skin deposition of the two nanosuspensions (NS HD1 I and NS HD2 I) were very similar, thus, demonstrating that the two crystal polymorphs, HD1 and HD2, behave in the same manner when applied as nanocrystals.

A useful dimensionless parameter that allows for the evaluation and comparison of different topical carriers is local drug accumulation efficiency (LAC). In our experiment, LAC values can easily be obtained as the ratio of DCF accumulated in the skin versus DCF delivered through the skin. LAC values obtained for the different applied formulations are listed in Table 4. The LAC value of both nanosuspensions was higher by a factor of 3.2–3.5 compared to the commercial gel formulation, suggesting that the main effect of nanocrystals was to increase the drug accumulation in the skin.

In order to understand the relationship between the amount of drug applied on the skin surface and the amount of drug actually accumulated or permeated, HD1 and HD2 nanosuspensions and coarse suspensions were also prepared using a double amount of DCF (0.0062 mol/100g) than that of commercial gel. In Figure 8, the cumulative amount of DCF recovered from the different skin strata is reported as the mean amount of drug per unit of surface area ($\mu$g/cm$^2$) after application of all the prepared formulations. As shown, when the same volume of suspension (coarse or na-

nosuspension) but with a double amount of the drug was applied, neither the accumulation nor the permeation of the drug was increased. Doubling the nanocrystal solid phase does not affect drug skin penetration and permeation because the DCF saturation solubility remain constant.



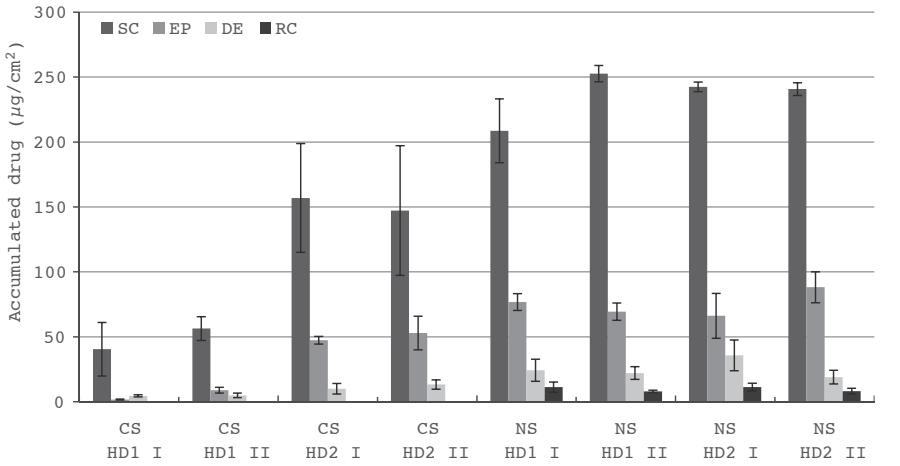


**Figure 8** Cumulative amount of DCF retained into and permeated through pig skin layers after 8 h application of nanosuspensions (NS) or coarse suspensions (CS) of HD1 and HD2 at two different concentrations: 0.0031 mol/100g (I) and 0.0062 mol/100g (II) SC, stratum corneum; Ep, epidermis; D, dermis; and RC, receptor compartment.

## References

[1] Warner TD, Giuliano F, Vojnovic I, Bukasa A, Mitchell JA, Vane JR. Nonsteroid drug selectivities for cyclo-oxygenase-1 rather than cyclo-oxygenase-2 are associated with human gastrointestinal toxicity: A full in vitro analysis. Proc Natl Acad Sci. 1999;96(13):7563–8.

[2] Gan TJ. Diclofenac: an update on its mechanism of action and safety profile. Curr Med Res Opin. Informa UK Ltd UK; 2010;26(7):1715–31.

[3] Odom DM, Mladsi DM, Saag KG, Sherif BN, Miles L, Ronquest N, et al. Relationship between diclofenac dose and risk of gastrointestinal and cardiovascular events: meta-regression based on two systematic literature reviews. Clin Ther. 2014;36(6):906–17.

[4] Williams HD, Trevaskis NL, Charman SA, Shanker RM, Charman WN, Pouton CW, et al. Strategies to address low drug solubility in discovery and development. Pharmacol Rev. 2013;65(1):315–499.

[5] Salazar J, Ghanem A, Müller RH, Möschwitzer JP. Nanocrystals: Comparison of the size reduction effectiveness of a novel combinative method with conventional top-down approaches. Eur J Pharm Biopharm. Elsevier B.V.; 2012;81(1):82–90.

[6] Dolenc A, Kristl J, Baumgartner S, Planinsek O. Advantages of celecoxib nanosuspension formulation and transformation into tablets. Int J Pharm. 2009;376(1-2):204–12.

[7] Singh SK, Srinivasan KK, Gowthamarajan K, Singare DS, Prakash D, Gaikwad NB. Investigation of preparation parameters of nanosuspension by top-down media milling to improve the dissolution of poorly water-soluble glyburide. Eur J Pharm Biopharm. 2011;78(3):441–6.

[8] Merisko-Liversidge E, Liversidge GG, Cooper ER. Nanosizing: a formulation approach for poorly-water-soluble compounds. Eur J Pharm Sci.

2003;18(2):113–20.

[9] Ghosh I, Schenck D, Bose S, Ruegger C. Optimization of formulation and process parameters for the production of nanosuspension by wet media milling technique: Effect of Vitamin e TPGS and nanocrystal particle size on oral absorption. Eur J Pharm Sci. 2012;47:718–28.

[10] Müller R., Jacobs C, Kayser O. Nanosuspensions as particulate drug formulations in therapy. Adv Drug Deliv Rev. 2001;47(1):3–19.

[11] Keck CM, Müller RH. Drug nanocrystals of poorly soluble drugs produced by high pressure homogenisation. Eur J Pharm Biopharm. 2006;62(1):3–16.

[12] Möschwitzer JP. Drug nanocrystals in the commercial pharmaceutical development process. Int J Pharm. 2013;453:142–56.

[13] Romero GB, Chen R, Keck CM, Müller RH. Industrial concentrates of dermal hesperidin smartCrystals(®) - production, characterization & long-term stability. Int J Pharm. 2014;

[14] Zhai X, Lademann J, Keck CM, Müller RH. Dermal nanocrystals from medium soluble actives - physical stability and stability affecting parameters. Eur J Pharm Biopharm. 2014;88(1):85–91.

[15] Lai F, Pireddu R, Corrias F, Fadda AM, Valenti D, Pini E, et al. Nanosuspension improves tretinoin photostability and delivery to the skin. Int J Pharm. 2013;458:104–9.

[16] Ghosh I, Michniak-Kohn B. Influence of critical parameters of nanosuspension formulation on the permeability of a poorly soluble drug through the skin--a case study. AAPS PharmSciTech. 2013;14(3):1108–17.

[17] Lai F, Sinico C, Ennas G, Marongiu F, Marongiu G, Fadda AM. Diclofenac nanosuspensions: influence of preparation procedure and crystal form on drug dissolution behaviour. Int J Pharm. 2009;373(1-2):124–32.

[18] Afolabi A, Akinlabi O, Bilgili E. Impact of process parameters on the breakage kinetics of poorly water-soluble drugs during wet stirred media milling: a microhydrodynamic view. Eur J Pharm Sci. 2014;51:75–86.



[19] Klug HP, Alexander LE. X-Ray Diffraction Procedures: For Polycrystalline and Amorphous Materials, 2nd Edition. Wiley-VCH. 1974;

[20] Giordano F, Rossi A, Pasquali I, Bettini R, Frigo E, Gazzaniga A, et al. Thermal degradation and melting point determination of diclofenac. J Therm Anal Calorim. Kluwer Academic Publishers; 2003;73(2):509–18.

[21] Palermo EF, Chiu J. Critical review of methods for the determination of purity by differential scanning calorimetry. Thermochim Acta. 1976;14(1-2):1–12.

[22] Noyes AA, Whitney WR. The rate of solution of solid substances in their own solutions. J Am Chem Soc. ACS Publications; 1897;19(12):930–4.

# 4. The effect of Transcutol® on skin penetration ability of diclofenac acid nanosuspensions



## 1. Introduction

There is great interest in the skin as route for both local and systemic of drug administration. Indeed, topical drug delivery has several advantages over other routes of administration such as reduction of drug systemic toxicity, improved bioavailability for drugs that suffer the gastrointestinal environment and/or hepatic first effects and also enhancement of drug local activity and patient compliance. However, the skin, in particular the stratum corneum (SC), forms a formidable barrier to drug penetration thereby limiting topical and transdermal bioavailability. In order to overcome the impermeability of intact human skin and to enhance drug transport across the skin, several strategies have been developed. These strategies include passive and active penetration enhancement and technologies to bypass the stratum corneum. They include chemical methods based on the use of different penetration enhancers [1–4] as well as physical methods (ionophoresis, electroporation and low-frequency ultra-sound) [5].

Transcutol® P (diethylene glycol monoethyl ether, TRC) is a powerful solubilizing agent used in several dosage forms and it seems to be very attractive as a penetration enhancer due to its non-toxicity, biocompatibility with the skin, miscibility with polar and non-polar solvents and optimal solubilizing properties for a number of drugs [6]. It has been suggested that Transcutol® can lead to formation of cutaneous depot of drugs due to its ability to cause intercellular lipids swelling without altering stratum corneum multiple bilayer structure [4,7,8]. However, Transcutol has also been reported to increase the skin accumulation of topically applied compounds without a concomitant increase in transdermal permeation [9].

Moreover, one approach to increase skin permeability of poorly water soluble drugs is the production of nanocrystals (pure drug only stabi-

lized with a small amount of stabilizer). Conversion of the microsized drug particles into nanocrystals not only increases the dissolution velocity [10,11], but also increases the saturation solubility, which significantly improves the bioavailability of the drug. An increase in the saturation solubility increases the concentration gradient between the dermally applied formulation and the skin [12,13].

The objective of this investigation was to develop Diclofenac acid (DCF) nanosuspensions obtained by the addition of a permeation enhancer, Transcutol, in the aqueous stabilizer solution and to study the effect of Transcutol on the transdermal permeation and skin accumulation of DCF nanocrystals. Diclofenac, 2-[(2,6-dichlorophenyl)amino] phenylacetic acid, is a potent nonsteroidal anti-inflammatory drug (NSAID) with a very low aqueous solubility and gastrolesive actions. It is used in inflammatory and painful conditions of rheumatic and nonrheumatic origin [14]. Three polymorphic forms of diclofenac acid are reported: two are monoclinic and are referred as HD1 (space group *P*21/*c*) and HD2 (space group *C*2/*c*). In both forms molecules are linked to each other through the carboxyl groups giving rise to centrosymmetric dimers [15]. Third polymorph is an orthorombic form (HD3, space group *Pcan*) where no intermolecular hydrogen bond is present [16]. In this study the polymorphic form HD2 has been used.

Characterization of DCF-TRC-nanosuspensions, prepared using the wet media milling technique, was carried out by different techniques: scanning electron microscopy (SEM), differential scanning calorimetry (DSC), X-ray powder diffractometry (XRPD), Fourier transform infrared spectroscopy and photon correlation spectroscopy (PCS). The influence of Transcutol concentration on skin penetration ability of DCF nanosuspensions was evaluated by *in vitro* skin penetration and permeation studies using



Franz diffusion vertical cells and newborn pig skin, in comparison with DCF nanosuspension without TRC, DCF coarse suspension and a commercial topical formulation containing diclofenac sodium.

## 2. Experimental

### 2.1 Materials

Diclofenac sodium salt (DCF-Na) was purchased from Galeno (Comeana, Italy). Diethylene glycol monoethyl ether (Transcutol® P, Trc) was kindly provided by Gattefosse (Saint Priest, France). DCF-Na commercial formulation, Diclofenac Sandoz® gel 1% is produced by Sandoz S.p.a. (Origgio, Varese, Italy). Kolliphor® P188 (Poloxamer 188) and all other reagents were purchased from Sigma–Aldrich (Milan, Italy).

### 2.2. Preparation of DCF acid

Diclofenac acid crystal form (DCF) was obtained following the procedure reported in a previous work [14]. Briefly, a saturated aqueous solution of diclofenac sodium salt was acidified with diluted HCl until a white precipitate of DCF acid was observed. The precipitate was filtered out, washed with bidistilled water to remove residual HCl and dried at 40°C overnight.

### 2.3. Preparation of DCF coarse suspension

The DCF coarse suspensions were prepared by dispersing DCF bulk powder in an aqueous system consisted of Poloxamer 188 (0.46% w/w) and Transcutol in concentrations of 0, 0.5, 1 or 5% (w/w) using an Ultra Turrax T25 basic (IKA, Werke, Germany) for 5 min at 6500 rpm. For the preparation, the same drug amount of the commercial gel formulation was used (3.1 mmol/100g).

### 2.4. Preparation and characterization of DCF nanosuspensions

Diclofenac nanosuspensions were prepared using a wet media milling technique. Drug bulk powder was dispersed in an aqueous system consisted of Poloxamer 188 (0.46% w/w) and Transcutol in concentrations of 0, 0.5, 1 or 5% (w/w) using an Ultra Turrax T25 basic for 5 min at 6500 rpm (Table 1).

This coarse suspension was divided in 1.5 ml conical microtubes containing about 0.4 g of 0.1-0.2 mm yttrium-stabilized zirconia-silica beads (Silibeads® Typ ZY Sigmund Lindner, Germany). The microtubes were oscillated at 3000 rpm for 60 minutes using a beads-milling cell disruptor equipment (Disruptor Genie®, Scientific Industries, USA). The obtained nanosuspensions of each microtubes were gathered and then separated from the milling beads by sieving. DCF acid nanosuspensions were prepared using both the same drug amount of the commercial gel formulation (3.1 mmol/100g).

The average diameter and polydispersity index (PI; a measure of the size distribution width) of the nanosuspensions were determined by photon correlation spectroscopy (PCS) using a Zetasizer nano (Malvern Instruments, Worcestershire, United Kingdom). Samples were backscattered by a helium–neon laser (633 nm) at an angle of 173° and a constant temperature of 25 °C. Zeta potential was estimated using the Zetasizer nano by means of the M3-PALS (Phase Analysis Light Scattering) technique. Just before the analysis, the DCF nanosuspensions were diluted with bidistilled water. DCF-Trc-nanosuspensions were evaluated using scanning electron microscopy (SEM) (S-4100, HITACHI). Samples were fixed on a brass stub using carbon double-sided, coated with gold blazers SCD 004 sputter coater for 2 minutes and observed under an excitation voltage of 5 kV.

**2.5. Solubility studies**

The water solubility of DCF acid was measured for the DCF bulk powder, coarse suspensions and nanosuspensions. Formulations (n=3) were kept under constant stirring for 48 h in a thermostated bath at 37 °C. At preselected time intervals, samples were withdrawn and centrifuged. 0.2 ml of the clear supernatant was filtrated, diluted with methanol and analyzed by HPLC. DCF content was quantified at 280.4 nm using a chromatograph Alliance 2690 (Waters, Milan, Italy), equipped with a photodiode array detector and a computer integrating apparatus (Empower 3). The column was a SunFire C18 (3.5 $\mu$m, 4.6 mm × 100 mm, Waters), and the mobile phase was a mixture of 30% water and 70% acetonitrile (v/v), delivered at a flow rate of 0.7 ml/min. A standard calibration curve was built up by using working standard solutions. Calibration graphs were plotted according to the linear regression analysis, which gave a correlation coefficient value (R2) of 0.999.



**2.6. Differential scanning calorimetry**

Differential scanning calorimetry (DSC) was performed with a Perkin Elmer DSC7, under a pure argon flux and with a heating rate of 10 °C/min in the temperature range from 30 to 190 °C. Each sample was accurately weighed (1–2 mg) in an aluminum pan, crimped and sealed. Temperature calibration was obtained using palmitic acid and indium before and after each measurement. At least three different measurements were made for each sample and average values of Tpeak (peak maximum) and Tonset (extrapolated onset temperature) were reported.

**2.7. X-ray powder diffractometry**

X-ray powder diffraction (XRPD) patterns were collected with a Seifert X3000 diffractometer operating at 35 mA and 40 kV using Cu K$\alpha$ radiation and equipped with a graphite monochromator on the diffracted beam. XRPD patterns were recorded in step scan mode in the range $3° \leq 2\theta \leq 45°$, with step size 0.05 $2\theta$ degree, collecting at least 1000 counts for each step. The divergence and receiving slits were chosen in order to ensure a high resolution mode for the crystalline phases. Attention was paid in the sample preparation in order to minimize preferred orientation. Average crystalline size was estimated by the Scherrer equation, where the integral breadth was corrected for instrumental broadening. The instrumental profile broadening was derived from the fitting of XRPD data ob-

tained from standard samples.

**2.8. Fourier transform infrared spectroscopy (FTIR)**

The FTIR spectra of the samples, dispersed in KBr pellet, were obtained using a Bruker Vector 22 spectrophotometer within the 4000— 400 cm−1 range. Transcutol spectrum was obtained dipping few drop of liquid sample onto KBr disk.

**2.9. In vitro skin penetration and permeation studies**

Experiments were performed on newborn pig skin using Franz vertical cells with an effective diffusion area of 0.785 $cm^2$, under non-occlusive conditions. One-day-old Goland—Pietrain hybrid pigs (~1.2 kg) were provided by a local slaughterhouse. The skin, stored at —80 °C, was pre-equilibrated in saline (0.9% w/v of NaCl) at 25 °C. Skin specimens (n = 12 per formulation) were sandwiched between donor and receptor compartments. The receptor was filled with 5.5 ml of saline, continuously stirred and thermostated at 37 ± 1 °C to reach the physiological skin temperature (i.e. 37 ± 1°C). 100 $\mu$l of each formulation were placed onto the skin surface. Experiments were carried out using DCF acid nanosuspensions and coarse suspensions with both the same drug amount of the commercial gel formulation (3.1 $\mu$moles). At regular intervals, up to 8 h, the receiving solution was entirely withdrawn, replaced with pre-thermostated (37 °C) fresh saline to ensure sink conditions and analysed by HPLC for drug content. After 8 h, the skin surface was gently washed (3 times) with 1 ml of distilled water and then dried with filter paper. The stratum corneum (SC) was removed by stripping with adhesive tape Tesa®AG (Hamburg, Germany). Each piece of the adhesive tape was firmly pressed on the skin surface and rapidly pulled off with one fluent stroke. Epidermis was separated from dermis with a surgical scalpel. Tape strips, epidermis and dermis were cut, placed each in a flask with methanol and sonicated for 4 min in an ice bath to extract the drug. The tapes and tissue suspensions were filtered out and assayed for drug content by HPLC.



**3. Results and Discussion**

**3.1. Preparation and characterization of DCF-TRC-nanosuspensions**

During this study, preparation, physico-chemical properties and (trans)dermal drug delivery ability of DCF-TRC-nanosuspensions were evaluated. In particular, the effect of different concentrations of Transcutol in the nanosuspension formulations (0.5, 1 and 5% for NS-TRC 0.5%, NS-TRC 1% and NS-TRC 5%, respectively) was studied and, as a comparison, a nanosuspensions without Transcutol (NS-TRC 0%) was prepared (Table 1). All nanosuspensions were prepared by the wet media milling technique, using as operating conditions 60 minutes of milling time at 3000 rpm and Poloxamer 188 (0.48% w/w) as stabiliser. The properties of freshly prepared nanosuspensions are shown in Table 2. As can be seen, nanosuspensions with Transcutol exhibited a mean diameter of ~350 nm and a polydispersity index ranging between 0.21 and 0.26, values greater than those of the nanosuspension without TRC (NS-TRC 0%). The zeta potential values were highly negative, ~-35 mV, and increasing TRC concentration increases the nanosuspension pH value which remains always acid (pH<6).

The morphological features of DCF nanocrystals were evaluated by SEM imaging. As seen in Figure 1, even with Transcutol, DCF nanocrystals were nanosized with smooth and rounded surfaces. However, particle size distribution is broader than nanosuspensions without TRC (see page 143), in accordance with the results obtained by PCS.

In the XRDP pattern of DCF nanosuspension without Transcutol and TRC-nanosuspensions (Figure 2), peaks due to polaxamer are visible (peaks around 19 and 23 2J degree) while no peaks due to bead are present. The XRDP results of nanosuspension indicate that no polymorphic transition took place during

**Table 1** Composition of DCF nanosuspensions

| **Components (% w/w)** | **Formulations** | | | |
|---|---|---|---|---|
| | NS-TRC 0% | NS-TRC 0.5% | NS-TRC 1% | NS-TRC 5% |
| **DCF** | 0.92 | 0.92 | 0.92 | 0.92 |
| **Poloxamer 188** | 0.46 | 0.46 | 0.46 | 0.46 |
| **Transcutol** | - | 0.5 | 1 | 5 |
| **Water** | 98.6 | 98.1 | 97.6 | 93.6 |

**Table 2** Average diameter (Z-AVE), polydispersity index (PI), Zeta potential (ZP) and pH of DCF freshly prepared nanosuspensions. Each value is the mean ± standard deviation of at least six experimental determinations.

| | Z-AVE (nm) | PI | ZP (mV) | pH |
|---|---|---|---|---|
| NS-TRC 0% | 279.2±8.12 | 0.17 ± 0.01 | -35.0 ± 1.32 | 4.4 |
| NS-TRC 0.5% | 346.1±14.17 | 0.21 ± 0.05 | -36.9 ± 2.86 | 5.28 |
| NS-TRC 1% | 355.7±3.31 | 0.26 ± 0.02 | -37.8 ± 0.87 | 5.13 |
| NS-TRC 5% | 349.5±14.32 | 0.22 ± 0.02 | -37.2 ± 1.10 | 5.95 |



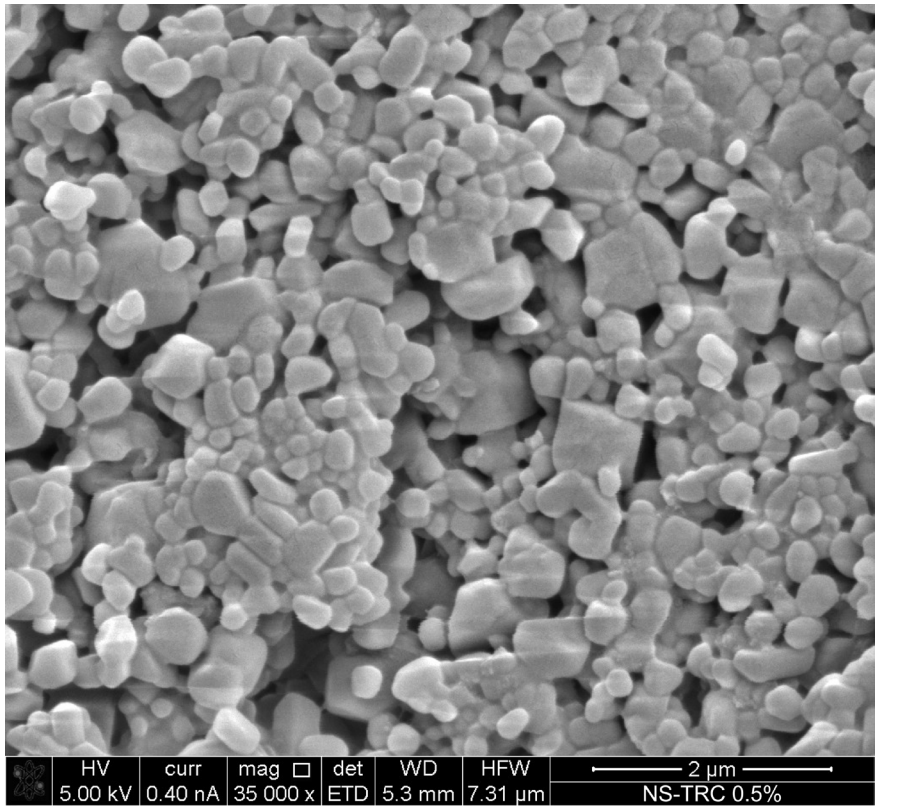


**Figure 1.a.** SEM images of Diclofenac acid (DCF) nanosuspensions with 0.5% TRC concentrations: NS-TRC 0.5%.

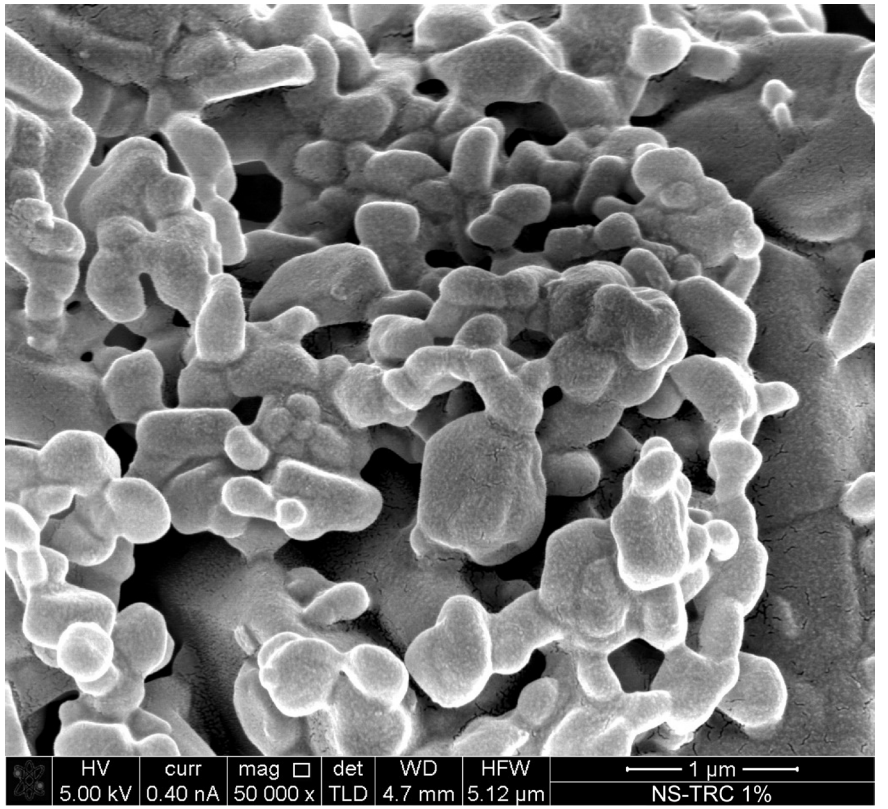


**Figure 1.b.** SEM images of Diclofenac acid (DCF) nanosuspensions with 1% TRC concentrations: NS-TRC 1%.



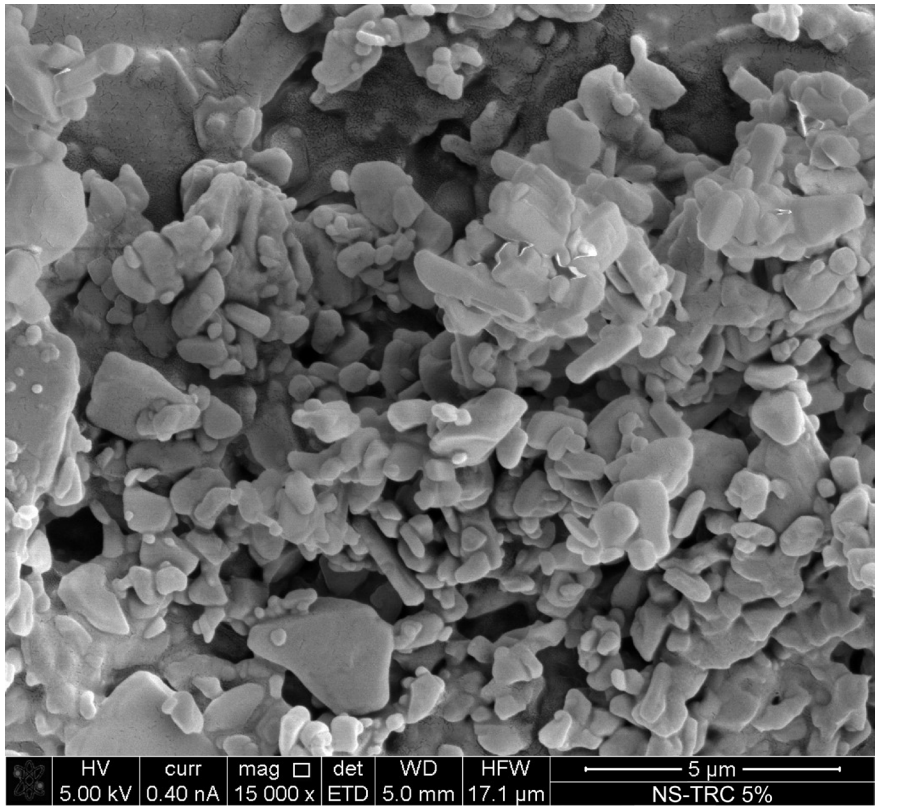


**Figure 1.c.** SEM images of Diclofenac acid (DCF) nanosuspensions with 5% TRC concentrations: NS-TRC 5%.

milling. In all these spectra the relative peak intensities due to DCF and Poloxamer phases have the trend of those of bulk samples. XRDP patterns of bulk DCF (Figure 2c), is in agreement with the HD2 monoclinic C2/c crystal structure and all peaks are indexed using these structural data [15]. Amorphous contribution of liquid Transcutol was not observed. In the nanosuspensions samples peaks due to HD2 phase were rather broad as a result of lower particle size, whose average values calculated according to Scherrer equation result in the nanometer range. The HD2 phase peaks width in the XRDP spectra of nanosuspensions prepared whitout Transcutol (Figure 2d) indicates a narrow crystalline size around 60 nm. The width analysis of the same peaks in the TRC-nanosuspensions leads to an average crystalline size around 84 nm for TRC 0.5% and TRC 1% while those of TRC 5% are smaller (77 nm).

In conclusion, the XRDP analysis indicates a crystalline average size in NS-TRC 0% lower than TRC-nanosuspensions samples. However, between TRC-nanosuspensions there are some differences: TRC 5% sample, containing the maximum amount of transcutol, shows the smallest average crystalline size.

DSC thermograms of nanosuspension formulations (Figure 3) show an endothermic peak around 50°C, due to Poloxamer melting. Thermogram of bulk DSC is characterized by a sharp endothermic peak centred around 177.9 °C followed by sample decomposition (Figure 3)[17]. NS-TRC 0% and TRC-nanosuspensions are similar, characterized by a broad faint peak with Tpeak centered around 160-161°C for TRC-nanosuspensions and around 152°C for NS-TRC 0%. In agreement with Van't Hoff equation [18] this behavior, lower Tpeak and broader peak, is expected for a very dispersed mixture like those of nanosuspension. Slightly differences in Tpeak of the nanosuspensions samples can be ascribed to very faint differences in average particles size, polidispersivity and different hydrogen bonds between DCF and Transcutol/Poloxamer. In agreement with this result the XRDP pattern of TRC 5% nanosuspension shows broader DCF peaks compared to TRC 0.5% and TRC 1% samples.

In Figure 4 the FTIR spectra of Poloxamer, Transcutol, NS-TRC 0%, TRC 5%, TRC 1% and TRC 0.5% nanosuspensions and bulk DCF samples are reported. The spectrum of Poloxamer 188, a non ionic triblock copolymers composed of a central hydrophobic chain of polyoxypropylene flanked by two hydrophilic chains of polyoxyethylene shows significant absorption bands due to OH (3600—3400 cm-1), C-O (1110cm-1) and C-H sp3 (2890 cm-1) stretching [19]. The transcutol spectrum is very similar to Poloxamer one: the absorption band due to OH (3600-3400 cm-1) is accompanied by that of methyl and methylene stretching (2982, 2927, 2875 cm-1). Bands due to CH3 and CH2 scissoring are also present in the region 1455-1382 cm-1. C-O stretching is also observed at 1102 cm-1 with OH bending at 1072cm-1.

In the bulk DCF sample the characteristic absorption bands of very strong intensities, due to C=O (1691 cm—1), COO- symmetric and asymmetric stretching (1578 cm—1, 1452 cm-1) and the absorption band at 3325 cm-1 due to N-H stretching, which is superimposed on that of the large OH stretching signal, were observed [20]. Distinct absorption bands at 1296 cm—1, 1196 cm—1 and 1156 cm-1 due to C—N stretching in secondary amines and C-C stretching vibrations in the aromatic ring at 1506 cm—1 were also observed. Further O—H stretching and out of plane bending vibrations were noted at 2682 cm—1 and 937 respectively. C—Cl stretching vibrations were observed at 766 cm—1 and 740 cm—1.

The FTIR spectra of NS-TRC 0% and TRC-nanosuspensions are very similar: all absorption bands ascribable both to polaxamer or transcutol and HD2 are evident. This result, in agreement with XRDP and DSC analysis, suggests that differences between these sam-

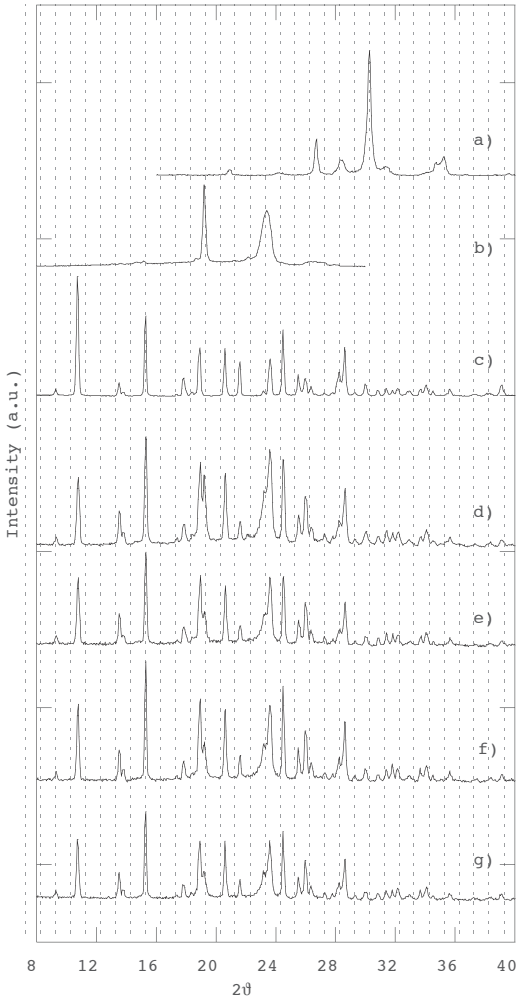


**Figure 2.** Experimental XRD spectra of a) Yttrium-stabilized zirconia-silica beads (beads), b) poloxamer, c) bulk DCF, d) DCF nanosuspension (without Transcutol), e) TRC 5%, f) TRC 1%, g) TRC 0.5% nanosuspensions samples.



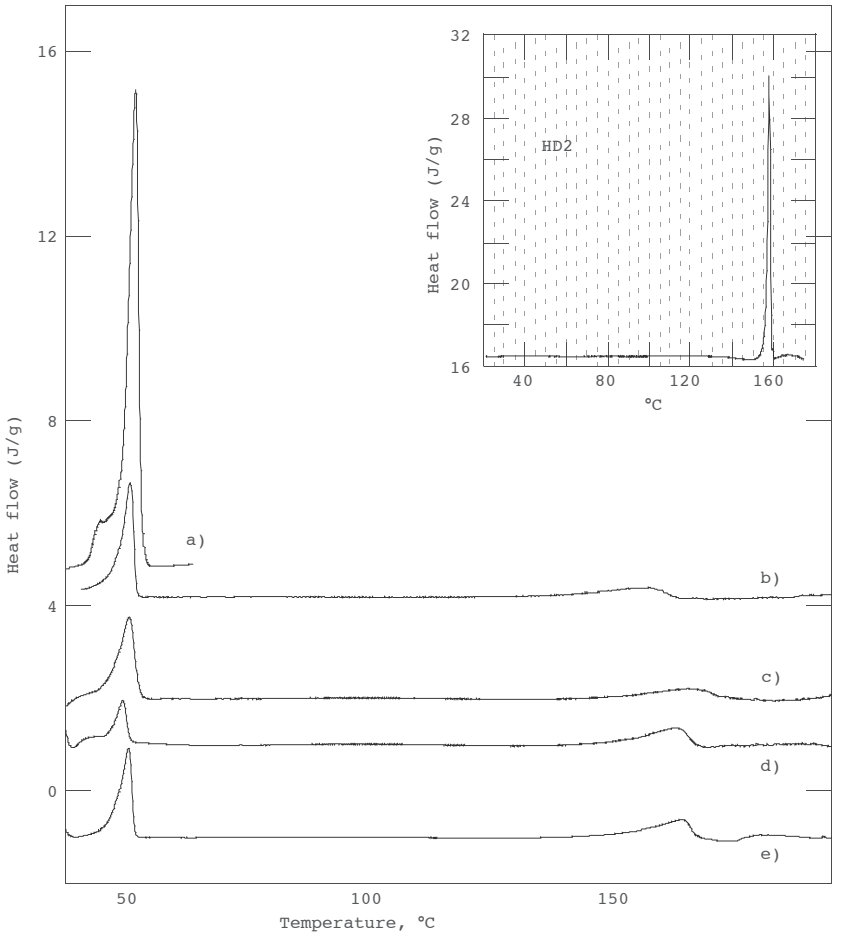


**Figure 3.** DSC thermograms of a) poloxamer, b) DCF nanosuspension (without Transcutol), c) Trc 5%, d) Trc 1%, e) Trc 0.5% nanosuspensions samples. DSC thermogram of bulk DCF is reported in the onset.

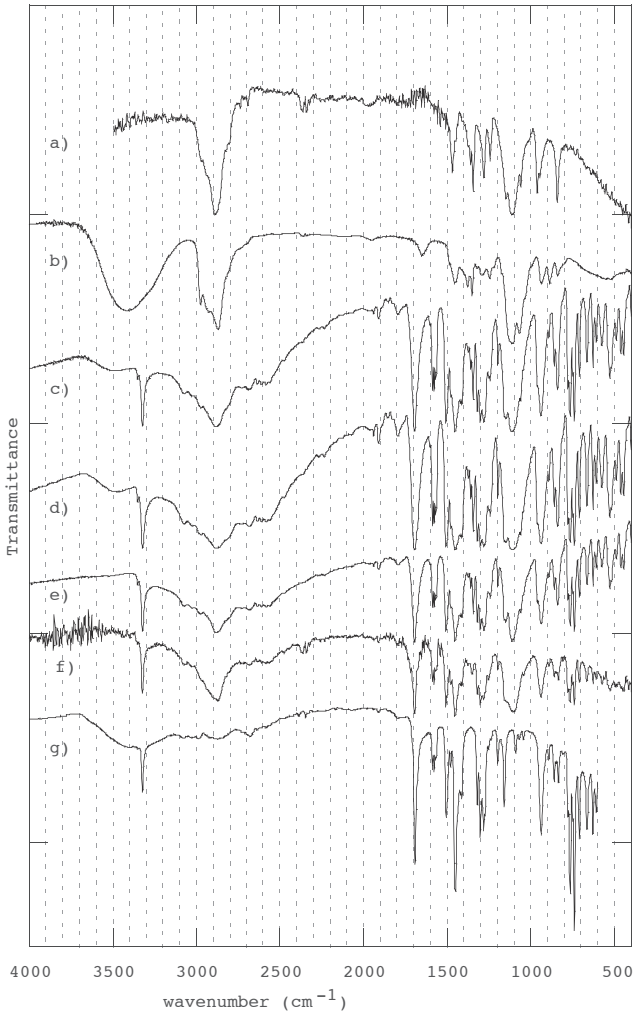


**Figure 4.** FT infrared spectra of a) poloxamer, b) transcutol, c) TRC 5%, d) TRC 1%, e) TRC 0.5%, f) TRC 0% nanosuspensions, g) bulk DCF samples.



ples should be traced to different morphology, dispersion degree and average crystallite size.

### 3.2. In vitro skin penetration and permeation studies

To evaluate the influence of Transcutol concentration on dermal and transdermal delivery of DCF when nanosuspensions are topically applied, *in vitro* penetration and permeation studies through newborn pig skin were carried out in non occlusive conditions using Franz diffusion cells. Coarse suspension and a commercial gel formulation were used as control. Figure 5 shows the % of delivered DCF to and accumulated in the skin strata for nanosuspensions prepared using different Transcutol concentration, coarse suspension and commercial formulation prepared using the same DCF molar concentration (3,1 mmol/100g), after an 8 h experiment. As previously reported (see page 148), nanosuspension prepared without Transcutol (NS-TRC 0%) enhanced DCF skin delivery compared to the coarse suspension and commercial gel formulation. In particular, commercial gel formulation showed the lowest drug delivery into the newborn pig skin (1.38% in the stratum corneum, 1.15% in the epidermis and 0.31% in the dermis).
Furthermore, the application of nanosuspensions and coarse suspension always gave the higher accumulation of DCF in the stratum corneum. In particular, nanosuspensions prepared without Transcutol (NS-TRC 0%) produced a drug accumulation in the SC approximately 16 times higher than the commercial gel and 2 times higher than the corresponding coarse suspension. In addition, nanosuspensions were able to improve DCF deposition, with respect to coarse suspensions, in the epidermis (6.1%) and dermis (3.3%).
As previously reported, this enhancement in DCF skin delivery when nanosuspensions are applied to the skin is correlated to an increased concentration gradient between formulation and skin due to the increased saturation solubil-

ity (Figure 6) according to the Freundlich–Ostwald equations, and increased dissolution rate of the nanocrystal formulation according to the Kelvin and Noyes–Whitney equations [21].

Unexpectedly, as reported in Figure 5 the increase of TRC in the nanosuspension formulations decreased the DCF skin delivery. In particular, nanosuspension prepared using 0,5% TRC (NS-TRC 0,5%) produced a drug accumulation in the SC similar to that of coarse suspension (~12.5%), while, the application of NS-TRC 1% and NS-TRC 5% reduced the DCF accumulation (7.8 and 4.9 % respectively). This unpredictable behavior can be explained considering the average diameter and saturation solubility values measured for the nanosuspension formulations obtained using different TRC concentrations. Indeed, the higher average diameter values of NS-TRC formulations could decrease the DCF dissolution velocity with respect to NS-TRC 0%. Moreover, although TRC is considered a powerful solubilizing agent, the increase of its concentration in the nanosuspension formulations determined the DCF solubility decrease (Figure 6). In particular, nanosuspension prepared without Transcutol (NS-TRC 0%) showed a solubility value of 83 $\mu$g/ml. This value decreased to 74, 65 and 53 $\mu$g/ml for NS-TRC 0,5%, NS-TRC 1% and NS-TRC 5% respectively. This solubility reduction leads to a decreased concentration gradient between formulation and skin, thus decreasing drug accumulation in the SC in comparison with the NS-TRC 0%.

On the contrary, application of NS-TRC gave DCF accumulation in the epidermis very similar to that obtained for NS-TRC 0% (6.1%, 8.7%, 7.1% and 6.1% for NS-TRC 0%, NS-TRC 0,5%, NS-TRC 1% and NS-TRC 5% respectively). Furthermore, the application of the nanosuspension formulation with the highest TRC concentration (NS-TRC 5%) gave a DCF permeation similar to that obtained for NS-TRC 0%. Probably, the high Transcutol concentration in the NS-TRC 5% formulation determined the swelling of the SC intercellular lipids reducing the ability of the outer skin strata to retain DCF molecules that easily accumulated in the deeper layers and permeated the skin.

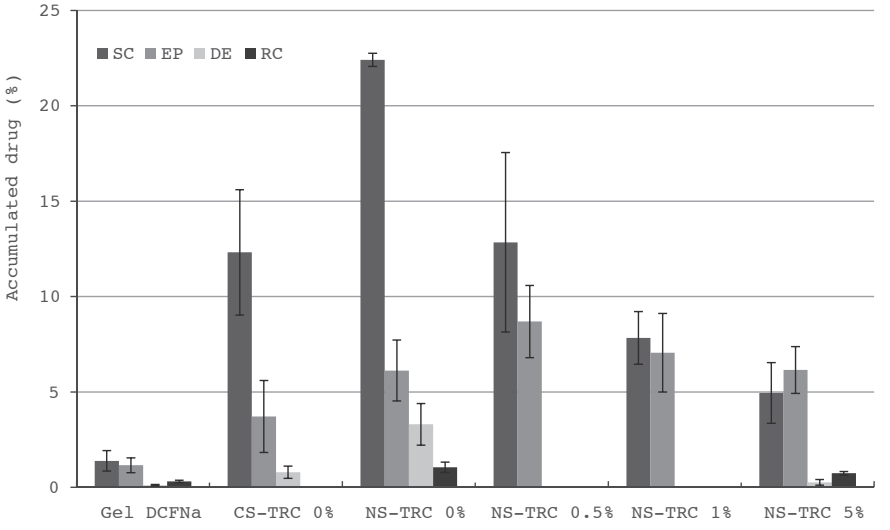


**Figure 5.** Cumulative amount of DCF retained into and permeated through mouse skin layers after 8 h application of different DCF-TRC-nanosuspensions (NS-TRC; DCF 3.1 mmol/100g) in comparison with DCF coarse suspension without TRC (CS-TRC 0%; DCF 3.1 mmol/100g) and Diclofenac Sandoz® gel 1% (3.1 mmol/100g). SC, stratum corneum; Ep, epidermis; D, dermis; and RC, receptor compartment.



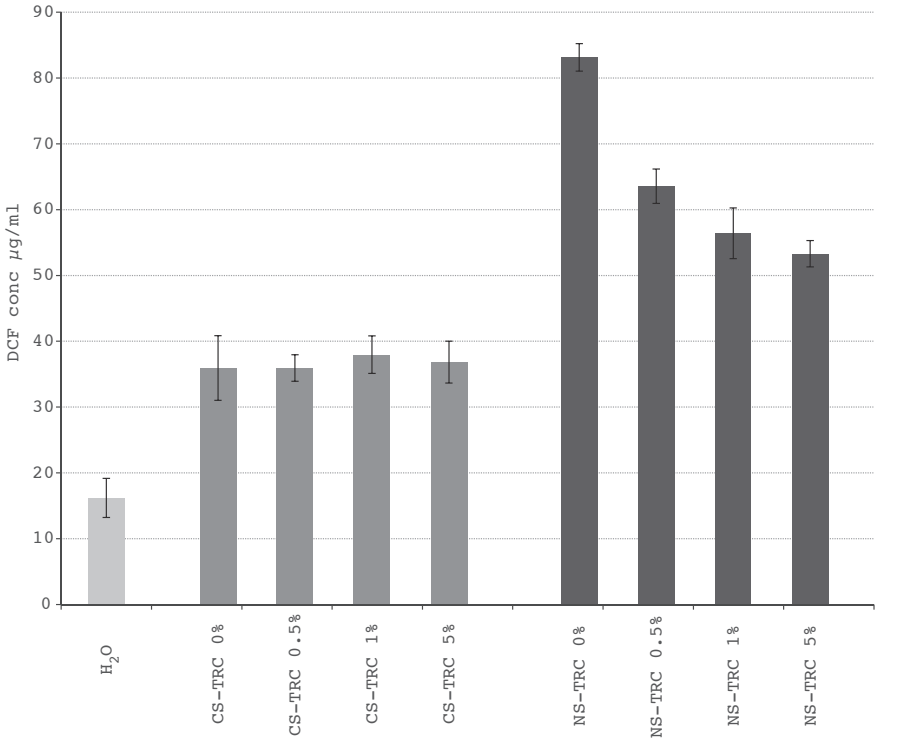


**Figure 6.** Water solubility of bulk DCF, DCF-TRC-nanosuspensions (NS) and DCF-TRC-coarse suspensions (CS) at 37 °C.

## References

[1] Thong H, Zhai H, Maibach H. Percutaneous penetration enhancers: An overview. Skin Pharmacol Physiol. 2007;20:272–82.

[2] Manconi M, Mura S, Sinico C, Fadda a. M, Vila a. O, Molina F. Development and characterization of liposomes containing glycols as carriers for diclofenac. Colloids Surfaces A Physicochem Eng Asp. 2009;342(1-3):53–8.

[3] Manconi M, Caddeo C, Sinico C, Valenti D, Mostallino MC, Biggio G, et al. Ex vivo skin delivery of diclofenac by transcutol containing liposomes and suggested mechanism of vesicle-skin interaction. Eur J Pharm Biopharm. Elsevier B.V.; 2011;78(1):27–35.

[4] Manconi M, Sinico C, Caddeo C, Vila AO, Valenti D, Fadda AM. Penetration enhancer containing vesicles as carriers for dermal delivery of tretinoin. Int J Pharm. 2011;412(1-2):37–46.

[5] Lavon I, Kost J. Ultrasound and transdermal drug delivery. Drug DiscovToday. 2004;9:670–6.

[6] Mura P, Faucci MT, Bramanti G, Corti P. Evaluation of transcutol as a clonazepam transdermal permeation enhancer from hydrophilic gel formulations. Eur J Pharm Sci. 2000;9(4):365–72.

[7] Panchagnula R, Ritschel WA. Development and evaluation of an intracutaneous depot formulation of corticosteroids using transcutol as a cosolvent: In-vitro, ex-vivo and in-vivo rat studies. J Pharm Pharmacol. 1991;43:609–14.

[8] Godwin DA, Felton LA, Kim NH. Influence of Transcutol® CG on the skin accumulation and transdermal permeation of ultraviolet absorbers. Eur J Pharm Biopharm. 2002;53:23–7.

[9] Ritschel WA, Panchagnula R, Stemmer K, Ashraf M. Development of an intracu-

taneous depot for drugs. Binding, drug accumulation and retention studies, and mechanism of depot. Skin Pharmacol Physiol. 1991;4:235–42.

[10] Buckton G, Beezer a. E. The relationship between particle size and solubility. Int J Pharm. 1992;82(3):7–10.

[11] Müller RH, Jacobs C, Kayser O. Nanosuspensions for the formulation of poorly soluble drugs. Pharmaceutical Emulsions and Suspensions. 2000. p. 383–407.

[12] Mishra PR, Al Shaal L, Müller RH, Keck CM. Production and characterization of Hesperetin nanosuspensions for dermal delivery. Int J Pharm. 2009;371(1-2):182–9.

[13] Al Shaal L, Shegokar R, Müller RH. Production and characterization of antioxidant apigenin nanocrystals as a novel UV skin protective formulation. Int J Pharm. 2011;420:133–40.

[14] Lai F, Sinico C, Ennas G, Marongiu F, Marongiu G, Fadda AM. Diclofenac nanosuspensions: influence of preparation procedure and crystal form on drug dissolution behaviour. Int J Pharm. 2009;373(1-2):124–32.

[15] Castellani C, Ottani S. Two Monoclinic Forms of Diclofenac Acid. Acta Crystallographica Section C Crystal Structure Communications. 1997. p. 794–7.

[16] Jaiboon N, Yos-In K, Ruangchaithaweesuk S, Chaichit N, Thutivoranath R, Siritaedmukul K, et al. New orthorhombic form of 2-[(2,6-dichlorophenyl) amino]benzeneacetic acid (diclofenac acid). Anal Sci. 2001;17(12):1465–6.

[17] Giordano F, Rossi A, Pasquali I, Bettini R, Frigo E, Gazzaniga A, et al. Thermal degradation and melting point determination of diclofenac. J Therm Anal Calorim. Kluwer Academic Publishers; 2003;73(2):509–18.

[18] Palermo EF, Chiu J. Critical review of methods for the determination of purity by differential scanning calorimetry. Thermochim Acta. 1976;14(1-2):1–12.



[19] Lai F, Pini E, Angioni G, Manca ML, Perricci J, Sinico C, et al. Nanocrystals as tool to improve piroxicam dissolution rate in novel orally disintegrating tablets. Eur J Pharm Biopharm. Elsevier B.V.; 2011;79(3):552–8.

[20] Jubert A, Massa NE, Tévez LL, Okulik NB. Vibrational and theoretical studies of the non-steroidal anti-inflamatory drugs Niflumic [2-3((3-trifluoromethyl)phenylamino)-3-pyridinecarboxylic acid]; Diclofenac [[2-(2,6-dichlorophenyl)amino]-benzeneacetic acid] and Indometacin acids [1-(4-chlorobenzo. Vib Spectrosc. 2005;37(2):161–78.

[21] Noyes AA, Whitney WR. The rate of solution of solid substances in their own solutions. J Am Chem Soc. ACS Publications; 1897;19(12):930–4.

# 5.Topical application of diclofenac acid nanosuspensions reduces skin inflammation in mice



## 1. Introduction

Inflammation is an essential protective process for preserving the integrity of the body against physical, chemical, infective, and autoimmune causes. However, the inflammatory response to such insults may erroneously lead to damaging of normal tissues, due to an overproduction of reactive oxygen species (ROS), nitric oxide (NO) and cytokines, such as tumor necrosis factor-alpha (TNF-α) [1–3].Therapeutic treatments involve the care of symptoms by interrupting the inflammatory process and, if possible, the native cause. Usually, inflammation is localized in a specific organ or apparatus, like skin, subcutaneous tissue, muscular or osteoarticular apparatus, and it can often become chronic. Long-term systemic treatments with steroidal or non-steroidal anti-inflammatory drugs can cause onset of several side effects and a low drug bioavailability at the site of action [4]. Topical administration may represent a valid alternative to the systemic treatment of local inflamed skin or muscle. In particular, nanosized formulations (e.g., nanocrystals in the range of 100-1000 nm) of anti-inflammatory drugs, which are usually poorly soluble in aqueous media, can be used to improve their local bioavailability and efficacy, minimizing side effects. Indeed, nanocrystals can increase drug bioavailability by enhancing its dissolution velocity and saturation solubility, thus, leading to an increased concentration gradient with a consequent improved drug penetration into the skin [5,6]. Nanocrystals are prepared as a suspension (nanosuspension) in a liquid dispersion medium, usually water, stabilized by a suitable surfactant and/or polymer. Nanosuspensions can be obtained by several technologies: milling, high-pressure homogenization, impinging jet, electro-spraying, liquid-based methods and supercritical fluid processes [7]. Compared to other nanosizing techniques, wet media milling, a typical top-down approach, is considered

a simple method that avoids organic solvents and is easy to scale-up [8]. During the milling process, drug crystals break into smaller particles thanks the energy and shear forces generated by the impaction of the milling pearls with the drug [9].
Nanocrystals can be delivered by various routes of administration, although product development is currently being mainly focused on the oral route [10]. Dermal use of nanocrystals of poorly soluble actives is a recent application. Indeed, up to 10 years ago, the dermal delivery of nanocrystals to enhance the local efficacy of actives has been completely neglected, both in pharmaceutical and cosmetic field [11], and, so far, relatively little is published about dermal delivery of nanocrystals [12–17]. Furthermore, to the best of our knowledge, there are no *in vivo* studies on the biological activity of drugs used in a nanocrystalline form and applied to the skin. Given that, in the present study, nanocrystals of diclofenac (2-(2-[(2,6-dichlorophenyl) amino]phenyl) acetic acid) (DCF) are proposed as a novel approach to treat skin inflammation, and their efficacy was validated in an animal model. DCF is one of the most potent and commercially successful non-steroidal anti-inflammatory drugs (NSAIDs). Due to several drawbacks when given orally, the DCF is preferably administered topically in long-term treatments, such as treatment of local muscle inflammation, in spite of low skin permeabilityof the drug. Currently available commercial topical preparations contain DCF in salt form, because of the DCF free acid very low aqueous solubility [18]. However, the lipophilicity of the DCF acid would allow a better penetration than hydrophilic DCF salts. Therefore, the aim of this work was to produce DCF acid nanocrystals, which are expected to readily penetrate into the skin by virtue of their dissolution properties. Characterization of DCF nanosuspensions, prepared using the wet media milling technique, was carried out by different techniques: scanning electron microscopy (SEM), differential scanning calorimetry (DSC), X-ray powder diffractometry, Fourier transform infrared spectroscopy and photon correlation spectroscopy (PCS).
Additionally, diffusion of DCF through mouse skin was investigated *ex vivo*, and the topical anti-inflammatory potential of the DCF nanosuspension was assessed *in vivo* by testing their activity against common inflammatory endpoints: inhibition of chemically induced oedema and leucocyte infiltration (reflected in myeloperoxidase–MPO-activity). TPA (12-O-tetradecanoylphorbol-13-acetate) is commonly used to induce inflammation in animal models [19]: it is known to trigger the activation of protein kinase C, the expression of a wide variety of pro-inflammatory cytokines, such as TNF-α, and the influx of neutrophils and other innate immune cells into skin, which closely resemble processes involved in chronic skin inflammation [20]. The therapeutic efficacy of the nanosuspension was compared with those of a DCF coarse suspension and a commercial topical preparation containing diclofenac diethylamine, Voltaren Emulgel®.



## 2. Experimental

### 2.1 Materials

Diclofenac sodium salt (DCF-Na) was purchased from Galeno (Comeana, Italy). Voltaren Emulgel®, an oily emulsion in aqueous gel containing 1.16% diclofenac diethylamine corresponding to 1% diclofenac sodium, was from Novartis Farma (Origgio,Varese, Italy). Kolliphor® P188 (Poloxamer 188), 12-O-Tetradecanoylphorbol 13-acetate (TPA) and all other reagents were purchased from Sigma–Aldrich (Milan, Italy).

### 2.2. Preparation of DCF acid

Diclofenac acid crystal form (DCF) was obtained following the procedure reported in a previous work [21]. Briefly, a saturated aqueous solution of diclofenac sodium salt was acidified with diluted HCl until a white precipitate of

DCF acid was observed. The precipitate was filtered out, washed with bidistilled water to remove residual HCl and dried at 40°C overnight.

**2.3. Preparation of DCF coarse suspension**

The DCF coarse suspension was prepared by dispersing DCF bulk powder in Poloxamer 188 bidistilled water solution (0.46% w/w) using an Ultra Turrax T25 basic (IKA, Werke, Germany) for 5 min at 6500 rpm. For the preparation, the same amount of drug of the commercial Voltaren Emulgel® was used (3.1 mmol/100g, CS DCF). Drug/surfactant ratio (w/w) was 2:1.

**2.4. Preparation and characterization of DCF nanosuspension**

The DCF nanosuspension was prepared using the wet media milling technique. Drug bulk powder was dispersed in a Poloxamer 188 aqueous solution using an Ultra Turrax T25 basic for 5 min at 6500 rpm (Table 1). This coarse suspension was divided in 1.5 ml conical microtubes containing about 0.4 g of 0.1-0.2 mm yttrium-stabilized zirconia-silica beads (Silibeads® Typ ZY, Sigmund Lindner, Germany).The microtubes were oscillated at 3000 rpm for 60 minutes using a beads-milling cell disruptor equipment (Disruptor Genie®, Scientific Industries, USA). The obtained nanosuspensions of each microtubes were gathered and then separated from the milling beads by sieving.

The DCF nanosuspension was prepared using the same amount of drug of the commercial Voltaren Emulgel® (3.1 mmol/100g, NS DCF). Drug/surfactant ratio (w/w) was 2:1 (Table 1).

The average diameter and polydispersity index (PI; a measure of the size distribution width) of the nanosuspension were determined by photon correlation spectroscopy (PCS) using a Zetasizer nano (Malvern Instruments, Worcestershire, United Kingdom). Samples were backscattered by a helium–neon laser (633 nm) at an angle of 173° and a constant temperature of 25 °C. Zeta potential



was estimated using the Zetasizer nano by means of the M3-PALS (Phase Analysis Light Scattering) technique. Just before the analysis, the DCF nanosuspension was diluted with bidistilled water.

DCF nanocrystals were evaluated using scanning electron microscopy (SEM) (S-4100, HITACHI). The sample was fixed on a brass stub using carbon double-sided, coated with gold blazers SCD 004 sputter coater for 2 minutes and observed under an excitation voltage of 10 kV.

**2.5. Solubility studies**

The solubility of DCF was measured for the DCF bulk powder, coarse suspension and nanosuspension. The formulations (n=3) were kept under constant stirring for 48 h in a thermostated bath at 37 °C. At preselected time intervals, samples were withdrawn and centrifuged. 0.2 ml of the clear supernatant was filtrated, diluted with methanol and analyzed by HPLC. DCF content was quantified at 280.4 nm using a chromatograph Alliance 2690 (Waters, Milan, Italy), equipped with a photodiode array detector and a computer integrating apparatus (Empower 3). The column was a SunFire C18 (3.5 $\mu$m, 4.6 mm × 100 mm, Waters), and the mobile phase was a mixture of 30% water and 70% acetonitrile (v/v), delivered at a flow rate of 0.7 ml/min.A standard calibration curve was built up by using working standard solutions. Calibration graphs were plotted according to the linear regression analysis, which gave a correlation coefficient value (R2) of 0.999.

**2.6. Differential scanning calorimetry**

Differential scanning calorimetry (DSC) was performed with a Perkin Elmer DSC7, under a pure argon flux and with a heating rate of 10 °C/min in the temperature range from 30 to 190 °C. Each sample was accurately weighed (1–2 mg) in an aluminum pan, crimped and sealed. Temperature calibration was obtained using palmitic acid and indium before and after each measurement. At least three different meas-

urements were made for each sample and average values of Tpeak (peak maximum) and Tonset (extrapolated onset temperature) were reported.

**2.7. X-ray powder diffractometry**

X-ray powder diffraction (XRPD) patterns were collected with a Seifert X3000 diffractometer operating at 35 mA and 40 kV using Cu Kα radiation and equipped with a graphite monochromator on the diffracted beam. XRPD patterns were recorded in step scan mode in the range 3° ≤2θ≤45°,with step size 0.05 2θ degree, collecting at least 1000 counts for each step. The divergence and receiving slits were chosen in order to ensure a high resolution mode for the crystalline phases. Attention was paid in the sample preparation in order to minimize preferred orientation. Average crystalline size was estimated by the Scherrer equation, where the integral breadth was corrected for instrumental broadening. The instrumental profile broadening was derived from the fitting of XRPD data obtained from standard samples.

**2.8. Fourier transform infrared spectroscopy (FTIR)**

The FTIR spectra of the samples, dispersed in KBr pellet, were obtained using a Bruker Vector 22 spectrophotometer within the 4000— 400 cm-1 range.

**2.9. Ex vivo and in vivo drug penetration and permeation studies in mice**

Male CD-1 mice (5—6 weeks old, 25—35 g) were obtained from Harlan Laboratories (S. Pietro al Natisone, Udine, Italy) and acclimatized for 1 week before use, with free access to food and water. All animal tests have been conducted in accordance with the guidelines for care and use of experimental animals of the European Communities Council Directive 86/609/EEC.

Mice were sacrificed and shaved. The skin from the dorsal region was excised and mounted on Franz diffusion vertical cells (effective diffusion area 0.785 $cm^2$), between donor and receptor compartments, with the stratum



corneum (SC) side facing the donor one. The receptor was filled with 5.5 ml of saline (NaCl 0.9%, w/v), continuously stirred and thermostated at 37 ± 0.5 °C. 20 μl of DCF nanosuspension, coarse suspension and Voltaren Emulgel® (n=6 per formulation) was applied on the skin surface (non-occlusive conditions). After 1, 2, 4, 6, 8, 23 and 24 h, the receiving solution was entirely withdrawn and analyzed by HPLC for drug content. After 24 h, the skin specimens were gently washed, and the SC removed by stripping with adhesive tape Tesa® AG (Hamburg, Germany). Epidermis was separated from dermis with a scalpel. Tape strips, epidermis and dermis were cut, each placed in a flask with methanol and sonicated for 4 min in an ice bath to extract the DCF. The tapes and tissue suspensions were filtered out and assayed for drug content by HPLC.

**2.10. Mice experimental design: oedema formation and myeloperoxidase determination**

The back skin of CD-1 mice (n=4 per group), housed and fed as above, was shaved one day before the experiment, and those animals showing no hair re-growth were used. TPA dissolved in acetone (243 μM; 3 μg/20 μl) was applied to the shaved dorsal area (approximately 2 $cm^2$) to induce cutaneous inflammation (day 1). Negative control mice received acetone only (20 μl). All test samples (20 μl), DCF nanosuspension, coarse suspension, Poloxamer and commercial Voltaren Emulgel®, were topically smeared over the same dorsal area 3 h after TPA application (non-occlusive conditions). The procedure was repeated (at 24-h intervals) on day 2 and 3. On day 4, mice were sacrificed by cervical dislocation.

The inhibitory effect of DCF formulations on TPA-induced skin inflammation was determined by two biomarkers: oedema formation and MPO activity. After 72 h of treatment (on day 4), the treated dorsal skin area of each mouse was excised and weighed to assess any increase indicative of oedema formation, and

immediately stored at −80 °C [20]. MPO assay was performed as previously reported [20]. Briefly, skin biopsies were homogenized and centrifuged. The supernatant was incubated with hydrogen peroxide and tetramethylbenzidine and then assayed for MPO activity spectrophotometrically at 620 nm. The MPO activity was calculated from the linear portion of a standard curve.

### 2.11. Statistical analysis of data

Data analysis was carried out with the software package R, version 2.10.1. Results are expressed as the mean ± standard deviation. Multiple comparisons of means (Tukey test) were used to substantiate statistical differences between groups, while Student's t-test was used for comparison between two samples. Significance was tested at the 0.05 level of probability (p).

## 3. Results and Discussion

### 3.1. Preparation and characterization of DCF nanosuspension

In this work, DCF acid nanosuspension was successfully prepared by the wet media milling technique. Composition and features of the freshly prepared nanosuspension are shown in Table 1. As can be seen, the nanosuspension exhibited a mean diameter of 279 nm and a low polydispersity index (0.17), that indicates a fairly narrow size distribution [9]. The zeta potential value was highly negative, -35 mV and the pH of the suspension was 4.4.

The morphological features of DCF nanocrystals were evaluated by SEM imaging. As seen in Figure 1, DCF crystals generated by milling technique have a regular shape with smooth and rounded surfaces, a narrow particle size distribution and diameters slightly less than 300 nm, as determined by PCS.

In addition to the PCS particle size measurements, the SEM images provided evidence that the prepared DCF nanocrystal suspensions were nanosized and homogenous in size and shape.



**Table 1.** Average diameter, polydispersity index (PI) and Zeta potential of Diclofenac acid (DCF) nanosuspension after milling

| Component | Stabilizer | Properties | | | |
|---|---|---|---|---|---|
| | | Particle size (nm) | PI | Zeta potential (mV)I | pH |
| DCF 0.92%(w/w) | Poloxamer 188 0.46%(w/w) | 279±7.7 | 0.17±0.01 | -35±1.3 | 4.4 |

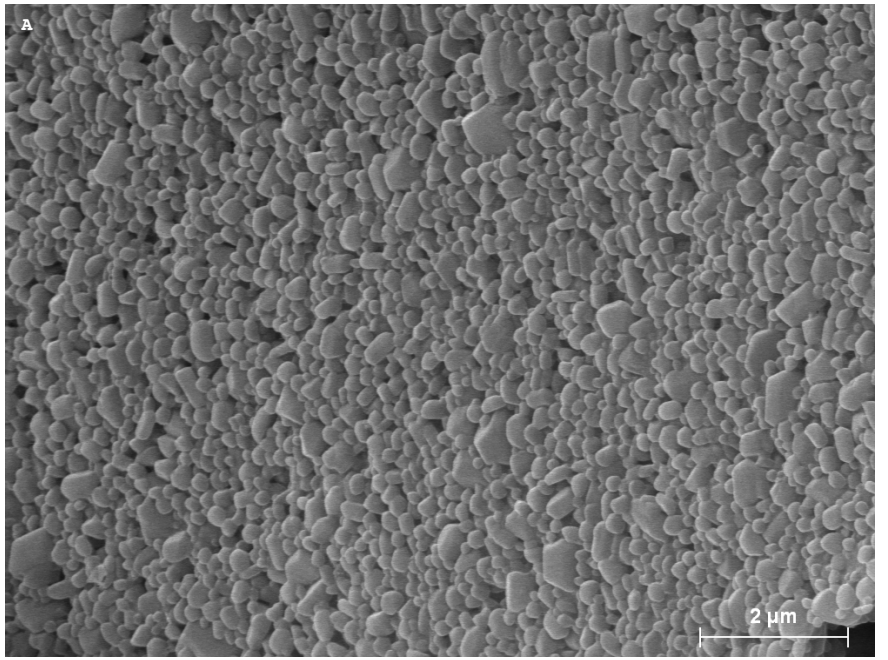


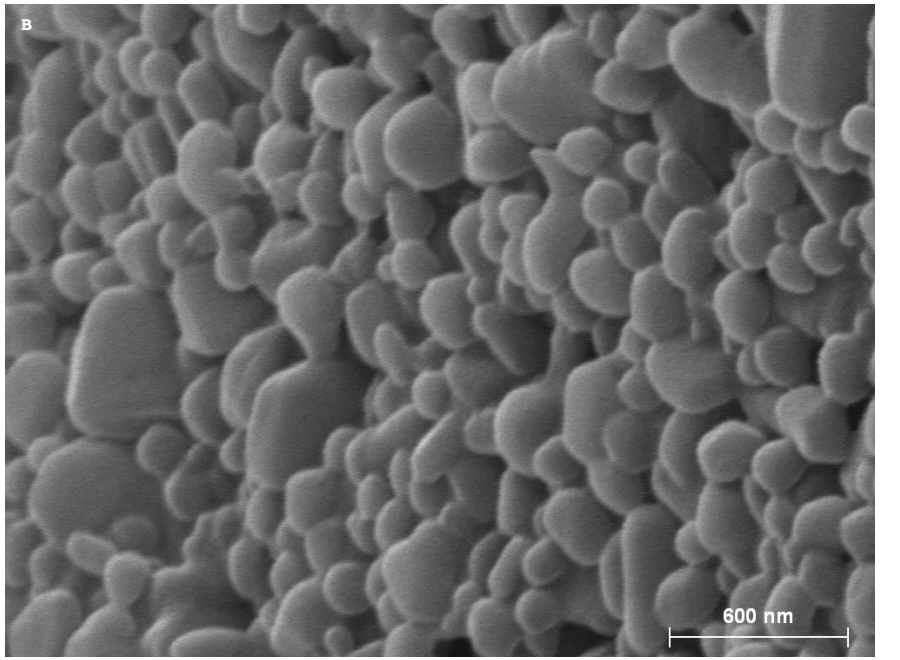


**Figure 1.** SEM images of Diclofenac acid (DCF) nanocrystals stabilized by poloxamer 188, (A) and (B), scale bars being 2 $\mu$m and 600 nm, respectively.

XRPD pattern of yttrium-stabilized zirconia-silica beads, poloxamer, bulk DCF, DCF nanosuspension and coarse suspension are reported in Figure 2. The diffraction pattern of poloxamer is characterized by a peak around 19° 2θ and a second one, larger, centred around 23° 2θ. XRPD of beads exhibits peaks due to crystalline yttrium and zirconium oxide mixture, with the strongest lines centred around 30.25 and 26.72 2θ degree. XRPD pattern of bulk DCF is in agreement with its monoclinic C2/c crystal structure typical to the DCF HD2 polymorph form [22] and all peaks were indexed using these structural data. No peaks due to others DCF polymorphic phases were observed in XRPD patterns.

In the XRPD pattern of DCF nanosuspension and coarse suspension, the characteristic peaks of poloxamer are visible (at 19 and 23 2θ degree), while the absence of bead signals confirms the effectiveness of the preparation process. Comparison of spectra of nano/coarse suspensions with bulk DCF allowed us to establish that no polymorphic transition of DCF took place during their production. Further, the relative peak intensities of DCF and poloxamer are the same of the raw materials (Figure 2).

DSC thermograms of nano and coarse suspensions show an endothermic peak around 50 °C, due to poloxamer melting (Figure 3). The thermogram of bulk DCF is characterized by a sharp endothermic peak centred around 177.9 °C followed by sample decomposition [23]. Nano and coarse suspensions display a very similar profile, characterized by a broad faint peak with Tpeak centered around 150-152 °C. According to Van't Hoff equation [24], this behavior (i.e. lower Tpeak and broader peak), is expected for a very dispersed mixture, like a nanosuspension. Slight differences in Tpeak of the suspensions are tentatively ascribed to very differences in average particle size, in agreement with XRDP results.

In Figure 4, the FTIR spectra of bulk DCF, poloxamer, nano and coarse suspensions are reported. In the bulk DCF, the characteristic absorption bands of very strong intensities, due to C=O (1691 cm—1), COO— symmetric and asymmetric stretching (1578 and 1452 cm—1, respectively) and the absorption band at 3325 cm—1 due to N-H stretching, which is superimposed on the large OH stretching signal, were observed [25]. The spectra also show distinct absorption bands at 1296, 1196 and 1156 cm—1, due to C—N stretching in secondary amines and C-C stretching vibrations in the aromatic ring at 1506 cm—1. Further, O—H stretching and out of plane bending vibrations are visible at 2682 and 937 cm—1, respectively, while C—Cl stretching vibrations can be seen at 766 and 740 cm—1. The spectrum of poloxamer 188 shows significant absorption bands due to OH (3600—3400 cm-1), C-O (1110 cm-1) and C-H sp3 (2890 cm-1) stretching[26].

The FTIR spectra of the nano and coarse suspensions are very similar: all the absorption bands ascribable both to poloxamer and DCF are evident. This result, in agreement with XRPD and DSC analyses, suggests that differences between these samples should be traced to the different morphology, dispersion degree, and average crystallite size.

An important investigational parameter for nanosuspensions is the determination of the saturation solubility. In this study the water solubility at 37 °C was evaluated for the DCF bulk powder, coarse suspension and nanosuspension.

The solubility of pure DCF was found to be 19.88 ± 2.63 μg/ml, which increased in the coarse suspension to 35.94 ± 4.91 μg/ml, and became even 83.14 ± 2.1 μg/ml in the nanosuspension. Therefore, it is confirmed that when particles are nanosized, saturation solubility of the drug increases, according to the Freundlich—Ostwald equations [27].

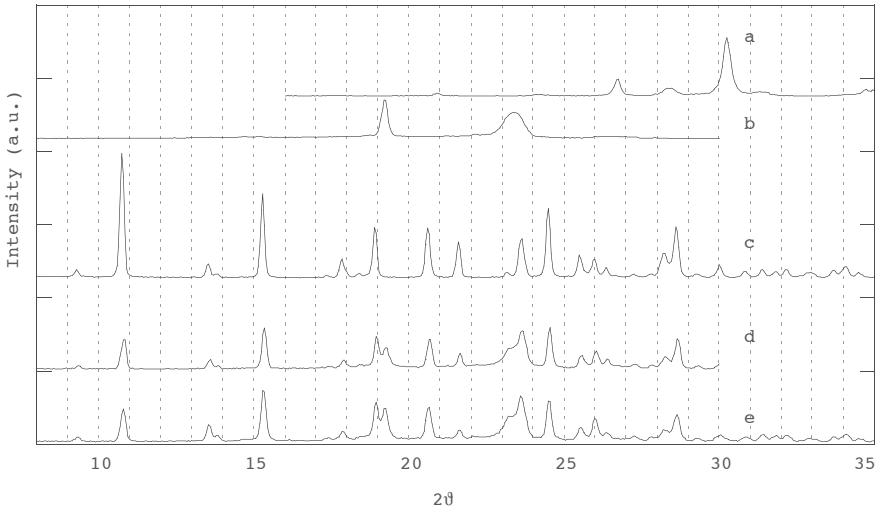


**Figure 2.** XRD spectra of a) Yttrium-stabilized zirconia-silica beads (beads), b) poloxamer, c) bulk DCF, d) DCF coarse suspension and e) DCF nanosuspension samples

**Figure 3** (next page). DSC thermograms of a) poloxamer, b) bulk DCF, c) DCF nanosuspension and d) DCF coarse suspension



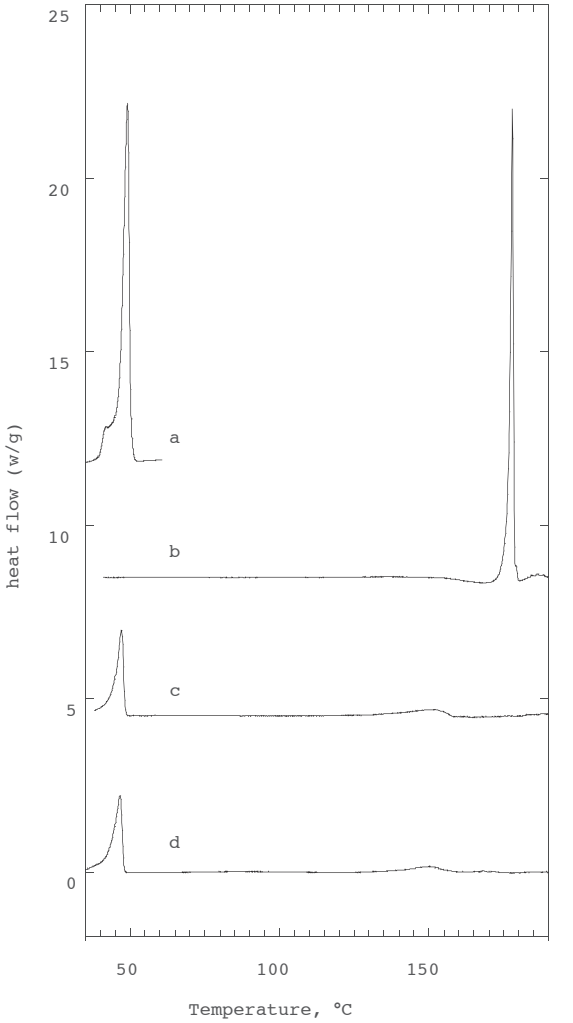

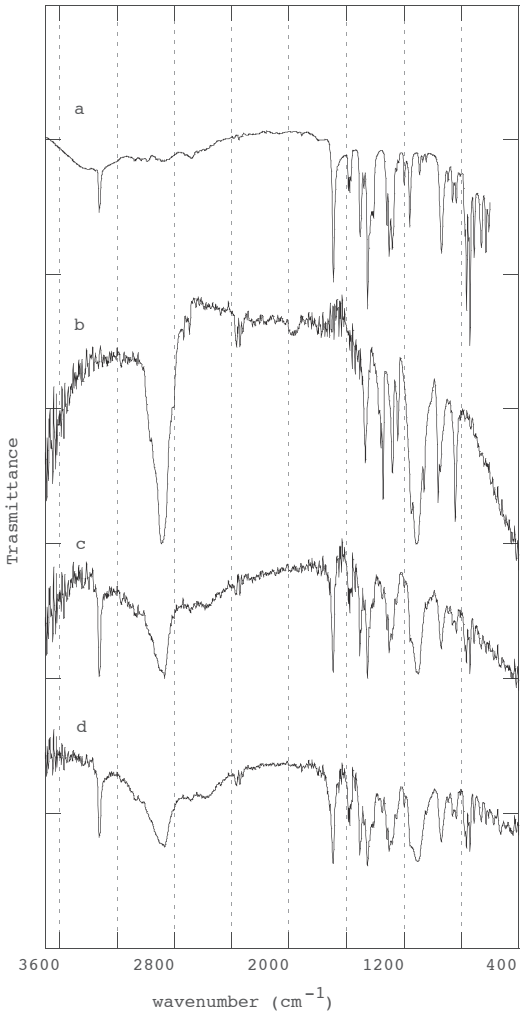


**Figure 4** FT infrared spectra of a) bulk DCF, b) poloxamer, c) DCF coarse suspension and d) DCF nanosuspension



### 3.2. Ex vivo skin penetration/permeation

The penetration ability of DCF in nanosuspension was evaluated on intact fullthickness mouse skin in comparison with the DCF coarse suspension and the commercial Voltaren Emulgel®. Experiments were carried out using 20 $\mu$l of the testing samples because this was found to be the appropriate dose in the proposed in vivo experimental protocol. The amount of drug accumulated into and permeated the whole skin is expressed as the percentage of the drug applied onto the skin. As reported in Table 2, Voltaren gave the highest permeation of DCF (50%), 1.7- and 2 fold higher than coarse- and nano-suspension, respectively. The flux (determined as the slope of the linear portion of the plot), was 1.7 fold than in coarse suspension and 1.3 fold than in nanosuspension. Moreover, it showed a negative lag time (calculated by extrapolating the linear portion of the curve to the abscissa), due to the rapid drug exit from the skin.

By contrast, nanosuspension provided the highest accumulation of DCF (42%; 2- and 5.3-fold higher than that of coarse suspension and Voltaren, respectively), the highest value of LAC (obtained as the ratio of drug accumulated in the skin versus drug delivered through the skin), 1.8- and 7-fold higher than course suspension and Voltaren, and the longest lag time.

More specifically, in Figure 5, the cumulative amount of DCF recovered from the different skin strata is reported as the mean amount of drug per unit of surface area ($\mu$mol/cm$^2$) after application of all the formulations tested. As can be seen, drug distribution in the different mouse skin strata was dissimilar. After application of the Voltaren formulation, drug deposition into the skin was only 0.010 $\mu$mol/cm$^2$ in the stratum corneum, 0.179 $\mu$mol/cm$^2$ in the epidermis and 0.086 $\mu$mol/cm$^2$ in the dermis while the highest amount of the drug was found in the receptor compartment (6 fold higher than

**Table 2** Percentage of accumulated (in the whole skin) and permeated drug (with respect to the drug applied onto the skin) and total drug delivered, Local Accumulation Efficiency (LAC) values: drug accumulated into the skin/drug delivered through the skin ratio, lag time (h) and steady-state flux (J μmol/cm2/h), after 24 h of diffusion experiments ex vivo of DCF nanosuspension (NS DCF) in comparison with DCF coarse suspensions (CS DCF) and Voltaren. Values are the means ± standard deviation (n = 6).

| Sample | Accumulated drug (% ± SD) | Permeated drug (% ± SD) | Total drug delivered (%) | LAC | Lag time (h) | J (μmol/cm²/h±SD) |
|---|---|---|---|---|---|---|
| Voltaren | 8±2.0 | 50±2.8 | 58 | 0.2 | -0.1 | 0.072±0.004 |
| CSDCF | 20±5.2 | 24±4.5 | 44 | 0.8 | 2.6 | 0.043±0.008 |
| NSDCF | 42±5.7 | 30±3.5 | 72 | 1.4 | 5.9 | 0.056±0.007 |

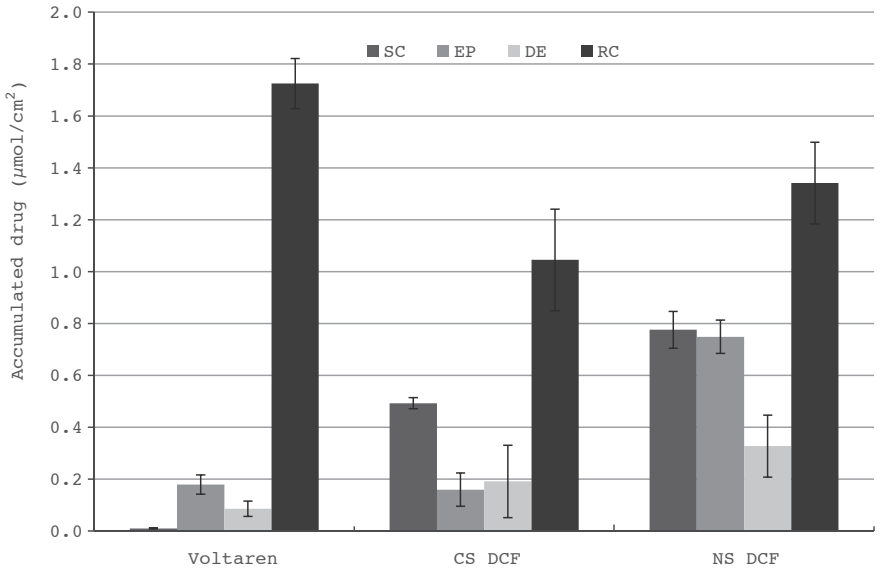


**Figure 5** Cumulative amount of DCF retained into and permeated through mouse skin layers after 24 h application of DCF nanosuspension (NS DCF, 31 mol/100g) in comparison with DCF coarse suspension (CS DCF,3.1 mmol/100g) and Voltaren® (3.1 mmol/100g). SC, stratum corneum; Ep, epidermis; D, dermis; and RC, receptor compartment.



the amount accumulated in the different skin layers). The application of coarse suspension gave the greatest accumulation of DCF in the SC, while the accumulation in the dermis and epidermis was three times lower. On the contrary, using nanosuspension, similar amount of DCF were found in epidermis (~0.76 μmol/cm²), where they reach significantly higher deposition than Voltaren or the coarse suspension. In the dermis, nanosuspension reached deposition extent higher than the coarse suspension (0.327 μmol/cm² vs 0.192 μmol/cm²) and even much higher than Voltaren (0.327 μmol/cm² vs 0.086 μmol/cm²).

*Ex vivo* results showed that nanosuspension was able to improve DCF acid cutaneous deposition and, at the same time, to reduce its permeation and flux, in comparison with Voltaren that provided a rapid and strong drug delivery to the receptor compartment (mimicking the systemic circulation). When coarse DCF is transformed into nanocrystals, drug saturation solubility increases, namely the dissolved DCF acid molecules in equilibrium with the solid phase increases, consequently, increasing the concentration gradient between the nanosuspension and the skin. Furthermore, the increase of the surface area in the nanosuspension also increases the dissolution rate: the DCF molecules dissolve quickly from the nanocrystals, which act as a depot in the water phase, and rapidly replace the DCF molecules penetrated from the water phase into the skin.

### 3.3. In vivo inflammatory response

TPA is routinely used in skin inflammation protocols, since it triggers different signal transduction pathways and cellular metabolic activities resulting in local inflammation, migration of leucocytes and swelling associated with increased vascular permeability [28,29].

In the short-term experiments presented in this paper, the skin of CD-1 mice was treated with TPA applications (once daily for three consecutive

days) to test whether topically applied DCF nanosuspension inhibited the development of acute, chemically induced inflammation. The more commonly used endpoints of acute inflammation are oedema, which is assayed by increase in weight, and neutrophil infiltration, which is measured by assaying for the neutrophil marker myeloperoxidase - MPO [30].

Our results, depicted in Figure 6a and b, show that the DCF nanosuspension partially suppressed TPA-induced oedema, providing an oedema inhibition of 50%, not statistically distinguishable from Voltaren Emulgel® ($p > 0.05$) (Figure 6a). The coarse suspension had a marginal inhibitory effect, and Poloxamer produced a slightly higher reduction of the oedema (23%). Furthermore, the DCF nanosuspension showed a superior ability to reduce significantly MPO activity in damaged tissue, than the coarse suspension, as shown by the higher inhibition value (86 vs 67%, Figure 6b). Most importantly, the nanosuspension was more effective than Voltaren Emulgel®, which achieved only 16% of MPO inhibition, thus, with no statistical significance compared to the TPA-treated skin. On the other hand, it was found that Poloxamer approached 29% MPO inhibition. Poloxamer is a nonionic block copolymer chemical surfactant known to have cytoprotective, anti-inflammatory activities, combined with minimal toxicity, due to its adherence to hydrophobic surfaces exposed after cell damage, restoring normal hydrated surfaces [31,32]. This can reasonably explain the ability of the surfactant to slightly modulate the inflammatory events triggered by TPA acute tissue damage.

The efficacy of the DCF nanosuspension was further confirmed by the macroscopic observation of the treated mouse skin. TPA-exposed mice showed cutaneous lesions that appeared as areas of red, crusted skin with thickened texture (Figure 7). The topical treatment with both the DCF coarse suspension and Poloxamer resulted in a moderate attenuation of the lesions, and when Voltaren Emulgel® was applied, the flaking, cracking and redness were still visible. On the contrary, a remarkable amelioration of the TPA injury was observed upon administration of the DCF nanosuspension, which had a softening effect on the skin showing only mild signs of irritation.

These results are in perfect agreement with *ex vivo* skin penetration/permeation experiments.



**4. Conclusions**

In this study, DCF nanosuspension was successfully prepared and characterized. *In vivo* and *ex vivo* results have proven the superior anti-inflammatory efficacy of the nanocrystal suspension and its actual ability to localize the drug in the site of inflammation, compared to a commercial product (Voltaren). In conclusion, this study highlights the great potential of using nanocrystal suspensions as an effective strategy to improve topical bioavailability of poorly water-soluble drugs as well as a valid therapeutic approach.

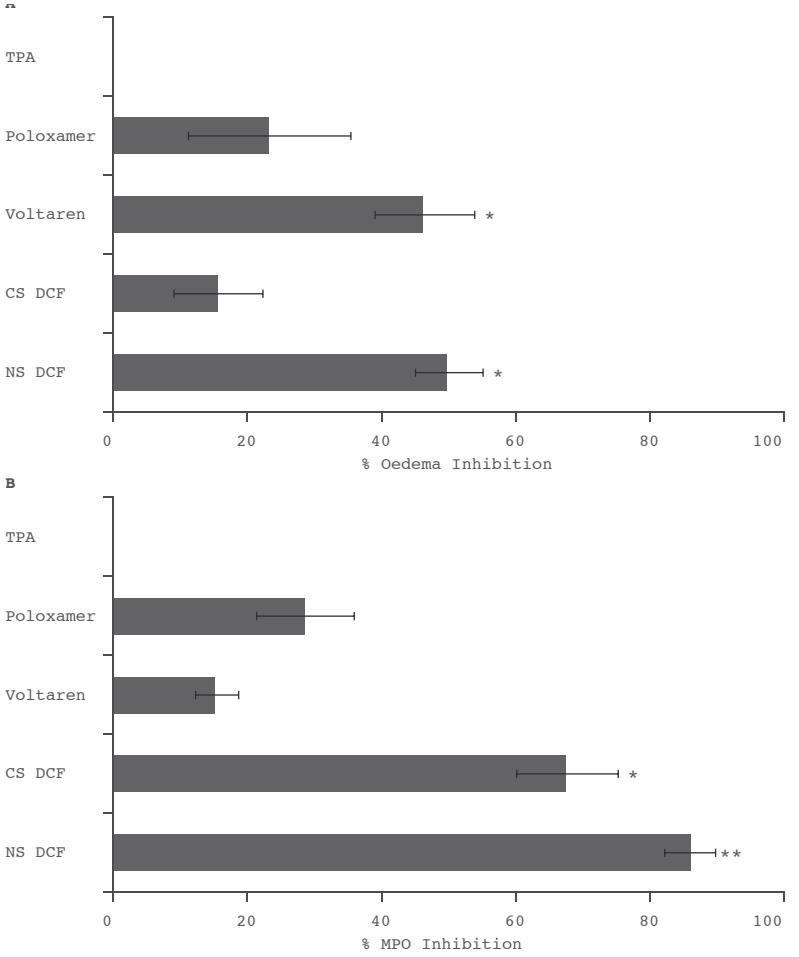


**Figure 6.** Percentage of mouse oedema and myeloperoxidase (MPO) inhibition obtained after TPA treatment followed by application of a Poloxamer water solution (0.46% w/v), Voltaren and DCF course (CS DCF) and nanosuspension (NS DCF), compared with TPA-only treated mice (positive control). Each bar is the mean ± S.D. of four animals (*p<0.05, **p<0.01, compared to TPA).



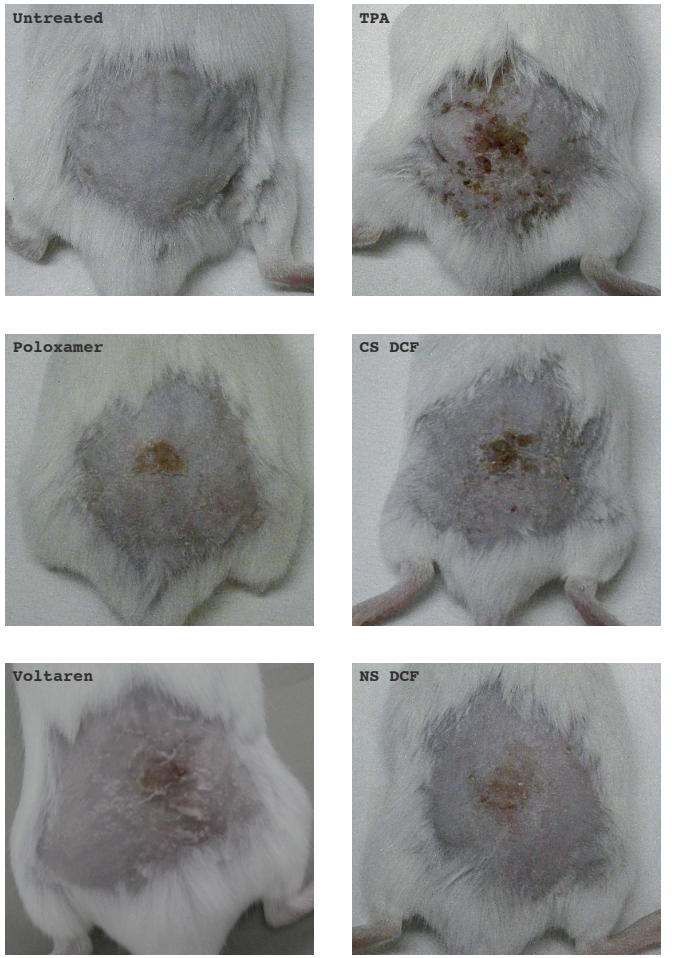


**Figure 7.** Photographs of dorsal skin of mice sacrificed on day 4: untreated, treated with TPA-only to induce inflammation, treated with TPA followed by the administration of a Poloxamer water solution (0.46% w/v), Voltaren and DCF course (CS DCF) and nanosuspension (NS DCF).

## References

[1] Standiford, J. T. Anti-inflammatory Cytokines and Cytokine Antagonists. Curr Pharm Des. 2000;6:633–49.

[2] Henderson WR. The Role of Leukotrienes in Inflammation. Ann Intern Med. 1994;121:684–97.

[3] Manconi M, Caddeo C, Sinico C, Valenti D, Mostallino MC, Biggio G, et al. Ex vivo skin delivery of diclofenac by transcutol containing liposomes and suggested mechanism of vesicle-skin interaction. Eur J Pharm Biopharm. Elsevier B.V.; 2011;78(1):27–35.

[4] Manca ML, Manconi M, Falchi AM, Castangia I, Valenti D, Lampis S, et al. Close-packed vesicles for diclofenac skin delivery and fibroblast targeting. Colloids Surfaces B Biointerfaces. 2013;111:609–17.

[5] Müller RH, Gohla S, Keck CM. State of the art of nanocrystals - Special features, production, nanotoxicology aspects and intracellular delivery. Eur J Pharm Biopharm. 2011;78:1–9.

[6] Romero GB, Chen R, Keck CM, Müller RH. Industrial concentrates of dermal hesperidin smartCrystals ® – production , characterization & long-term stability. Int J Pharm. 2015;482:54–60.

[7] Pawar VK, Singh Y, Meher JG, Gupta S, Chourasia MK. Engineered nanocrystal technology: in-vivo fate, targeting and applications in drug delivery. J Control Release. 2014;183:51–66.

[8] Merisko-Liversidge E, Liversidge GG. Nanosizing for oral and parenteral drug delivery: A perspective on formulating poorly-water soluble compounds using wet media milling technology. Adv Drug Deliv Rev. 2011;63:427–40.

[9] Patravale VB, Date A a, Kulkarni RM. Nanosuspensions: a promising drug delivery strategy. J Pharm Pharmacol. 2004;56(1992):827–40.

[10] Möschwitzer JP. Drug nanocrystals in the commercial pharmaceutical development process. Int J Pharm. 2013;453:142–56.

[11] Petersen R. Nanocrystals for use in topical formulations and method of production thereof. PCT/EP2007/009943. 2006.

[12] Ghosh I, Michniak-Kohn B. Influence of critical parameters of nanosuspension formulation on the permeability of a poorly soluble drug through the skin--a case study. AAPS PharmSciTech. 2013;14(3):1108–17.

[13] Romero GB, Chen R, Keck CM, Müller RH. Industrial concentrates of dermal hesperidin smartCrystals® – production, characterization & long-term stability. Int J Pharm. Elsevier B.V.; 2015;482:54–60.

[14] Piao H, Kamiya N, Hirata A, Fujii T, Goto M. A novel solid-in-oil nanosuspension for transdermal delivery of diclofenac sodium. Pharm Res. 2008;25:896–901.

[15] Lai F, Pireddu R, Corrias F, Fadda AM, Valenti D, Pini E, et al. Nanosuspension improves tretinoin photostability and delivery to the skin. Int J Pharm. 2013;458:104–9.

[16] Zhai X, Lademann J, Keck CM, Müller RH. Nanocrystals of medium soluble actives - Novel concept for improved dermal delivery and production strategy. Int J Pharm. 2014;470:141–50.

[17] Kobierski S, Ofori-Kwakye K, Müller RH, Keck CM. Resveratrol nanosuspensions: Interaction of preservatives with nanocrystal production. Pharmazie. 2011;66:942–7.

[18] Goh CF, Lane ME. Formulation of diclofenac for dermal delivery. Int J Pharm. 2014;473(1-2):607–16.

[19] Murakawa M, Yamaoka K, Tanaka Y, Fukuda Y. Involvement of tumor necrosis factor (TNF)-α in phorbol ester 12-O-tetradecanoylphorbol-13-acetate (TPA)-induced skin edema in mice. Biochem Pharmacol. 2006;71:1331–6.



[20] Caddeo C, Sales OD, Valenti D, Saurí AR, Fadda AM, Manconi M. Inhibition of skin inflammation in mice by diclofenac in vesicular carriers: Liposomes, ethosomes and PEVs. Int J Pharm. 2013;443:128–36.

[21] Lai F, Sinico C, Ennas G, Marongiu F, Marongiu G, Fadda AM. Diclofenac nanosuspensions: influence of preparation procedure and crystal form on drug dissolution behaviour. Int J Pharm. 2009;373(1-2):124–32.

[22] Castellani C, Ottani S. Two Monoclinic Forms of Diclofenac Acid. Acta Crystallographica Section C Crystal Structure Communications. 1997. p. 794–7.

[23] Giordano F, Rossi A, Pasquali I, Bettini R, Frigo E, Gazzaniga A, et al. Thermal degradation and melting point determination of diclofenac. J Therm Anal Calorim. Kluwer Academic Publishers; 2003;73(2):509–18.

[24] Palermo EF, Chiu J. Critical review of methods for the determination of purity by differential scanning calorimetry. Thermochim Acta. 1976;14(1-2):1–12.

[25] Jubert A, Massa NE, Tévez LL, Okulik NB. Vibrational and theoretical studies of the non-steroidal anti-inflamatory drugs Niflumic [2-3((3-trifluoromethyl)phenylamino)-3-pyridinecarboxylic acid]; Diclofenac [[2-(2,6-dichlorophenyl)amino]-benzeneacetic acid] and Indometacin acids [1-(4-chlorobenzo. Vib Spectrosc. 2005;37(2):161–78.

[26] Lai F, Pini E, Angioni G, Manca ML, Perricci J, Sinico C, et al. Nanocrystals as tool to improve piroxicam dissolution rate in novel orally disintegrating tablets. Eur J Pharm Biopharm. Elsevier B.V.; 2011;79(3):552–8.

[27] Müller RH, Peters K. Nanosuspensions for the formulation of poorly soluble drugs. Int J Pharm. 1998;160(2):229–37.

[28] Gebhardt C, Breitenbach U, Tuckermann JP, Dittrich BT, Richter KH, Angel P. Calgranulins S100A8 and S100A9 are negatively regulated by glucocorticoids in a c-Fos-dependent manner and overexpressed throughout skin carcinogenesis. Oncogene. 2002;21:4266–76.

[29] Goel G, Makkar HPS, Francis G, Becker K. Phorbol esters: structure, biological activity, and toxicity in animals. Int J Toxicol. 2007;26:279–88.

[30] Gordon JS, Wolanin PM, Gonzalez A V, Fela D a, Sarngadharan G, Rouzard K, et al. Topical N-acetyl-S-farnesyl-L-cysteine inhibits mouse skin inflammation, and unlike dexamethasone, its effects are restricted to the application site. J Invest Dermatol. 2008;128:643–54.

[31] Harting MT, Jimenez F, Kozar R a., Moore F a., Mercer DW, Hunter RL, et al. Effects of poloxamer 188 on human PMN cells. Surgery. 2008;144:198–203.

[32] Hunter RL, Luo AZ, Zhang R, Kozar R a., Moore F a. Poloxamer 188 inhibition of ischemia/reperfusion injury: Evidence for a novel anti-adhesive mechanism. Ann Clin Lab Sci. 2010;40(2):115–25.